THE UNIVERSITY OF MICHIGAN

INDUSTRY PROGRAM OF THE COLLEGE OF ENGINEERING

EFFECT OF INELASTIC ACTION ON THE BEHAVIOR OF STRUCTURES DURING EARTHQUAKES

Spiro S. Thomaides

A dissertation submitted in partial fulfillment
of the requirements for the degree of
Doctor of Philosophy in the
University of Michigan
1961

June, 1961

IP-519

ACKNOWLEDGMENT

I wish to express my appreciation to each of the members of my doctoral committee for their kind assistance and helpful discussions during the course of this work. Especially, I wish to express my profound gratitude to Professor Glen V. Berg, Chairman of the committee, whose constant guidance and advice have been invaluable.

This dissertation is part of ORA Project No. 02881, "A Study of the Energy Functions for Structures Subjected to Earthquakes," administered by The University of Michigan's Office of Research Administration, and directed by Professor G. V. Berg, under whom I had the privilege of working. The project was sponsored by the National Science Foundation under Grant No. 7316. I am grateful to the Foundation for its financial support.

The University of Michigan's Computing Center kindly made available the high-speed digital computer, without which the computations could not have been made. The U.S. Coast and Geodetic Survey furnished the accelerogram records from which the digital accelerograms were prepared. The secretaries of the Department of Civil Engineering typed the first draft of the dissertation, and the staff of the Industry Program of the College of Engineering did the final typing and reproduction. I am sincerely thankful to each of these persons for their contribution.

TABLE OF CONTENTS

LIST OF TABLES

LIST OF FIGURES

LIST OF FIGURES (CONT'D)

LIST OF FIGURES (CONT'D)

LIST OF FIGURES (CONT'D)

LIST OF FIGURES (CONT'D)

NOMENCLATURE

Symbols are defined where they first appear in the text. Those which appear frequently are listed below for reference.

D	energy dissipated through inelastic deformation
E	energy input
K	kinetic energy
L	duration of earthquake
L	energy dissipated in viscous damping
N	number of stories
Q	resistance force
Q_y	yield strength
T	undamped natural period
U	strain energy
V	shear resistance
V_y	yield shear strength
c	coefficient of viscous damping
g	acceleration due to gravity
h	time interval
i	index, floor, or story
k	stiffness
m	mass
q	resistance force per unit mass
q_y	yield level
r	ratio of base yield shear strength to total weight of building

t	time
x	lateral displacement relative to the ground
x_p	total plastic displacement
x_r	residual displacement
x_y	limiting elastic displacement
y	ground displacement
Δ	forward difference
β	fraction of critical damping
ζ	ratio of stiffness in the inelastic region to stiffness in the elastic region
ξ	story deflection
ξ_y	limiting elastic story deflection
τ	time parameter of integration
$\lvert\ \rvert$	absolute value

CHAPTER I

INTRODUCTION

Linear dynamic analysis of the response of buildings to earthquake indicates that buildings subjected to strong-motion earthquakes, even if heavily damped, will experience lateral loads considerably larger than those specified by the current building codes. This is especially true for buildings of small natural period. Yet, the history of earthquake damage shows that buildings designed for lateral loads lower than those prescribed by codes have withstood major earthquakes while undergoing distortions causing cracking of concrete or masonry walls. The uncalculated reserve strength of the structural and nonstructural elements may not be sufficient by itself to explain the relatively small damage.

Energy dissipation has been recognized by engineers as an important factor in explaining the observed behavior of structures during strong-motion earthquakes. For low distortion values, energy dissipated in the nonstructural elements may be more important than energy dissipated in the structural elements through inelastic deformation in protecting the traditional type of building (steel-frame with masonry or concrete walls). With the present architectural trend towards lighter and lighter buildings and the use of the modern type of fenestration, the ductile properties of the structural elements become increasingly important until the energy dissipated in the structural elements through inelastic deformation becomes the predominant component of the total dissipated energy.

Current building codes are based largely on results obtained from linear dynamic analysis. Yet the seismic lateral loads recommended

for design purposes are numerically much lower than those calculated analytically. The codes rely upon the energy-absorbing properties of the structural and nonstructural elements, although this is not stated explicitly. But the codes make no distinction between lightly and heavily damped buildings, and also (with the exception of the proposal of the Structural Engineers Association of California) do not take into account the ductile properties of the structural elements.

The history of earthquake damage, together with the experimental work of several investigators on hysteretic properties of structural materials,[1-3] suggest that an approach incorporating energy dissipated through inelastic deformation may be advantageous for the design of earthquake-resistant buildings. This study is concerned with the behavior of buildings with hysteretic load-deflection relations during earthquakes.

Recent investigations on the inelastic response of structures to earthquake motion comprise, among others:

(1) an analysis by R. Tanabashi,[4] applicable to multi-degree-of-freedom systems for several types of pulse series representing idealized earthquake motion;

(2) a detailed analysis by G. V. Berg,[5] applicable to multi-degree-of-freedom systems for actual earthquake accelerograms;

(3) a study by G. N. Bycroft, M. J. Murphy, and K. J. Brown,[6] giving inelastic results of an electric analog (simulating simple damped structures) for an actual earthquake accelerogram;

(4) a study by R. M. Sheth,[7] investigating the effect of inelastic action on the response of simple structures for actual earthquake accelerograms by means of a high-speed digital computer; and

(5) a study by J. Penzien, dealing with the dynamic response of simple[8] and multi-story[9] elasto-plastic structures for an actual earthquake accelerogram by means of a high-speed digital computer.

Simplified design procedures based upon energy absorption through inelastic deformation comprise:

(1) Housner's limit design,[10,11] according to which a building can be designed for a seismic lateral load lower than that calculated from linear dynamic analysis, provided the structural elements of the building have the capacity to dissipate an adequate amount of energy through inelastic deformation; and

(2) Blume's reserve energy technique,[12,13] which attempts to reconcile the seismic coefficients stipulated by current building codes with those calculated from linear dynamic analysis.

The purpose of this study is to analyze the effect of energy absorption through inelastic deformation on the behavior of buildings during earthquakes, in the hope that ultimately earthquake-resistant design procedures will be improved by making use of inelastic dynamic analysis.

All the investigations have been carried out with the aid of a high-speed digital computer using the accelerograms obtained from the four strongest U.S. earthquakes recorded to date.

The study comprises:

(1) the translation of the accelerogram records, furnished by the U.S. Coast and Geodetic Survey, into punched-card accelerograms to be used as input data by the computer (Chapter II);

(2) a review of linear dynamic analysis and its deficiency when applied to strong-motion earthquake-resistant design (a brief account of the velocity spectrum technique is given and the importance of inelastic action is shown) (Chapter III);

(3) the evaluation and interpretation of deflection spectra showing the effect of elasto-plastic action on lateral deflections of simple (one-story) buildings, followed by an investigation of the residual lateral deflections at the end of the earthquake (Chapter IV);

(4) the evaluation and interpretation of energy input spectra showing the effect of elasto-plastic action on the energy imparted to simple buildings by strong-motion earthquakes (Chapter V);

(5) an analysis of the effect of elasto-plastic action in reducing the seismic lateral loads (Chapter VI);

(6) an investigation of the behavior of simple buildings with bilinear (elastic-strain-hardening) hysteresis during strong-motion earthquakes (Chapter VII); and

(7) the extension of the above investigations to four-story idealized shear buildings (Chapter VIII).

CHAPTER II

ACCELEROGRAMS OF STRONG-MOTION EARTHQUAKES

The strongest U.S. earthquakes for which accelerograms have been recorded to date are the following:

El Centro, California,	December 30, 1934
El Centro, California,	May 18, 1940
Olympia, Washington,	April 13, 1949
Taft, California,	July 21, 1952

The accelerogram records consisting of the three components of motion for each of the above earthquakes were furnished by the U.S. Coast and Geodetic Survey. Figure 1 shows a typical accelerogram record.

Each accelerogram was approximated quite closely by a series of straight-line segments. As there are no indications on an accelerogram record from which the true base line (the zero axis) can be established, a temporary base line, usually the reference line shown in the records, was adopted. Then the time-acceleration coordinates corresponding to the intersection point of every two successive line segments were scaled to a convenient scale and punched on IBM cards. The coordinates of seven points were punched on every card, plus an index number so that the machine could check the card sequence and identify the earthquake component.

The number of points required to describe the significant part, around 30 seconds, of an earthquake component accelerogram varied from 380 to 710. It was noted that, for all four earthquakes, the number of

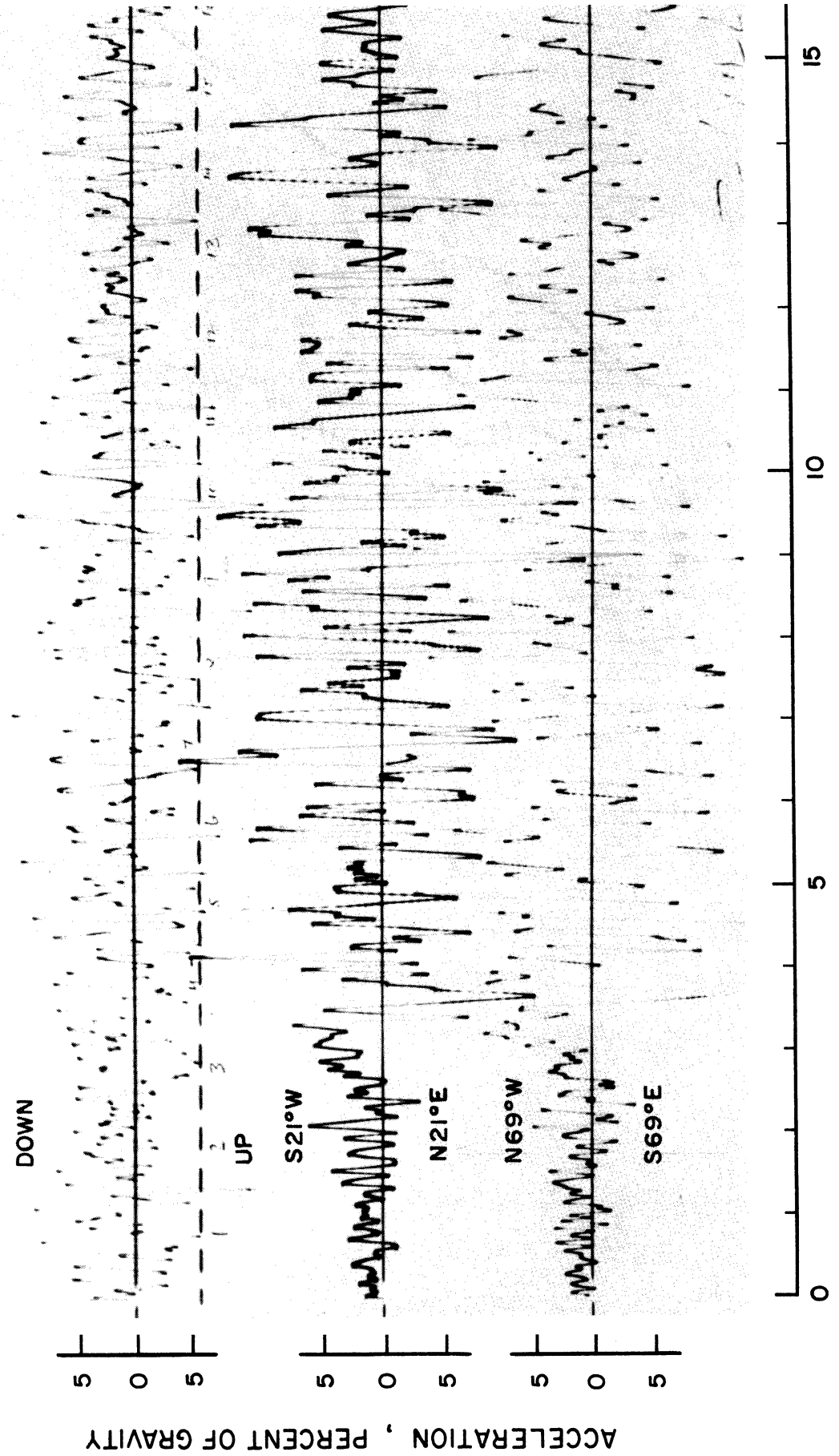

Figure 1. Accelerograms, Taft, California, Earthquake of July 21, 1952. Components: Vertical, S21°W, N69°W.

points required to describe the accelerogram corresponding to the vertical component was larger than the number of points required by the accelerogram of either horizontal component.

At first, it was expected that reasonable ground velocity and ground displacement curves could be obtained upon integration of the accelerograms, if the latter were modified by referring the acceleration ordinates to a new base line parallel to the temporary base line and located so that, with zero initial ground velocity and zero initial ground displacement, the terminal ground velocity would be zero.

To modify the accelerograms, the computer was first instructed to calculate the terminal ground velocity by integrating numerically the straight-line-segmented accelerogram, that is,

$$\dot{y}(L) = \frac{1}{2} \sum_{i=1}^{N-1} (\ddot{y}_i + \ddot{y}_{i+1})(t_{i+1} - t_i) ,$$

in which y is the ground displacement, dots define differentiation with respect to time, L is the time duration of the accelerogram, t is the time corresponding to the ground acceleration ordinate, and N is the number of points which describe the accelerogram.

Then, to reduce the terminal ground velocity to zero, the computer was further instructed to move the temporary base line by an amount equal to $-(\dot{y}(L)/L)$ and in a direction parallel to itself. In so doing the computer referred the ground acceleration ordinates to the new base line. It was then instructed to multiply the time-acceleration coordinates by the appropriate scale factors and punch out the coordinates of four points per card, plus a card sequence number, and an identification number identifying the earthquake component.

Double integration of the straight-line-segmented accelerogram was performed numerically by the computer in accordance with the equations given below:

$$\dot{y}_{i+1} = \dot{y}_i + \frac{t_{i+1} - t_i}{2} (\ddot{y}_i + \ddot{y}_{i+1})$$

and

$$y_{i+1} = y_i + (t_{i+1} - t_i)\dot{y}_i + \frac{(t_{i+1} - t_i)^2}{6} (2\ddot{y}_i + \ddot{y}_{i+1}) .$$

This generated curves showing high ground displacements and notably high permanent ground displacements corresponding to the vertical earthquake components, going up to 135 inches. Such high ground displacements did not actually occur. To obtain more reasonable results, it was decided to modify the accelerogram records further. The curves obtained from the first modification will be referred to as preliminary curves.

With the purpose of reducing the ground displacements throughout the earthquake duration, it was decided to fit to the preliminary ground-displacement curve a third-order polynomial, $a_o + a_1 t + a_2 t^2 + a_3 t^3$,

make $\int_o^L [y(t) - (a_o + a_1 t + a_2 t^2 + a_3 t^3)]^2 \, dt$ a minimum (best fitting in the sense of least squares), and let the modified ground motion read as follows:

$$y^*(t) = y(t) - a_o - a_1 t - a_2 t^2 - a_3 t^3 \qquad y^*(0) = - a_o$$

$$\dot{y}^*(t) = \dot{y}(t) - a_1 - 2a_2 t - 3a_3 t^2 \qquad \dot{y}^*(0) = - a_1$$

$$\ddot{y}^*(t) = \ddot{y}(t) - 2a_2 - 6a_3 t \qquad \ddot{y}^*(0) = \ddot{y}(0) - 2a_2$$

In the above equations, y is the preliminary ground displacement and y^* is the ground displacement as last modified. A third-order polynomial

was chosen because the shape of most of the preliminary ground displacement curves was approximately that of a third-order polynomial. The coefficients a_i ($i = 0, 1, 2, 3$) were evaluated by the computer.

Figure 2 shows the preliminary and last modified ground-velocity and ground-displacement curves for the vertical component of the El Centro, California, earthquake of May, 1940.

The last modification is analogous to assuming that the true base line has the ordinates $(2a_2 + 6a_3t)$ from the preliminary base line; by this, the originally adopted temporary line is given a further shifting, this time accompanied by a rotation. This modification also introduces nonzero initial conditions. One cannot claim zero initial conditions since the accelerometer has to be triggered by a ground motion before it starts recording. Finally, this modification yields a nonzero terminal ground velocity, which condition is possible since only the first 30 seconds of the accelerogram record were used.

It is interesting to note that this last modification generated maximum offsets from the preliminary base line ranging from 0.006 in. to 0.024 in., which, multiplied by their respective acceleration scales, correspond to 0.001 g and 0.003 g, g being the acceleration due to gravity.

Response calculations later showed that accelerogram modifications of the type and order of magnitude described above generally had no significant effect upon the response of structures.

To verify whether the approximation of an accelerogram record by a series of straight-line segments was sufficiently accurate, the

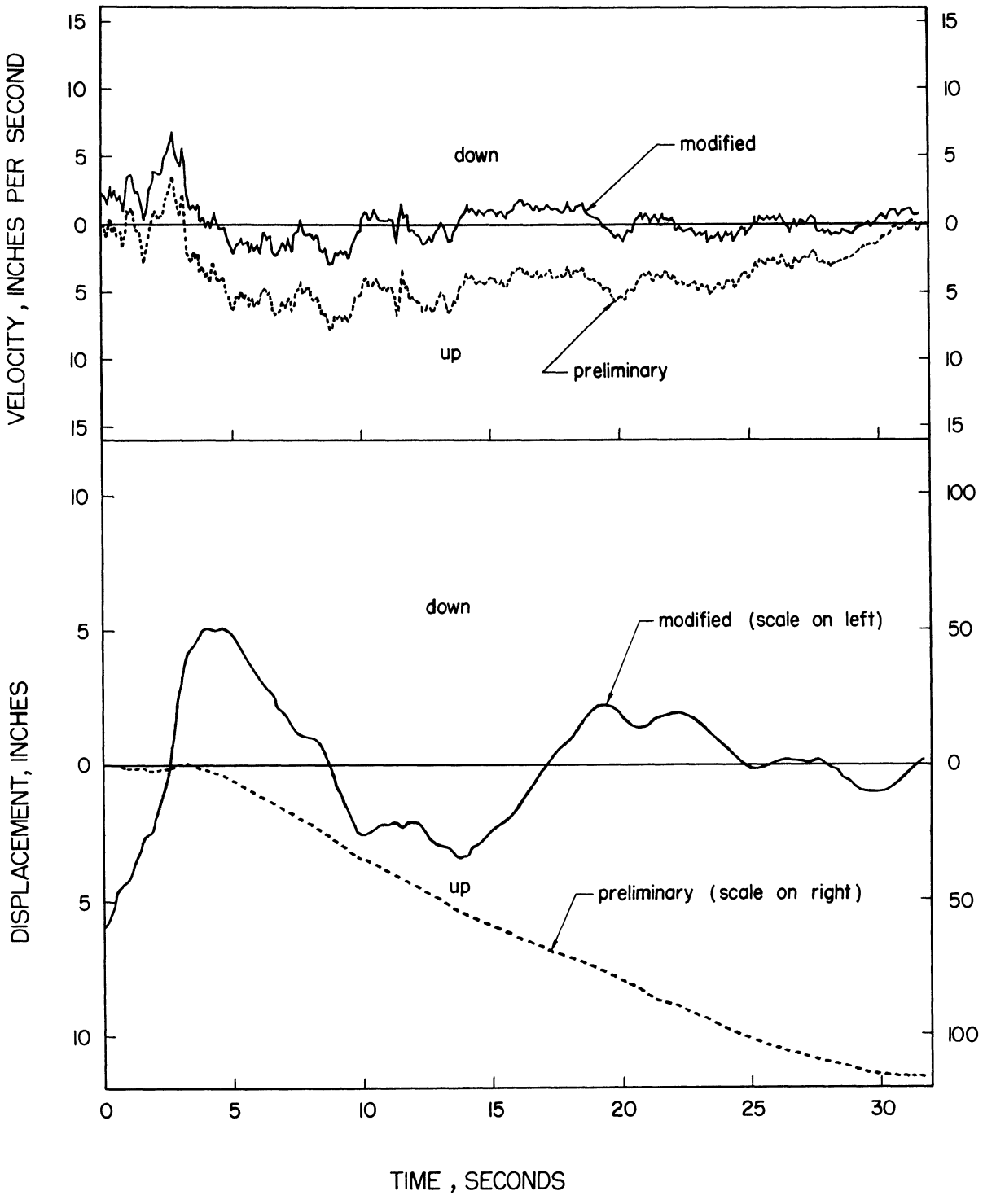

Figure 2. Ground Velocity (upper), Ground Displacement (lower), El Centro, California, Earthquake of May 18, 1940. Vertical Component.

response spectra of linear systems were calculated from the punched-card accelerograms and the results were compared with those which had been obtained by means of an electric analog computer.[14] The comparison showed close agreement.

Although there may be other ways to adjust the accelerogram records, the above procedure was adopted for all accelerograms because it generated acceptable ground-velocity and ground-displacement curves. Also, the curves thus obtained for the El Centro, California, earthquake of May, 1940, were compared with the curves published[15] for that earthquake and were found to be reasonably similar.

CHAPTER III

REVIEW OF LINEAR DYNAMIC ANALYSIS; ITS DEFICIENCY WHEN APPLIED TO EARTHQUAKE-RESISTANT DESIGN

If we assume (1) that a simple (one-story) building frame with foundations rigidly built upon a firm ground can be represented by a linear damped oscillating system, consisting of one mass, spring, and a viscous damper, as shown in Figure 3; (2) that the spring and damper are weightless; and (3) that all motion takes place in the direction in which the spring and damper act, then, when the system is subjected to an earthquake ground motion, the equation of motion will read as follows:

$$m(\ddot{x}+\ddot{y}) + c\dot{x} + kx = 0 \tag{3.1}$$

or

$$m\ddot{x} + c\dot{x} + kx = -m\ddot{y} \tag{3.2}$$

where

m	is the mass,	$(FL^{-1}T^2)$*
c	is the coefficient of viscous damping,	$(FL^{-1}T)$
k	is the spring constant (stiffness),	(FL^{-1})
x	is the displacement of the mass relative to the ground, a function of time,	(L)
y	is the ground displacement, a known function of time,	(L)

and dots define differentiation with respect to time.

---

* Dimensions are shown in units of force, length, and time.

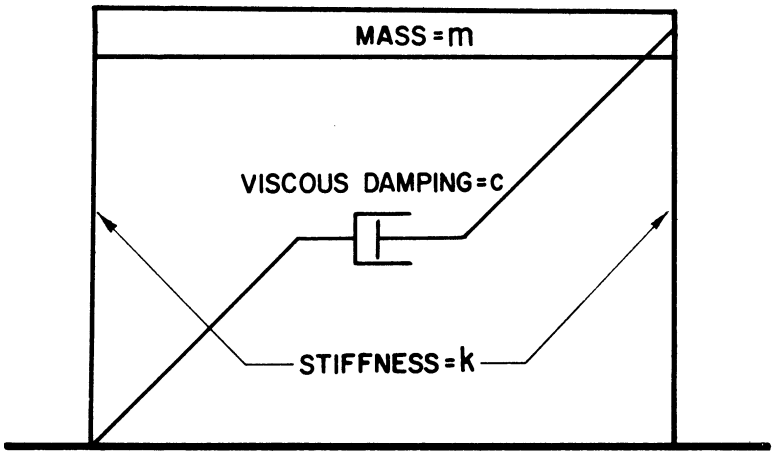

SIMPLE DAMPED ELASTIC FRAME

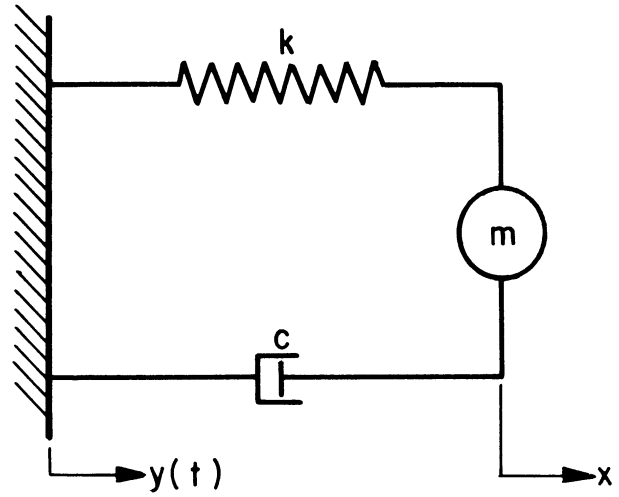

EQUIVALENT DAMPED SPRING AND MASS SYSTEM

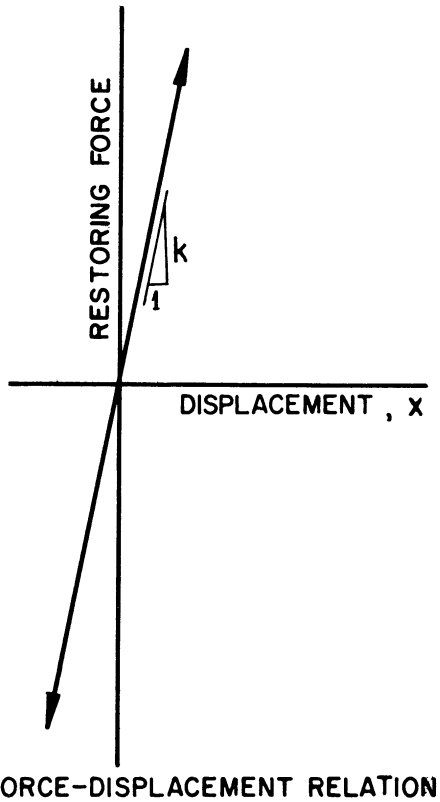

FORCE-DISPLACEMENT RELATION

Figure 3. Simple Building Frame Represented by a Linear Damped Oscillating System.

If we define

$$\left.\begin{aligned} T &= 2\pi\sqrt{\frac{m}{k}} \;=\; \text{the undamped natural period} \qquad (T) \\ \text{and} \qquad & \\ \beta &= \frac{Tc}{4\pi m} \;=\; \text{the fraction of critical damping} \end{aligned}\right\} , \quad (3.3)$$

then, in view of Equations (3.2) and (3.3),

$$\ddot{x} + \frac{4\pi}{T}\beta\dot{x} + \left(\frac{2\pi}{T}\right)^2 x = -\ddot{y} \quad . \qquad (3.4)$$

Mathematically, the solution to Equation (3.4), for zero initial conditions, is given by Duhamel's integral as follows:

$$x = -\frac{T}{2\pi\sqrt{1-\beta^2}} \int_0^t \ddot{y}(\tau) e^{-\frac{2\pi}{T}\beta(t-\tau)} \sin\frac{2\pi}{T}\sqrt{1-\beta^2}\,(t-\tau)\,d\tau \quad , \qquad (3.5)$$

where

t is the time

and

τ is the variable of integration.

For the encountered values of damping, $\beta \leq 0.20$, the term $\sqrt{1-\beta^2}$ can be considered to be very nearly equal to 1. Hence Equation (3.5) can be rewritten as follows:

$$x \approx -\frac{T}{2\pi} \int_0^t \ddot{y}(\tau) e^{-\frac{2\pi}{T}\beta(t-\tau)} \sin\frac{2\pi}{T}(t-\tau)\,d\tau \quad . \qquad (3.6)$$

The maximum absolute value of the integral in Equation (3.6) is designated by S_v,[16] where the subscript v is used because the physical dimensions of the integral are those of velocity. For small damping values like the encountered ones, S_v is practically equal to the maximum absolute value of the velocity of the system relative to the ground.

Hence

$$S_V = \left| \int_0^t \ddot{y}(\tau) e^{-\frac{2\pi}{T}\beta(t-\tau)} \sin \frac{2\pi}{T}(t-\tau) d\tau \right|_{max} \qquad (3.7)$$

$\approx$ maximum absolute value of velocity relative to the ground

and

$$\left| \dot{x} \right|_{max} \approx \frac{T}{2\pi} S_V \ . \qquad (3.8)$$

If a number of values of S_V are calculated for different natural periods and different values of damping, the resulting family of curves, plotted as S_V against natural period for fixed values of damping, constitute the velocity response spectrum[16] which is characteristic of the considered earthquake.

Typical velocity response spectra are shown in Figure 4. These are plots of $|\dot{x}|_{max}$, computed from the punched-card accelerograms by integrating numerically the differential equation of motion, that is, Equation (3.4).

Response spectra for most of the strong-motion earthquakes of record have been computed by means of an electric analog computer at the Earthquake Research Laboratory of the California Institute of Technology.[14]

S_V has a simple relation with the maximum strain energy developed in the structure during the earthquake action. If U designates the maximum strain energy per unit mass, then

$$U = \frac{1}{m}\left\{\frac{1}{2}[(k)|x|_{max}|x|_{max}]\right\} \ . \qquad (3.9)$$

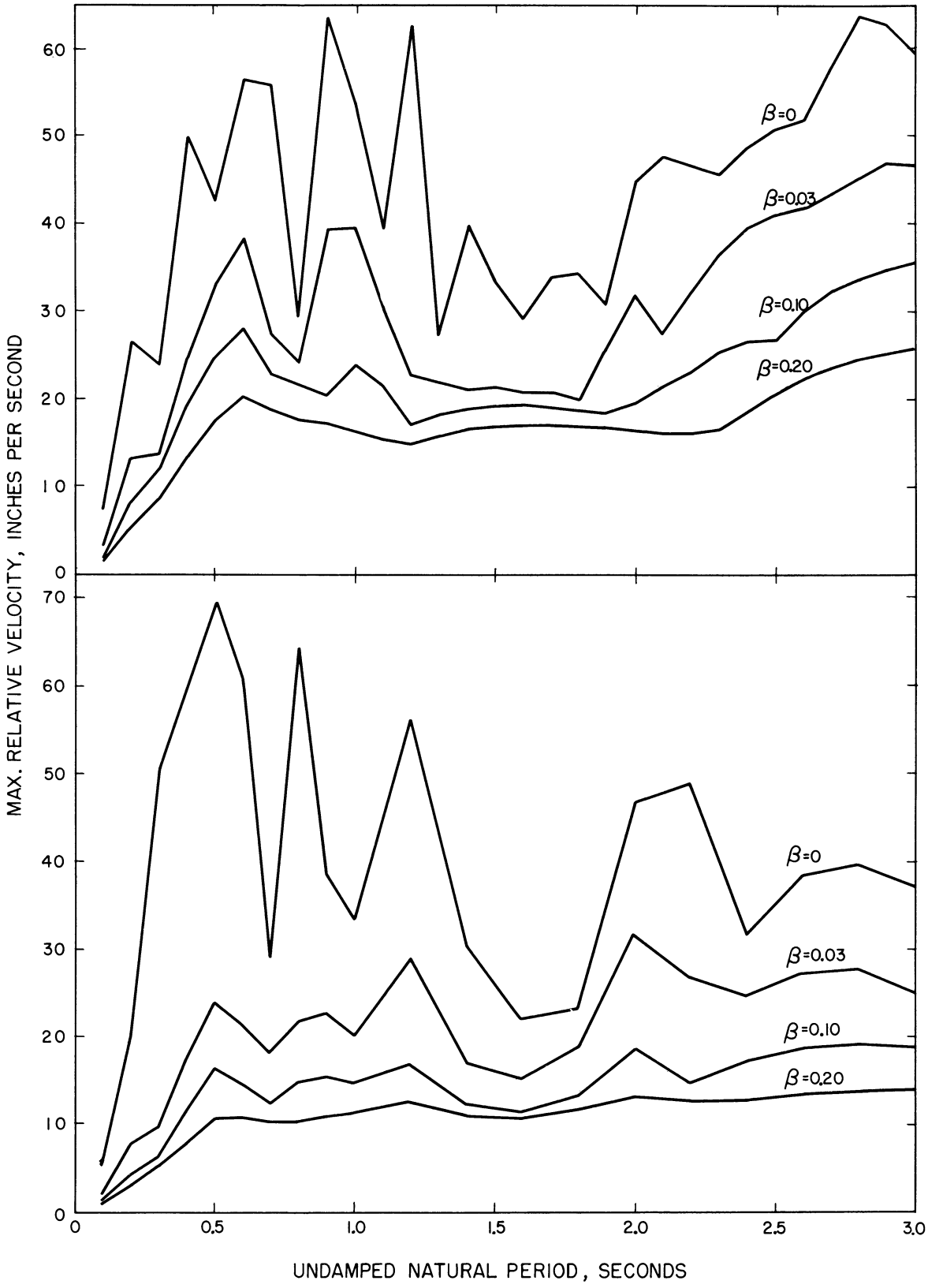

Figure 4. Velocity Spectra, El Centro, California, Earthquake of May 18, 1940. Components: N-S (upper), E-W (lower).

In view of Equations (3.3) and (3.8), Equation (3.9) becomes:

$$U = \frac{1}{2} S_v^2 \ . \tag{3.10}$$

From $|x|_{max}$, the earthquake maximum base shear V_B can be determined as follows:

$$V_B = k|x|_{max} \ . \tag{3.11}$$

In the case of a multi-story building frame, for every mode there is an equivalent one-story frame giving the same base shear as the corresponding mode of the multi-story frame. The equivalent one-story frame corresponding to the r-th mode of a multi-story frame has the following properties:

$$\left.\begin{aligned} m_{er} &= \frac{\left[\sum_{i=1}^{N} m_i \phi_{ir}\right]^2}{\sum_{i=1}^{N} m_i \phi_{ir}^2} \\ k_{er} &= \left(\frac{2\pi}{T_r}\right)^2 m_{er} \\ V_{Br} &= k_{er}|x_{er}|_{max} \end{aligned}\right\} \ , \tag{3.12}$$

where

m_{er} is the mass of the equivalent one-story frame giving the same base shear as the r-th mode of the multi-story frame, $(FL^{-1}T^2)$

m_i is the mass at the i-th floor level of the multi-story frame, $(FL^{-1}T^2)$

ϕ_{ir} is the r-th mode displacement of the i-th floor level,

k_{er} is the stiffness of the equivalent one-story frame corresponding to the r-th mode, (FL^{-1})

T_r is the natural period of the r-th mode of the multi-story frame, (T)

V_{Br} is the maximum base shear if the multi-story frame vibrated in the r-th mode, (F)

x_{er} is the displacement of the mass m_{er} relative to the ground. (L)

The vertical distribution of the base shear V_{Br} over the floor levels of the multi-story frame is determined from:

$$F_{ir} = V_{Br} \frac{m_i \phi_{ir}}{\sum_{i=1}^{N} m_i \phi_{ir}} \qquad (i = 1, 2, \ldots, N) , \qquad (3.13)$$

in which F_{ir} is the lateral load applied at the i-th floor level if the frame vibrated in the r-th mode. The derivation of Equations (3.12) and (3.13) is given in Appendix A.

The velocity response spectrum as defined above is concerned with maximum values of velocity acquired by systems of different periods. Since, in general, these velocities do not occur at the same time, the superposing of the individual mode maximum base shears as determined from the response spectrum will yield an approximate (overestimated) total base shear.

It has been suggested[17] that magnifying the maximum response of the first mode by a constant factor to account for the effect of

higher modes is not entirely rational, because the higher modes have a different effect at different heights. Instead, a better estimate can be made if a certain fraction of the maximum response of the second and third modes is added to the maximum response of the first mode.

S_V is related to the seismic lateral load coefficient C in the expression determining the earthquake maximum base shear as follows:

$$V_B = Cmg = k|x|_{max} = k(\frac{T}{2\pi} S_V)$$

or

$$C = (\frac{1}{g})(\frac{k}{m})(\frac{T}{2\pi} S_V) \quad .$$

In view of Equation (3.3), the above equation becomes:

$$C = (\frac{1}{g})(\frac{2\pi}{T} S_V) \quad . \qquad (3.14)$$

For each horizontal component of the four strongest U.S. earthquakes on record, the seismic lateral load coefficients were computed for systems of different natural periods and for different values of damping. The results, plotted against natural period for fixed values of damping, are shown in Figures 5-8.

These figures indicate seismic lateral load coefficients as high as 0.55 for buildings represented by linear dynamic systems, even if damped as heavily as 0.20 of critical damping. Design for such lateral forces may not be practicable because of the high cost entailed. On the other hand, after an intensive study of the history of earthquake damage, it has been reported that buildings designed for considerably lower seismic coefficients and subjected to major earthquakes

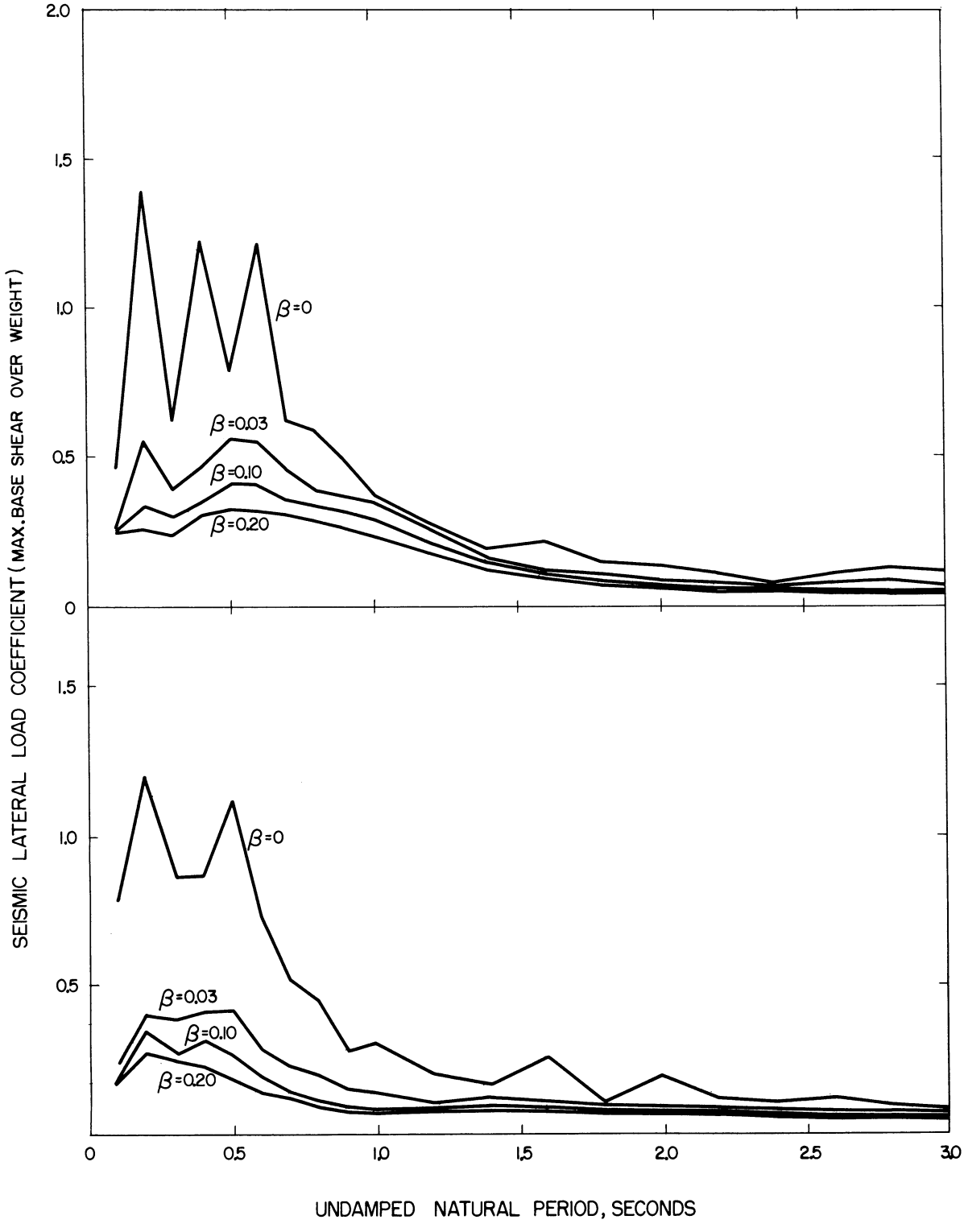

Figure 5. Seismic Lateral Load Coefficients, El Centro, California, Earthquake of December 30, 1934. Components: N-S (upper), E-W (lower).

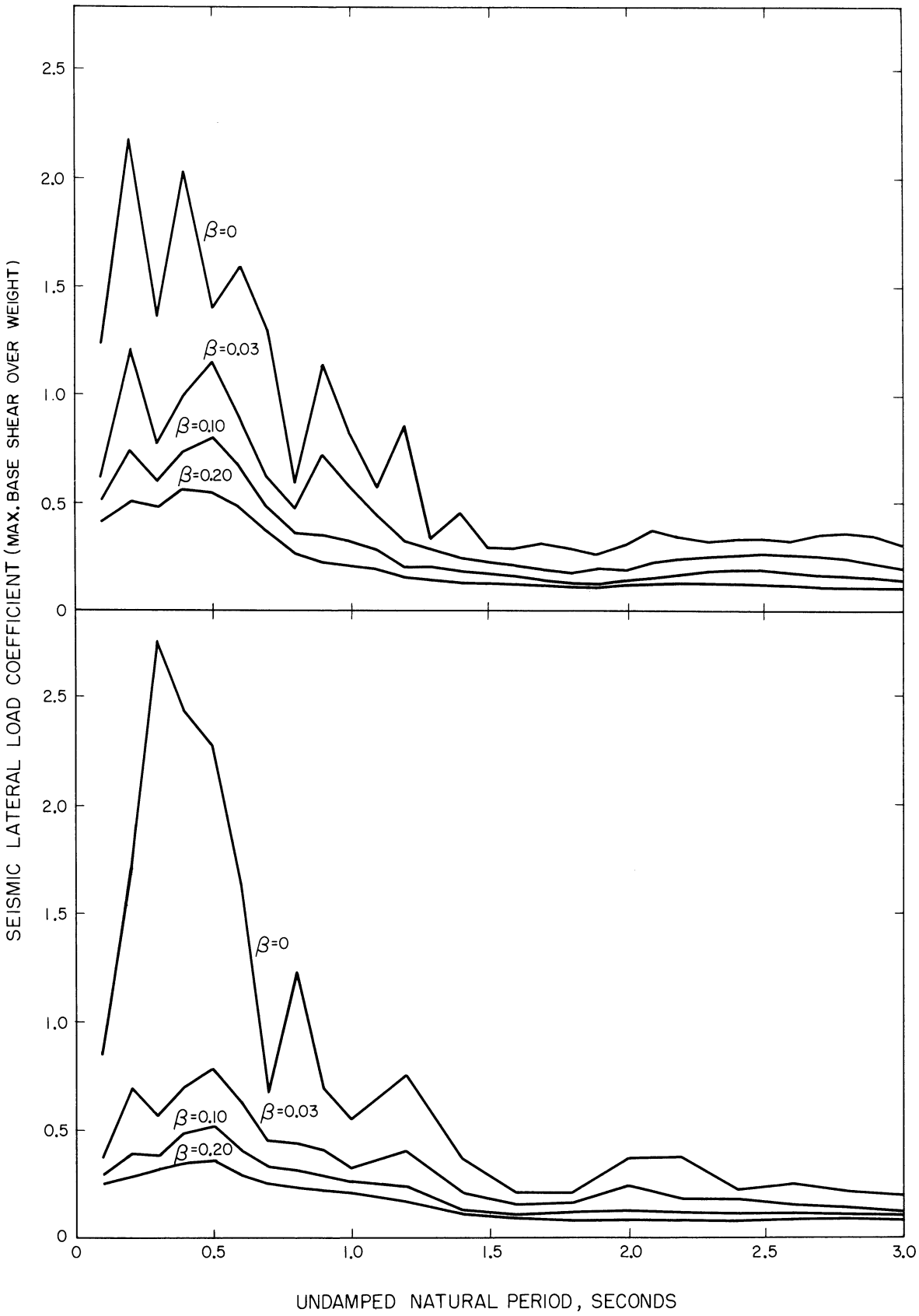

Figure 6. Seismic Lateral Load Coefficients, El Centro, California, Earthquake of May 18, 1940. Components: N-S (upper), E-W (lower).

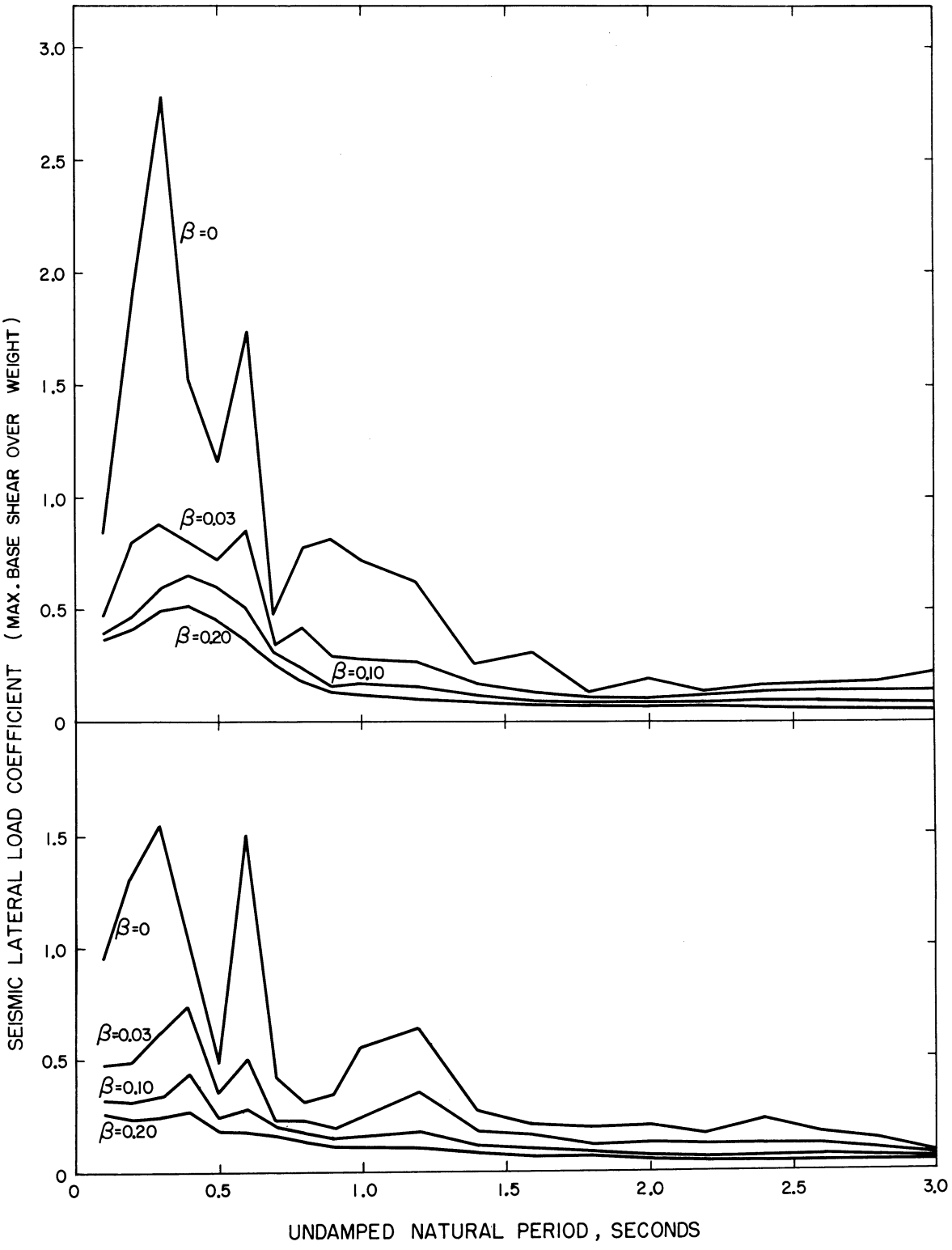

Figure 7. Seismic Lateral Load Coefficients, Olympia, Washington, Earthquake of April 13, 1949. Components: N80°E (upper), N10°W (lower).

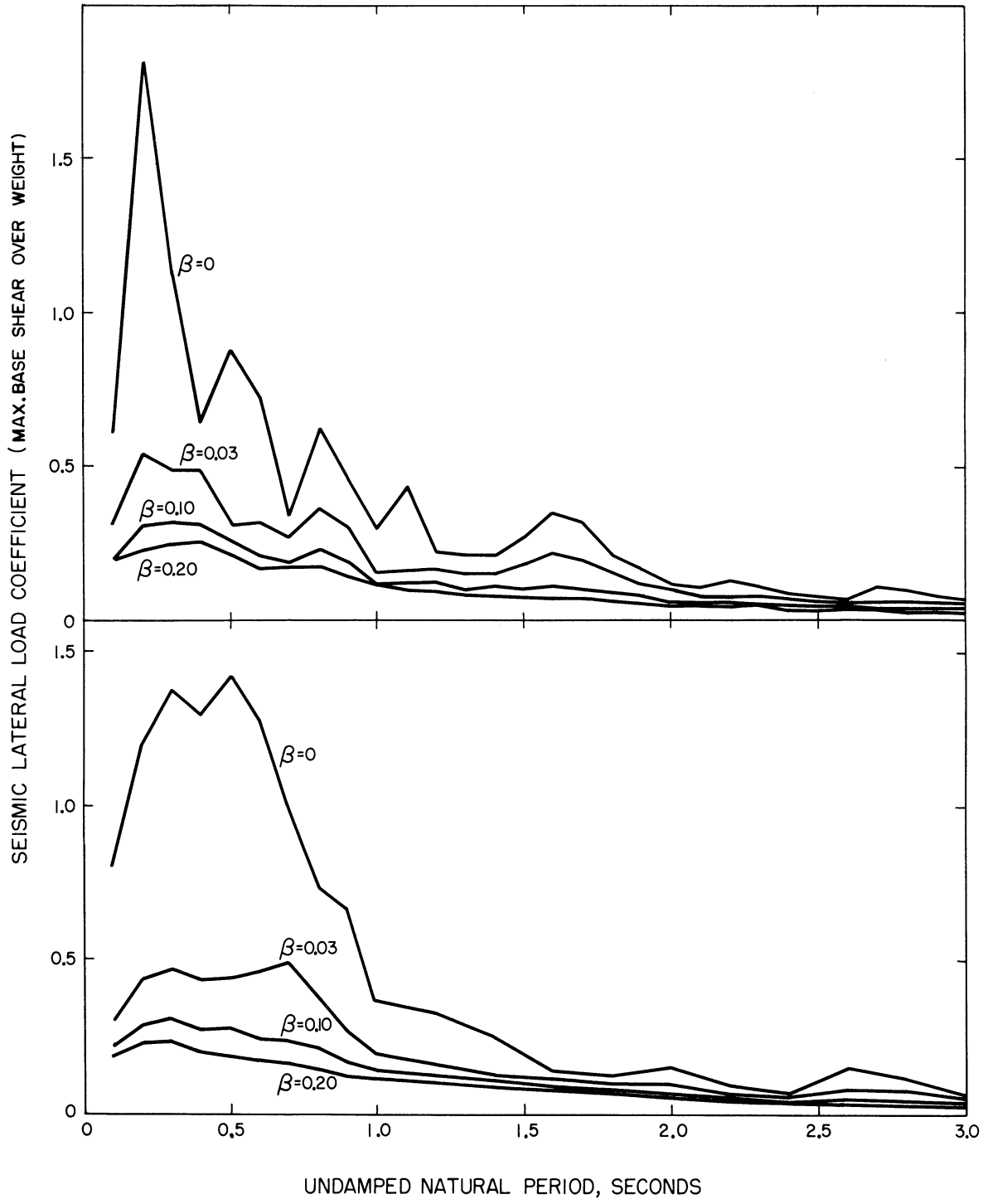

Figure 8. Seismic Lateral Load Coefficients, Taft, California, Earthquake of July 21, 1952. Components: N69°W (upper), S21°W (lower).

did not reveal any structural damage. In such cases, damping alone is not sufficient to account for the absence of damage in the structures. Energy dissipation through inelastic deformation, which is ignored by linear dynamic analysis, is recognized by engineers as an important factor in explaining the observed behavior of structures during strong-motion earthquakes.

CHAPTER IV

EFFECT OF ELASTO-PLASTIC ACTION ON LATERAL DEFLECTIONS OF SIMPLE BUILDINGS SUBJECTED TO EARTHQUAKES

With the present architectural trend towards lighter buildings, in which lightweight materials with slight rigidity replace the traditional masonry or concrete walls, the flexibility of the building becomes an important design factor if the building is to resist earthquake action successfully. Large lateral deflections, besides causing property damage such as plaster cracking, glass breakage, etc., are also a considerable life hazard. The danger of broken glass falling from a tall building is obvious. Moreover, in the case of nonlinear behavior, it could be expected that a building, designed for a seismic lateral load coefficient lower than that indicated by linear dynamic analysis, might become unusable because of the possibility of resulting increased lateral deflections causing large permanent sets, even though the structural elements might still have adequate strength for structural safety. Therefore the following investigations were made:

1. The effect of inelastic action on lateral deflections. The maximum lateral deflections of different buildings, assumed to yield safely, were calculated and compared with the corresponding ones calculated from linear dynamic analysis.
2. The permanent sets. The residual lateral deflections at the end of each earthquake analysis were calculated to determine whether they were within acceptable limits.

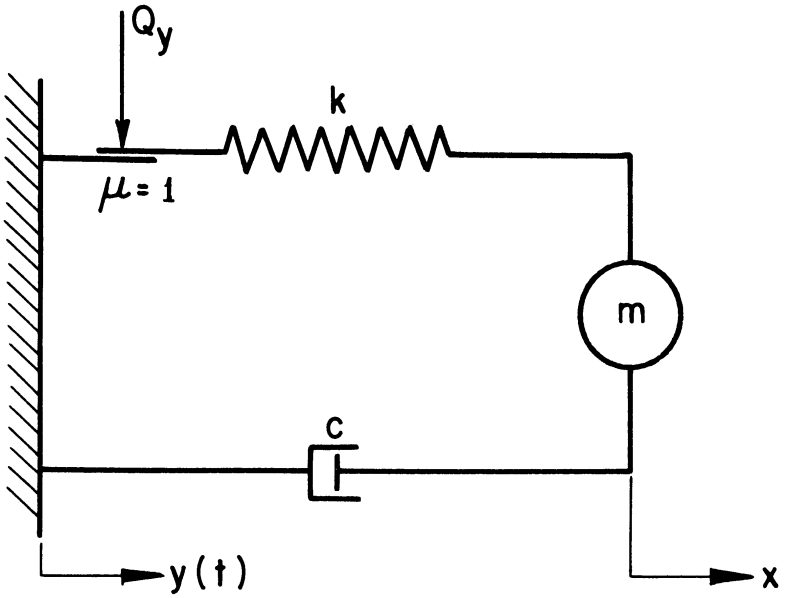

Figure 9. Equivalent Nonlinear Damped Oscillating System.

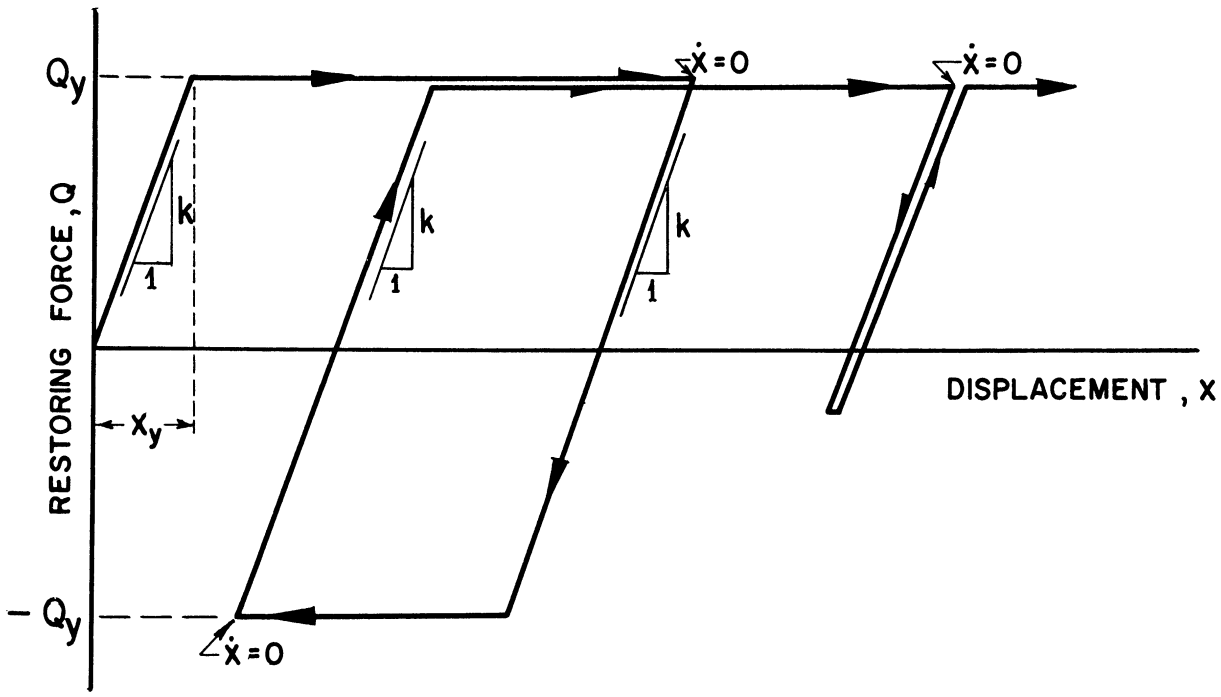

Figure 10. Idealized Force-Displacement Diagram.

To simplify the proceedings, only simple (one-story) buildings were considered. The study was based upon the following three assumptions:

1. The structural elements have a large capacity for energy absorption through inelastic deformation, enabling buildings rigidly built upon firm ground to yield safely.
2. The building frame can be represented by an equivalent nonlinear damped oscillating system as shown in Figure 9, consisting of one mass, a spring, a viscous damper, and a friction plate with a coefficient of slipping friction μ. The use of a simplified dynamic model reduces the complexity of the building frame to the point where computations are practicable.
3. Reverse loadings of complete buildings produce load-deflection curves mirroring the curves for the first loading and unloading cycle[18] (neglecting softened features and a decaying ultimate strength). This behavior was represented by an idealized force-displacement curve of the elasto-plastic type, chosen for its simplicity.

Assuming that the load-deflection characteristics of a complete building can be described by an elasto-plastic curve, as shown in Figure 10, then the spring force-displacement relations for the equivalent system will read as follows:

$$\left.\begin{aligned} \dot{Q} = k\dot{x} \quad &\text{if} \quad -Q_y < Q < Q_y \\ &\text{or if} \quad Q = Q_y \quad \text{and} \quad \dot{x} < 0 \\ &\text{or if} \quad Q = -Q_y \quad \text{and} \quad \dot{x} > 0 \\ \dot{Q} = 0 \quad &\text{if} \quad Q = Q_y \quad \text{and} \quad \dot{x} \geq 0 \\ &\text{or if} \quad Q = -Q_y \quad \text{and} \quad \dot{x} \leq 0 \end{aligned}\right\} , \qquad (4.1)$$

where

Q is the spring force, a function of time, (F)

Q_y is the yield strength of the spring, (F)

k is the spring constant (stiffness), (FL^{-1})

x is the displacement of the mass relative to the ground, a function of time, (L)

and dots define differentiation with respect to time.

Designating the slip of the friction plate by ψ, a function of time, then, according to Figures 9 and 10,

$$\left.\begin{array}{lll} \dot{\psi} = 0 & \text{if} & -Q_y < Q < Q_y \\ \text{or} & \text{if} & Q = Q_y \quad \text{and} \quad \dot{x} \leq 0 \\ \text{or} & \text{if} & Q = -Q_y \quad \text{and} \quad \dot{x} \geq 0 \end{array}\right\} . \qquad (4.2)$$

If it is assumed that the spring, damper, and friction plate of the equivalent oscillating system are weightless and that all motion takes place in the direction in which the spring and damper act, then, when the system is subjected to an earthquake ground motion, the equation of motion will read as follows:

$$m(\ddot{x} + \ddot{y}) + c\dot{x} + Q = 0 \qquad (4.3)$$

or

$$m\ddot{x} + c\dot{x} + Q = -m\ddot{y} \quad . \qquad (4.4)$$

From the second definition of Equation (3.3),

$$c = \frac{4\pi}{T} m \beta \ .$$

Hence Equation (4.4) can be rewritten as follows:

$$m\ddot{x} + \frac{4\pi}{T} m \beta \dot{x} + Q = -m\ddot{y} \qquad (4.5)$$

or

$$\ddot{x} + \frac{4\pi}{T}\beta\dot{x} + \frac{Q}{m} = -\ddot{y} \quad . \tag{4.6}$$

Define

$$\left.\begin{aligned} q &= \frac{Q}{m} \qquad (LT^{-2}) \\ \text{and} \\ q_y &= \frac{Q_y}{m} = \text{the yield level} \qquad (LT^{-2}) \end{aligned}\right\} \quad . \tag{4.7}$$

The yield level q_y is the acceleration of the system that will just cause the spring force to attain its yield strength Q_y.

Based on Equations (4.6) and (4.7), the differential equation of motion, reduced to a unit mass basis, will read as follows:

$$\ddot{x} + \frac{4\pi}{T}\beta\dot{x} + q = -\ddot{y} \quad . \tag{4.8}$$

In view of Equation (4.7) and the first definition of Equation (3.3) which gives

$$\frac{k}{m} = \left(\frac{2\pi}{T}\right)^2 \quad ,$$

the spring force-displacement relations given by Equation (4.1), reduced to a unit mass basis, become:

$$\left.\begin{aligned} \dot{q} = \left(\frac{2\pi}{T}\right)^2 \dot{x} \qquad & \text{if} \quad -q_y < q < q_y \\ \text{or} \quad & \text{if} \quad q = q_y \quad \text{and} \quad \dot{x} < 0 \\ \text{or} \quad & \text{if} \quad q = -q_y \quad \text{and} \quad \dot{x} > 0 \\ \dot{q} = 0 \qquad & \text{if} \quad q = q_y \quad \text{and} \quad \dot{x} \geq 0 \\ \text{or} \quad & \text{if} \quad q = -q_y \quad \text{and} \quad \dot{x} \leq 0 \end{aligned}\right\} \quad . \tag{4.9}$$

Equation (4.8) was integrated numerically by the computer for each earthquake analysis for specified values of yield level, damping, and natural period. Since the maximum response was of primary concern rather than the complete time history of the response, the computer was instructed to evaluate the response at small time intervals and record the maximum response. The Runge-Kutta third-order procedure,[5][19] a single-step method well suited to high-speed digital computers, was used for the numerical integration. This method is advantageous for the study under consideration, because the functions at time $t + h$ (h being a specified time interval) are evaluated from those at time t, which therefore permits one to change the time interval h at any step of the integration, and because it does not require any special starting procedure for the initial steps of the integration. The formulas used in the Runge-Kutta method are given in Appendix B.

To adapt the equation of motion to the Runge-Kutta procedure, the second-order differential equation was replaced by the following two simultaneous first-order differential equations:

$$\left.\begin{aligned} \dot{x} &= v \\ \text{and} \qquad \dot{v} &= \ddot{x} = -\left(\ddot{y} + \frac{4\pi}{T}\beta v + q\right) \end{aligned}\right\} \quad . \tag{4.10}$$

To overcome the difficulty caused by the discontinuity of $\dot{q}$ whenever the system was entering the plastic region, the differential relations of Equation (4.9) were replaced by the following equivalent difference relations:

$$\left.\begin{aligned} \Delta q &= \left(\frac{2\pi}{T}\right)^2 \Delta x \quad \text{if} \quad -q_y \le q + \left(\frac{2\pi}{T}\right)^2 \Delta x \le q_y \\ \Delta q &= q_y - q \quad \text{if} \quad q + \left(\frac{2\pi}{T}\right)^2 \Delta x > q_y \\ \Delta q &= -q_y - q \quad \text{if} \quad q + \left(\frac{2\pi}{T}\right)^2 \Delta x < -q_y \end{aligned}\right\} . \qquad (4.11)$$

An exact solution cannot be claimed when finite differences are introduced in place of differentials. Nevertheless, by making the time interval small enough and by assuming that $\dot{x}$ does not change sign during the interval, a close approximation to the exact solution can be obtained.

A small time interval was also required to insure a sufficient accuracy in the numerical solution of differential equations; in fact, it was specified that the time interval h was not to exceed the twentieth of the natural period of the system considered. However, for the undamped and lightly damped cases, when high yield levels were considered, it was necessary to reduce the above limit considerably to bring the discrepancies resulting from the numerical solution within the range of tolerance.

At every step of the integration, the computer was instructed to calculate the difference between the time at the end of the accelerogram segment involved in that particular step and the time at the beginning of the same step; this difference was then compared to the specified time interval h. Whenever the difference was found smaller than h, it was used as the integration time interval; otherwise, the specified time interval h was used. In the latter case the ground acceleration at time $t + h$ was evaluated from that at time t by linear interpolation between the two adjacent ground accelerations involved in that particular step of the integration.

When the computer had completed an earthquake analysis by advancing step by step through the solution, it was instructed to calculate the magnitude of the permanent set, which is given by:

$$|x_r| = |x(L) - (\frac{T}{2\pi})^2 q(L)| \qquad (4.12)$$

where

x_r is the residual displacement (permanent set) (L)

and

L is the time duration of the accelerogram (around 30 seconds).

Equations (4.10) and (4.12) were solved for each horizontal earthquake component for five yield levels, that is, q_y = 0.01 g, 0.03 g, 0.06 g, 0.12 g and ∞. Infinity represents a yield level high enough so that the same nonlinear damped system can serve as a linear damped system. The low yield levels 0.03 g and 0.01 g were considered for the purpose of finding the extent to which the yield level can be lowered without causing lateral deflections significantly larger than those calculated from completely elastic dynamic analysis. For each yield level, three values of damping, β = 0.03, 0.10, and 0.20, were considered as well as the undamped case. The undamped case served as a comparison basis in investigating the effect of damping. The value 0.03 of critical damping was chosen because it is about as low as is encountered in structures; the values 0.10 and 0.20 of critical damping were chosen because they may correspond to moderately and heavily damped frame buildings, respectively. For the undamped case and for each value of damping, natural periods ranging from 0.10 to 3.0 seconds were considered.

The calculated maximum lateral deflections and permanent sets were plotted against natural periods, for yield levels varying from completely elastic down to 0.01 g and for fixed values of damping ranging from 0 to 0.20 of critical damping. Maximum lateral deflection is plotted in Figures 11-14 and permanent set, in Figures 15-18.

Figures 11-14 permit a comparison of the maximum lateral deflections calculated from elasto-plastic behavior with the corresponding ones calculated from completely elastic behavior. The comparison, at all levels of damping, shows that:

1. The maximum lateral deflections of buildings with a yield level as low as 0.01 g are appreciably increased for all the considered earthquake components, except for those of the Olympia earthquake for which the increase is not as noticeable as for the others.
2. The maximum lateral deflections corresponding to a 0.03 g yield level are, in general, moderately increased.
3. Generally, the yield levels 0.06 g and 0.12 g do not cause any significant increase in the maximum lateral deflections; moreover, they reduce the maximum lateral deflections of a great number of systems.

Contrary to what might have been expected, the above observations indicate that, when subjected to strong-motion earthquake action, simple buildings, designed for seismic lateral load coefficients lower than those indicated by linear dynamic analysis but with yield levels not lower than 0.06 g, will undergo lateral deflections seldom exceeding those calculated from completely elastic behavior, and often lower.

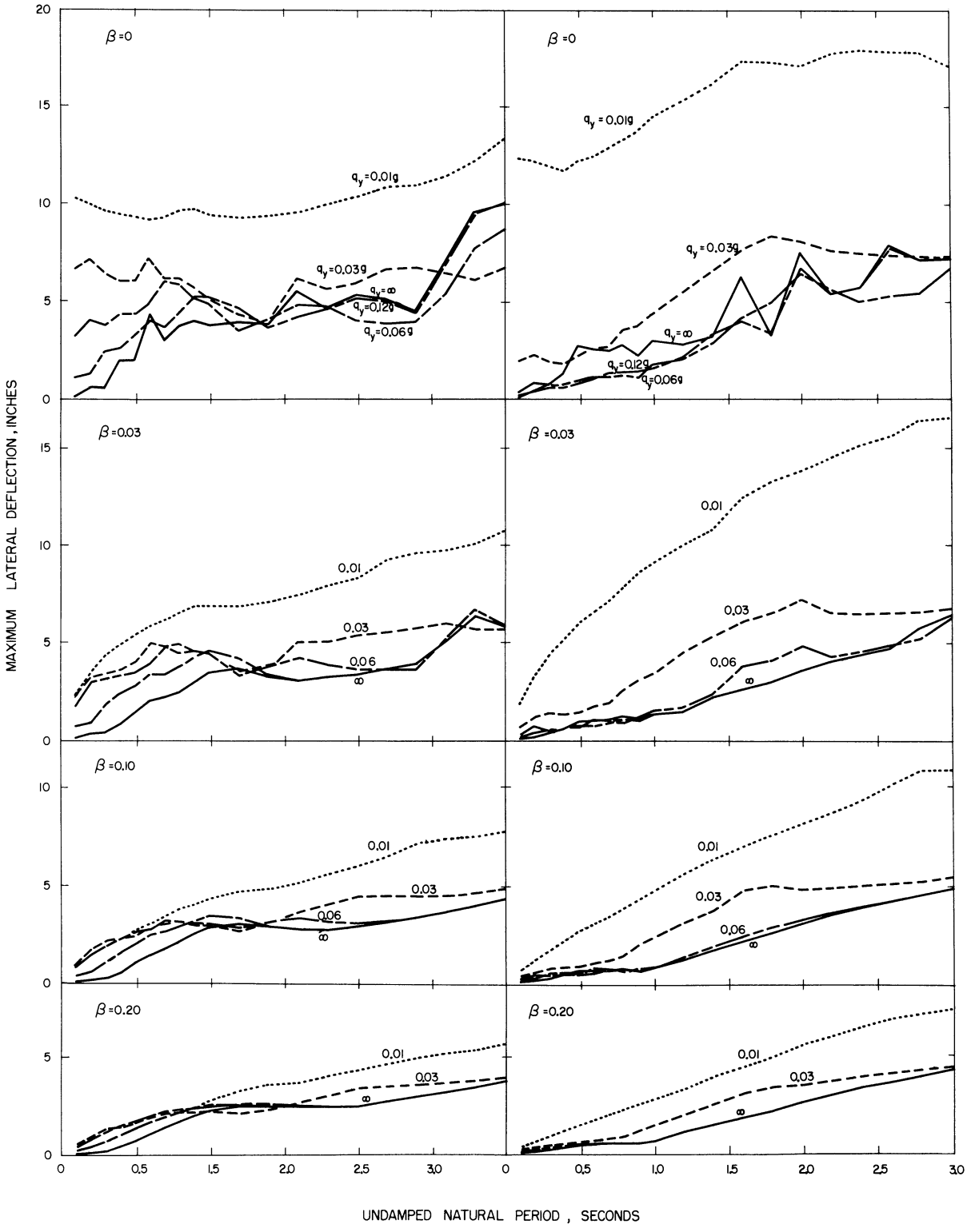

Figure 11. Lateral Deflection Spectra, El Centro, California, Earthquake of December 30, 1934. Components: N-S (left), E-W (right).

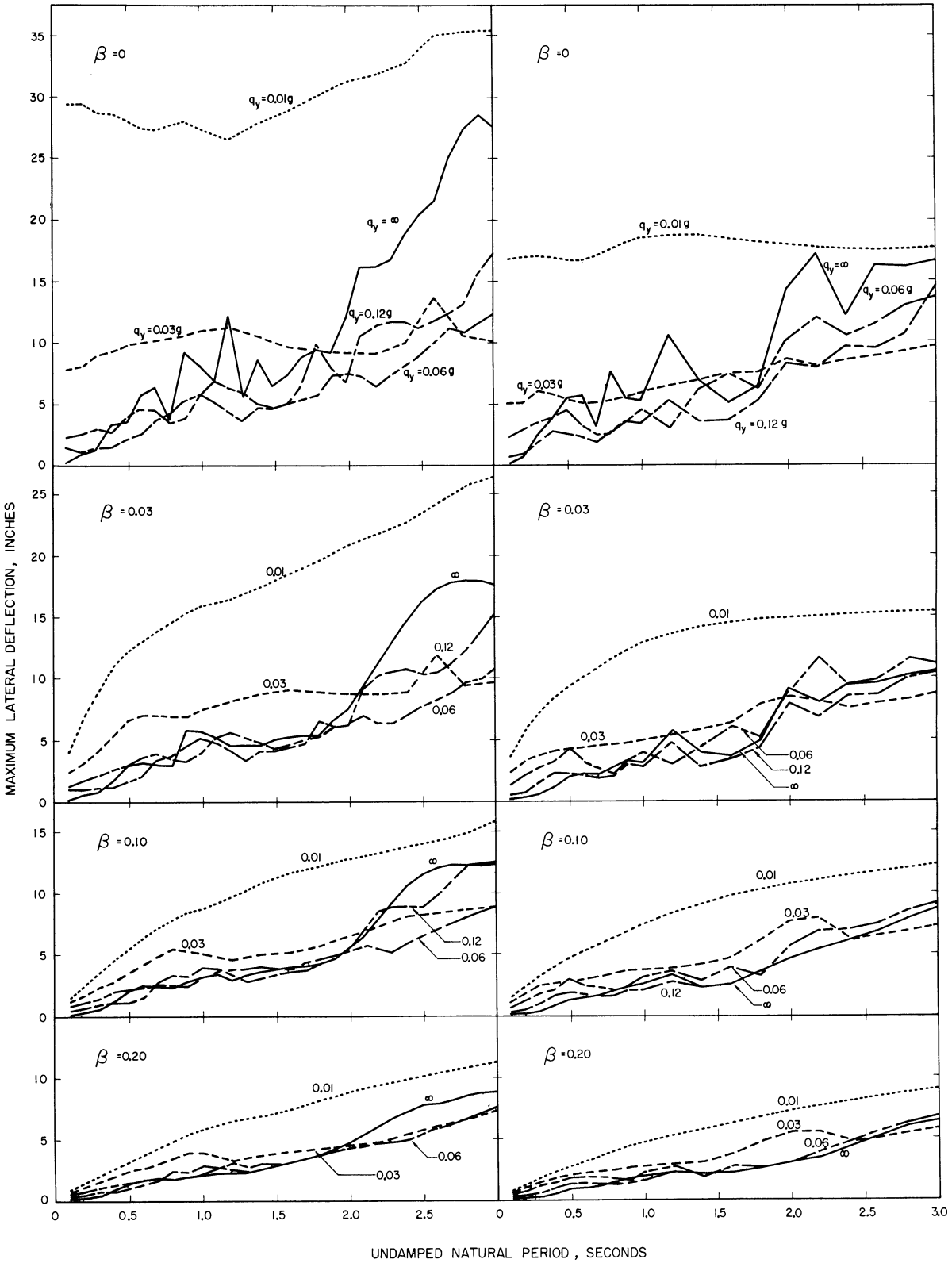

Figure 12. Lateral Deflection Spectra, El Centro, California, Earthquake of May 18, 1940. Components: N-S (left), E-W (right).

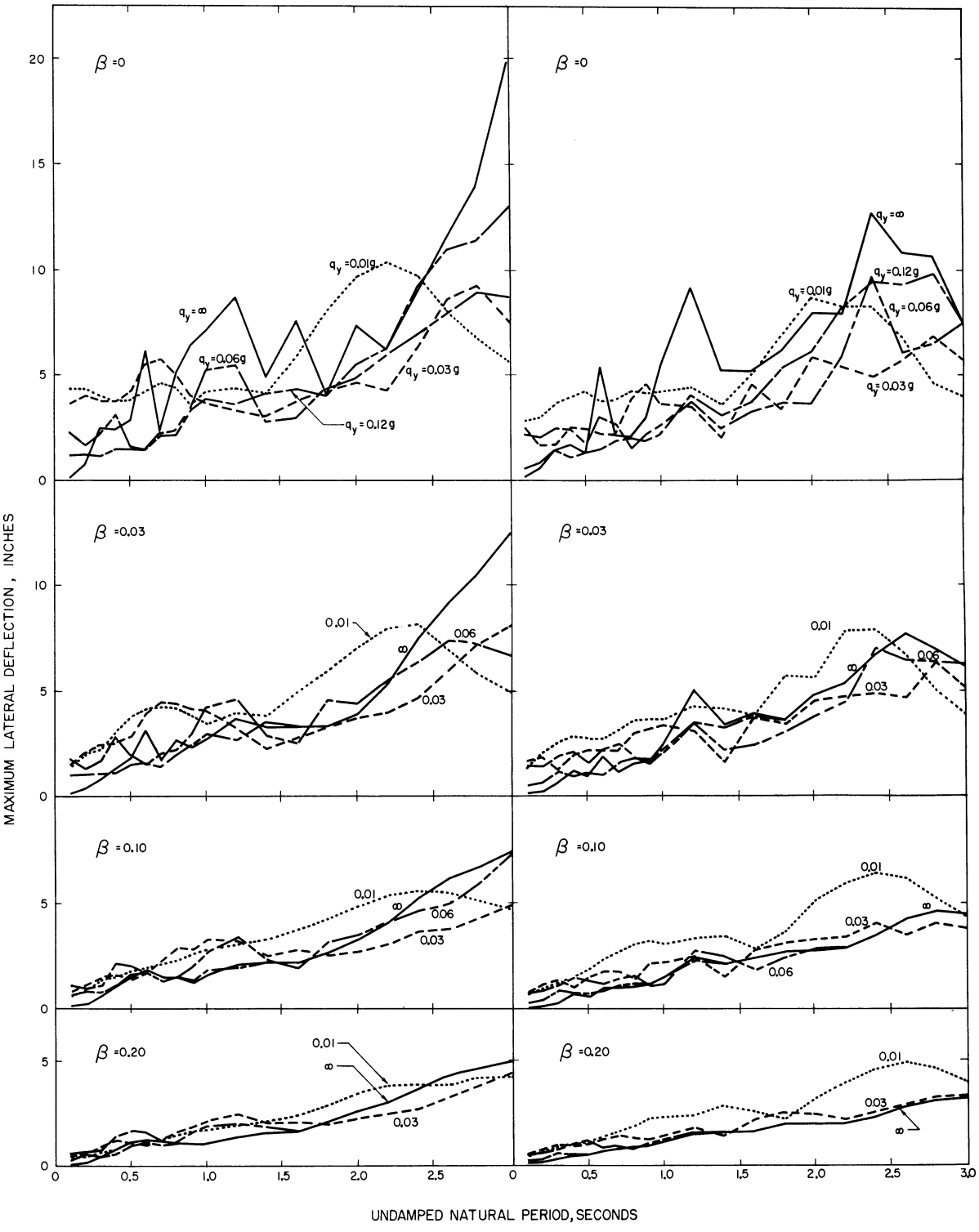

Figure 13. Lateral Deflection Spectra, Olympia, Washington, Earthquake of April 13, 1949. Components: N80°E (left), N10°W (right).

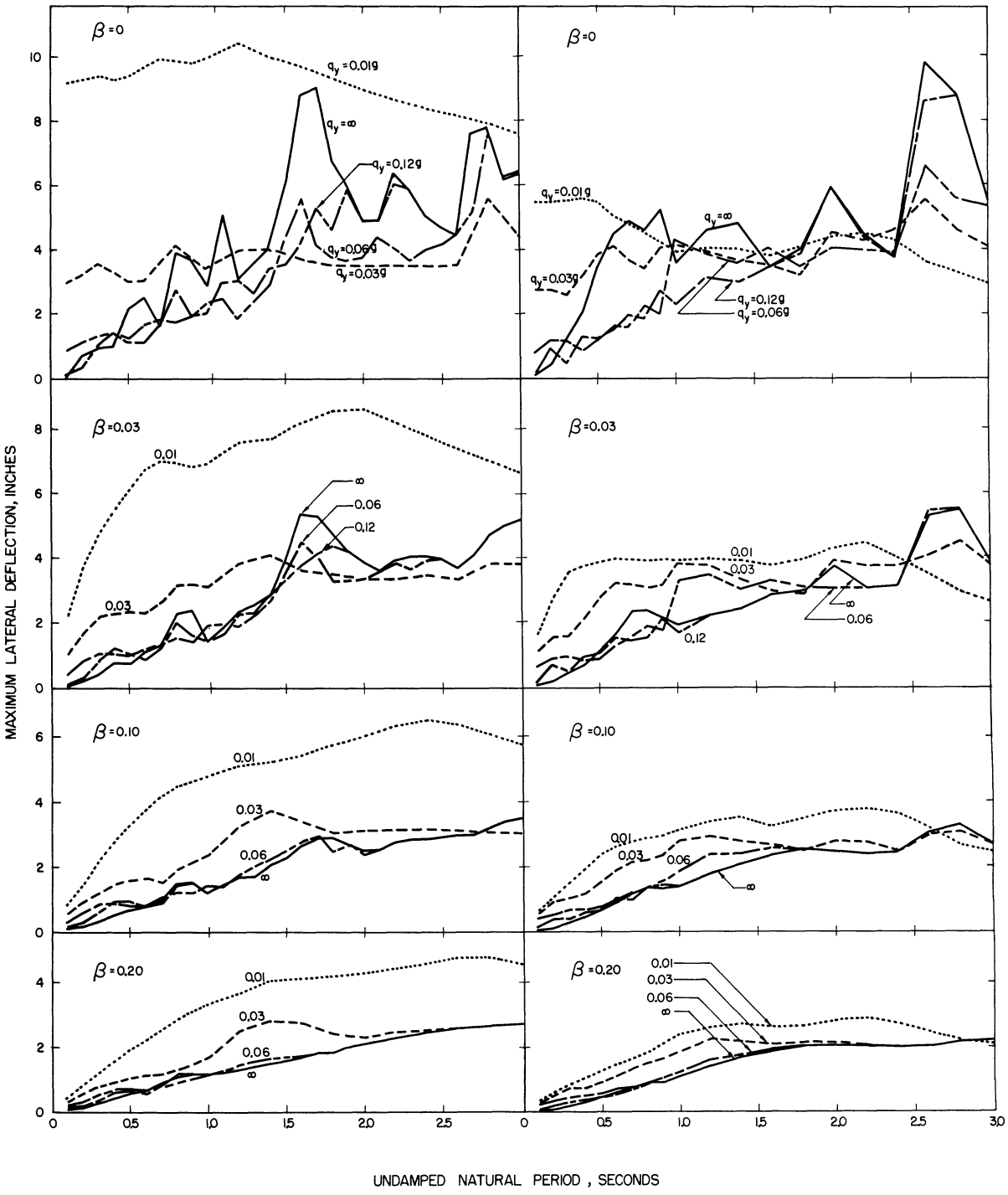

Figure 14. Lateral Deflection Spectra, Taft, California, Earthquake of July 21, 1952. Components: N69°W (left), S21°W (right).

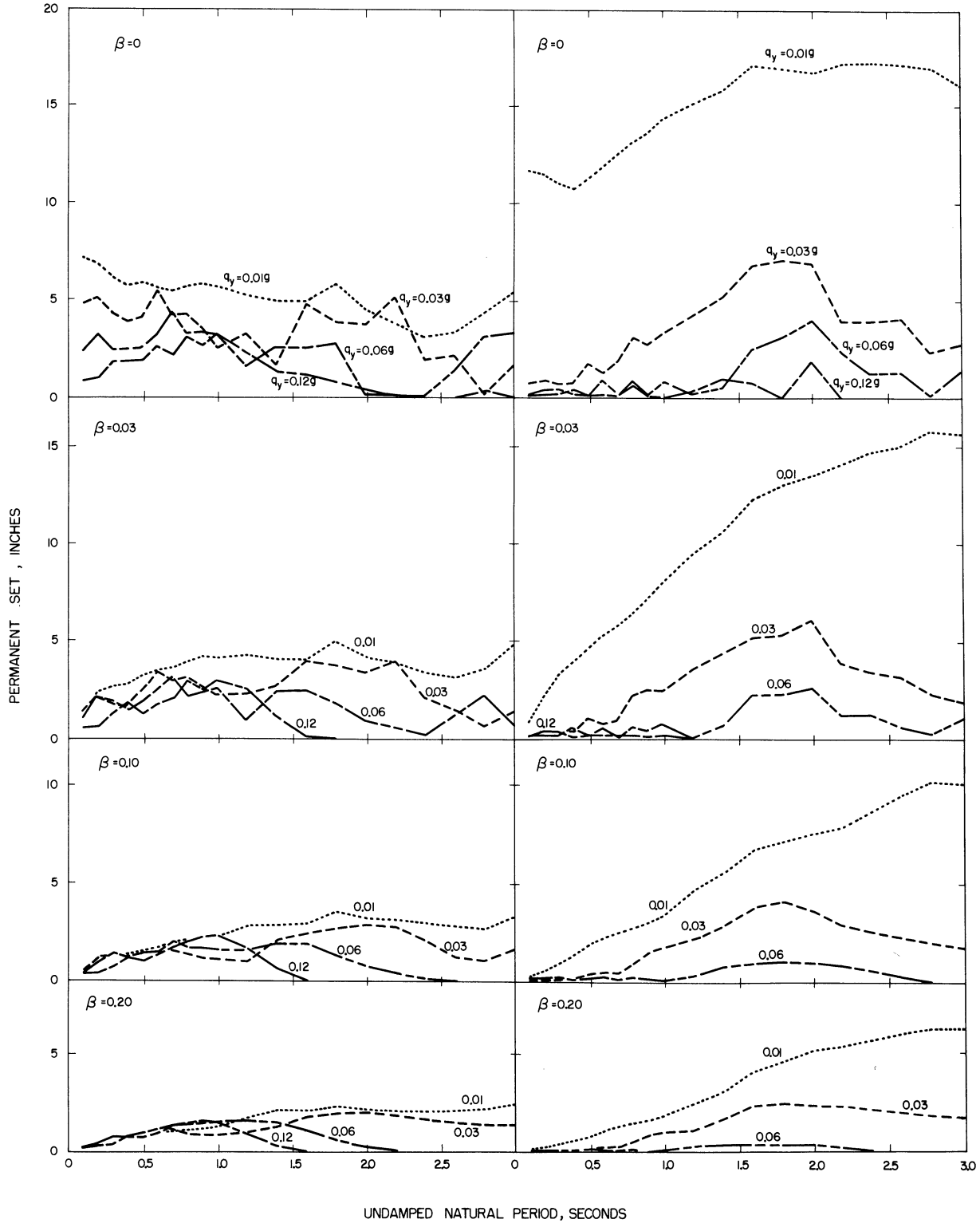

Figure 15. Permanent Sets, El Centro, California, Earthquake of December 30, 1934. Components: N-S (left), E-W (right).

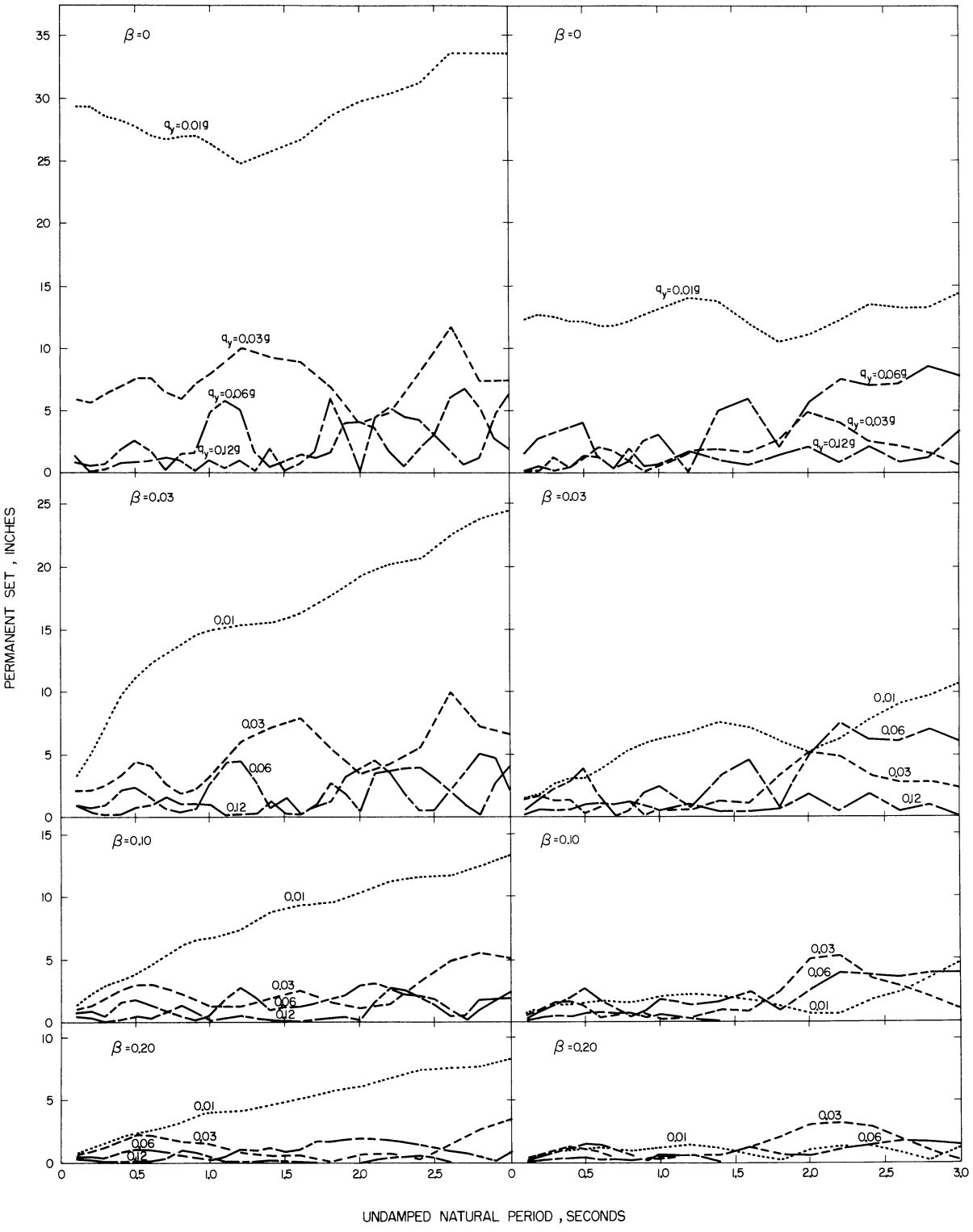

Figure 16. Permanent Sets, El Centro, California, Earthquake of May 18, 1940. Components: N-S (left), E-W (right).

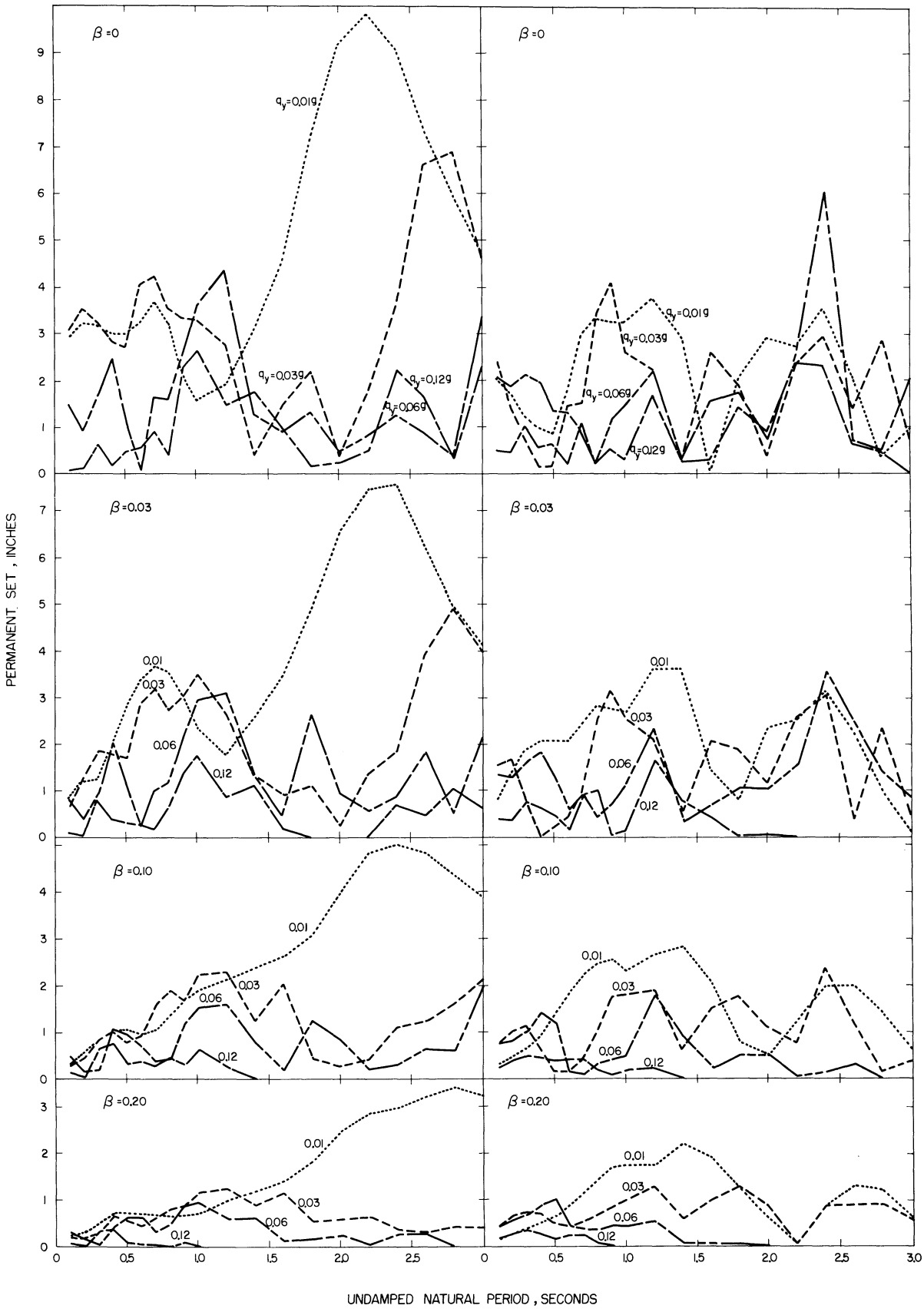

Figure 17. Permanent Sets, Olympia, Washington, Earthquake of April 13, 1949. Components: N80°E (left), N10°W (right).

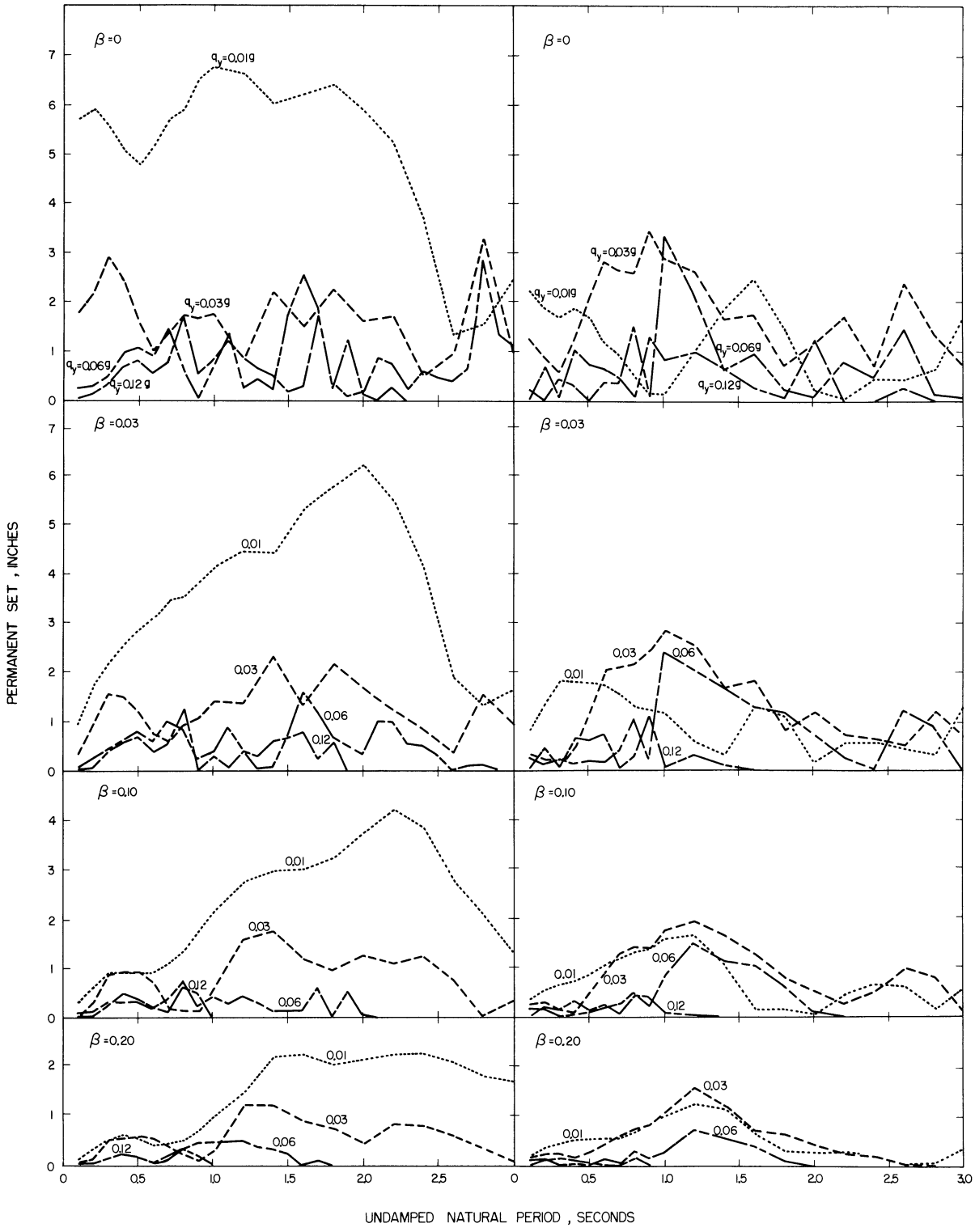

Figure 18. Permanent Sets, Taft, California, Earthquake of July 21, 1952. Components: N69°W (left), S21°W (right).

Figures 11-14, studied with respect to the effect of damping on the response of buildings, also show that the first increment of damping, from 0 to 0.03, reduces very effectively the lateral deflections at all yield levels.

Figures 15-18 show that, for the values of damping and natural period generally encountered in buildings, the permanent sets resulting from yield levels not lower than 0.06 g seem to be within acceptable limits.

The results obtained from the above investigations indicate that a strong-motion earthquake-resistant design incorporating energy absorption through plastic deformation can be attempted, provided the yield level is not lower than 0.06 g.

CHAPTER V

EFFECT OF ELASTO-PLASTIC ACTION ON THE ENERGY IMPARTED TO SIMPLE BUILDINGS BY EARTHQUAKES

An earthquake in itself is caused by a release of energy due to displacements on fault planes inside the earth's crust. Consequently, a building subjected to earthquake action is fed with energy. A part of this energy is stored by the building in the form of strain and kinetic energy and the remaining energy is dissipated through damping. At any time, the sum of the stored energy and the dissipated energy is equal to the total energy input. When the energy imparted to the building is greater than its strain-energy capacity, then, there remains an excess energy which will have to be absorbed in some way. For this there are two possibilities:

1. If the capacity of the structural elements of the building is adequate for dissipating this excess energy through inelastic deformation, the building will survive.
2. If the structural elements have no or only inadequate capacity for energy dissipation through inelastic deformation, then, this excess energy will be dissipated through complete or partial structural damage.

As a relatively large capacity for dissipating energy seems highly desirable in strong-motion earthquake-resistant design, knowledge of the type and amount of dissipated energy becomes important. Such knowledge could also explain damage or absence of damage in buildings that have been subjected to earthquake action.

This chapter deals with the energy functions (energy input and its components) as related to the three structural parameters, namely, natural period, damping, and yield strength. In particular, it deals with the effect of elasto-plastic action on the energy imparted to buildings by strong-motion earthquakes. Again, to simplify the proceedings, only one-story buildings were considered and the study was based on the same assumptions stated in the previous chapter. In fact, the computer evaluated the energy input and its components while it evaluated the response of the system at small time intervals and it was instructed to record the maximum values of the above functions.

The equations of energy input and its components will be derived on a unit mass basis from Equation (4.8).

If $f(t)$ is the force per unit mass exerted on the system by the foundation, then from Equation (4.8)

$$f(t) = - \left(\frac{4\pi}{T} \beta \dot{x} + q\right) . \tag{5.1}$$

Therefore, the energy input per unit mass is

$$E(t) = - \int \left(\frac{4\pi}{T} \beta \dot{x} + q\right) dy ,$$

but

$$dy = \dot{y} dt$$

thus

$$E(t) = - \int_0^t \left(\frac{4\pi}{T} \beta \dot{x} + q\right) \dot{y} d\tau . \tag{5.2}$$

The stored energy is resolved into strain energy, recoverable when the system returns to its equilibrium position, and kinetic energy. The strain energy per unit mass is

$$U(t) = \frac{1}{2} (q)(\frac{Q}{k}) \quad . \tag{5.3}$$

From the first definition made in Equation (4.7),

$$Q = qm$$

and from the first definition made in Equation (3.3)

$$\frac{m}{k} = (\frac{T}{2\pi})^2 \quad .$$

Hence Equation (5.3) can be rewritten as follows:

$$U(t) = \frac{1}{2} (\frac{T}{2\pi} q)^2 \quad . \tag{5.4}$$

The kinetic energy per unit mass is

$$K(t) = \frac{1}{2} (\dot{x} + \dot{y})^2 \quad . \tag{5.5}$$

The dissipated energy is resolved into energy dissipated through viscous damping and energy dissipated through plastic deformation. The energy dissipated through viscous damping per unit mass is

$$L(t) = \int \frac{4\pi}{T} \beta \dot{x} dx \quad ,$$

but

$$dx = \dot{x} dt$$

thus

$$L(t) = \frac{4\pi}{T} \beta \int_0^t \dot{x}^2 \, d\tau \quad . \tag{5.6}$$

From Figure 10 and the differential relations given by Equation (4.9), $\dot{D}$, the rate of energy dissipated through plastic deformation, has to obey the following relations:

$$\left.\begin{array}{lll} \dot{D} = 0 & \text{if} & -q_y < q < q_y \\ \text{or} & \text{if} & q = q_y \quad \text{and} \quad \dot{x} \leq 0 \\ \text{or} & \text{if} & q = -q_y \quad \text{and} \quad \dot{x} \geq 0 \\ \dot{D} = q_y \dot{x} & \text{if} & q = q_y \quad \text{and} \quad \dot{x} > 0 \\ \dot{D} = -q_y \dot{x} & \text{if} & q = -q_y \quad \text{and} \quad \dot{x} < 0 \end{array}\right\} . \qquad (5.7)$$

The energy integrals, as given by Equations (5.2) and (5.6), were adapted to the Runge-Kutta procedure of numerical integration by replacing each energy integral by its rate of change.

From Equation (4.10),

$$\dot{x} = v$$

and if we define

$$\dot{y} = z ,$$

then

$$\left.\begin{array}{l} \dot{E} = - \left(\frac{4\pi}{T} \beta v + q\right) z \\ \dot{L} = \frac{4\pi}{T} \beta v^2 \end{array}\right\} . \qquad (5.8)$$

To overcome the difficulty caused by the discontinuity of $\dot{D}$ whenever the system was entering the plastic region, the differential relations given by Equation (5.7) were replaced by equivalent difference relations which read as follows:

$$\left.\begin{aligned} \Delta D &= 0 && \text{if} \quad -q_y \le q + \left(\frac{2\pi}{T}\right)^2 \Delta x \le q_y \\ \Delta D &= q_y\left(\Delta x - \left(\frac{T}{2\pi}\right)^2 \Delta q\right) && \text{if} \quad q + \left(\frac{2\pi}{T}\right)^2 \Delta x > q_y \\ \Delta D &= -q_y\left(\Delta x - \left(\frac{T}{2\pi}\right)^2 \Delta q\right) && \text{if} \quad q + \left(\frac{2\pi}{T}\right)^2 \Delta x < -q_y \end{aligned}\right\} \quad . \quad (5.9)$$

The same conditions stated in the previous chapter made the use of equivalent difference relations possible.

For each earthquake analysis, the computer, advancing step by step through the solution and reaching the end of the accelerogram, evaluated the response and energy functions of systems of different natural periods for different values of damping and for a specified yield level.

To check for any possible errors or inaccuracies that might have occurred in the proceedings, the following tests were made:

Prior to any solution involving actual earthquake data, checks for digital errors were performed by using as input simple waves for which the exact solutions were analytically worked out. These digital checks showed an accuracy to four significant digits.

The energy balance, i.e., the difference between the energy input and the sum of the energy components, was calculated to serve as a detector of any possible machine or numerical error that might have occurred during an earthquake analysis run. For this, the computer was instructed to calculate the energy balance at the end of each solution, which balance theoretically should have been equal to zero. In most cases the energy-balance discrepancy was below 5% of the energy input; only in one or two cases did it go up to 7%. In trial solutions, it

was found that reducing the integration time interval brought the discrepancy almost down to zero. But as the above discrepancies were found tolerable, it was considered unnecessary to reduce the integration time interval throughout all the earthquake analyses, as this would have required considerably longer computer time for the completion of the study.

Since the study under consideration concerns a nonlinear problem, investigations were carried out to determine whether the problem was not inherently ill-conditioned. If it were, small variations in the punched-card accelerograms could induce significantly large variations in the response and energy components. Several solutions were computed five times. In the first computation, the punched-card accelerogram was used without any modification, but for the other four computations the computer was instructed to modify the accelerogram by inserting a distinct perturbation in each computation. The first perturbation consisted of a 10% magnification in all accelerogram ordinates, which caused magnifications ranging from 3% to 25% in displacement response and 17% to 21% in energy input. In systems with completely elastic behavior, the same perturbation would have caused magnifications of 10% in response and 21% in energy input. The second perturbation consisted of a 21% magnification in all accelerogram ordinates, which caused magnifications ranging from 5% to 46% in response and 36% to 49% in energy input as compared to 21% and 46%, respectively, for completely elastic behavior. The third perturbation increased the odd-numbered accelerogram ordinates by 0.01 g and decreased the even-numbered ordinates by the same amount. The fourth perturbation differed from the third in

that the odd-numbered ordinates were reduced and the even-numbered ordinates were increased. These last two perturbations had practically no effect. The results obtained from the above perturbations led to the conclusion that the problem in this study is not inherently ill-conditioned.

Figures 19-22 show the values of maximum energy input plotted against natural period, for yield levels varying from completely elastic down to 0.01 g and for fixed values of damping ranging from 0 to 0.20 of critical damping.

These figures permit a comparison of the values of maximum energy input calculated from elasto-plastic behavior with the corresponding values calculated from completely elastic behavior. This comparison, at all levels of damping, shows:

1. that energy absorption through plastic deformation has a remarkable smoothing effect upon the energy input curves and that the lower the yield level, the smoother the energy-input curve; and
2. that, on the average, a decrease in yield level is accompanied by a decrease in energy input. But, for very short natural periods of about 0.4 seconds or less, when the natural period decreases, the energy-input curves of higher yield levels drop more rapidly than those of lower yield levels.

The values of maximum energy input and total dissipated energy are plotted on Figures 23 and 24 against natural period, for values of damping varying from 0 to 0.20 of critical damping and at fixed

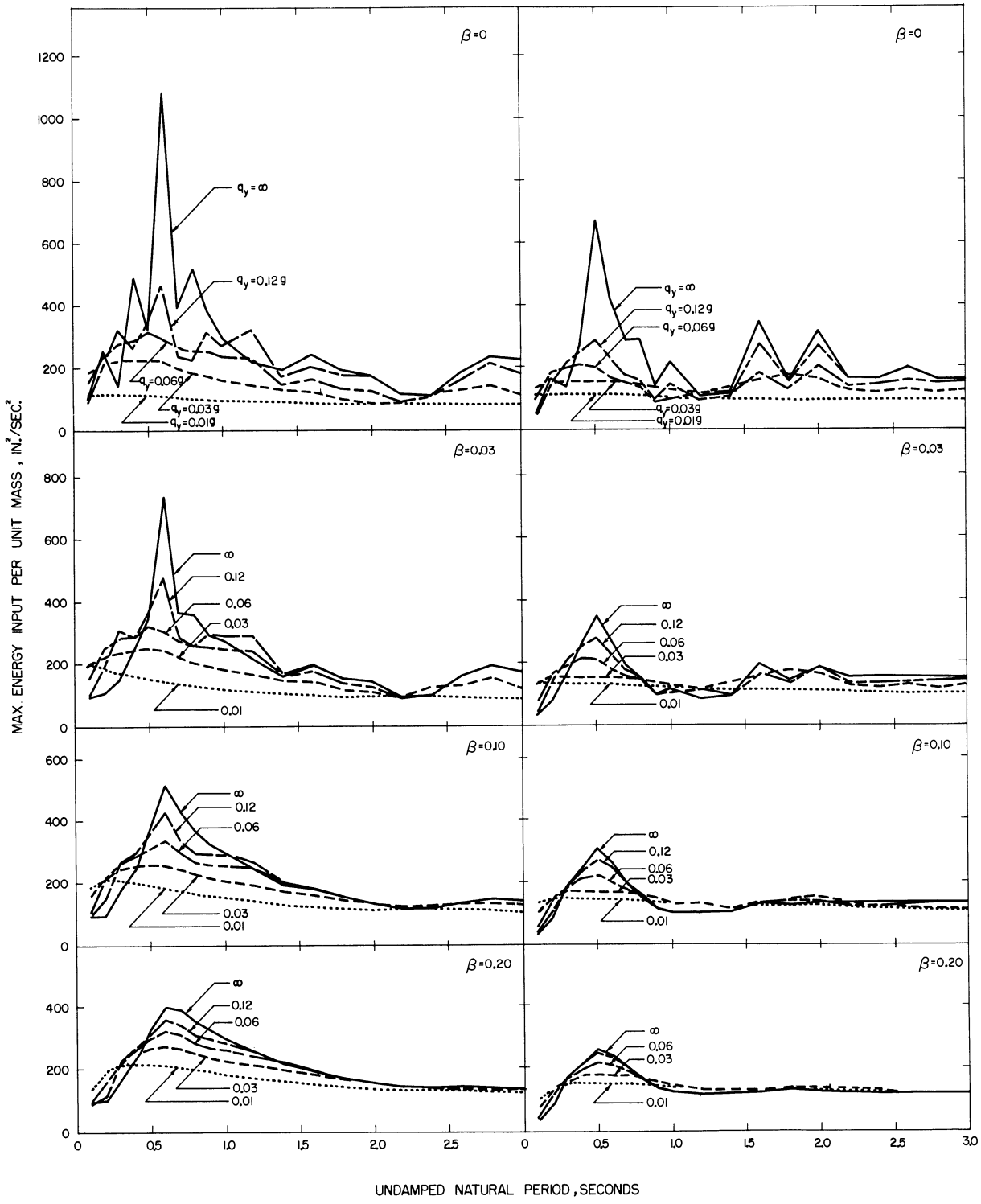

Figure 19. Energy Input Spectra, El Centro, California, Earthquake of December 30, 1934. Components: N-S (left), E-W (right).

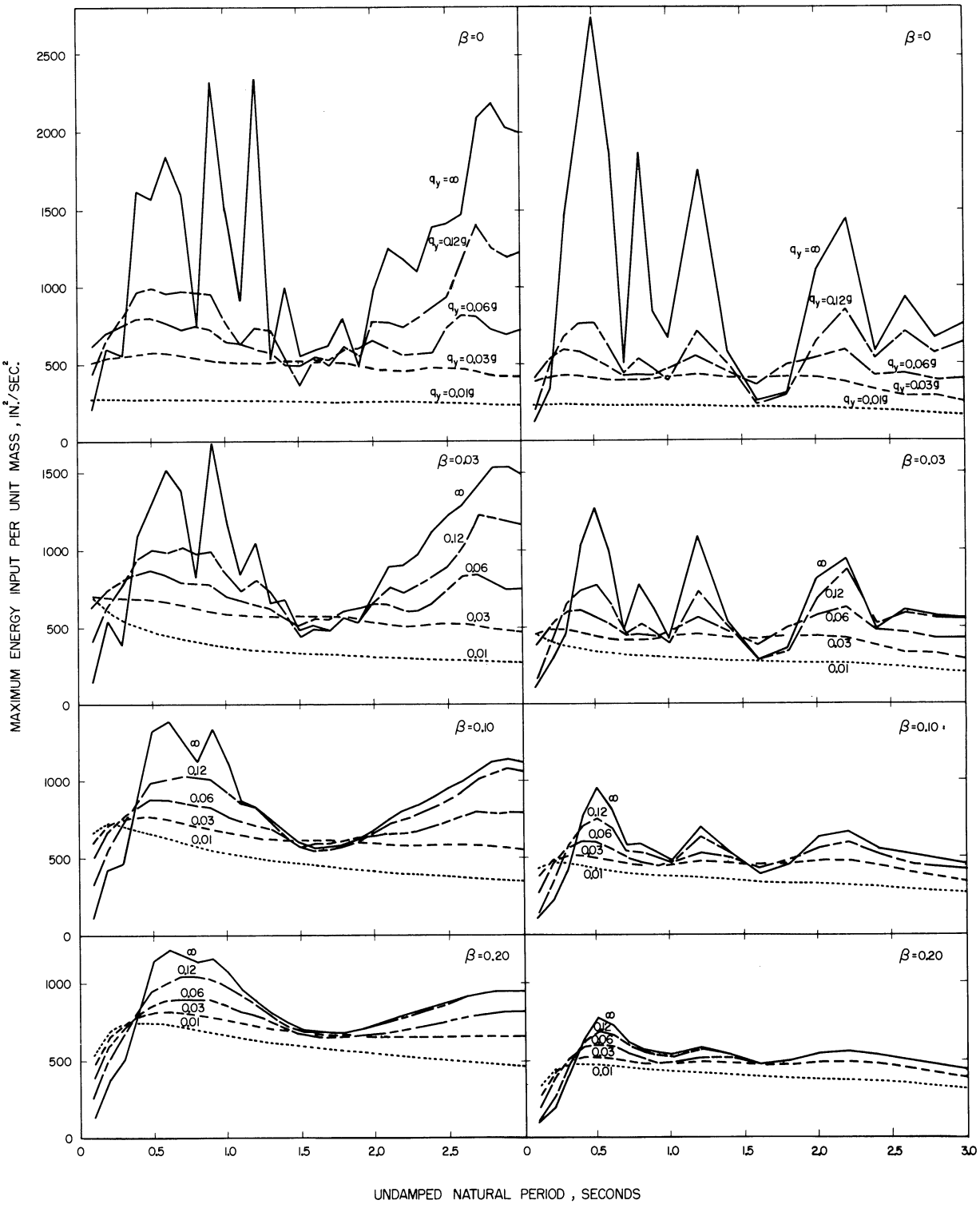

Figure 20. Energy Input Spectra, El Centro, California, Earthquake of May 18, 1940. Components: N-S (left), E-W (right).

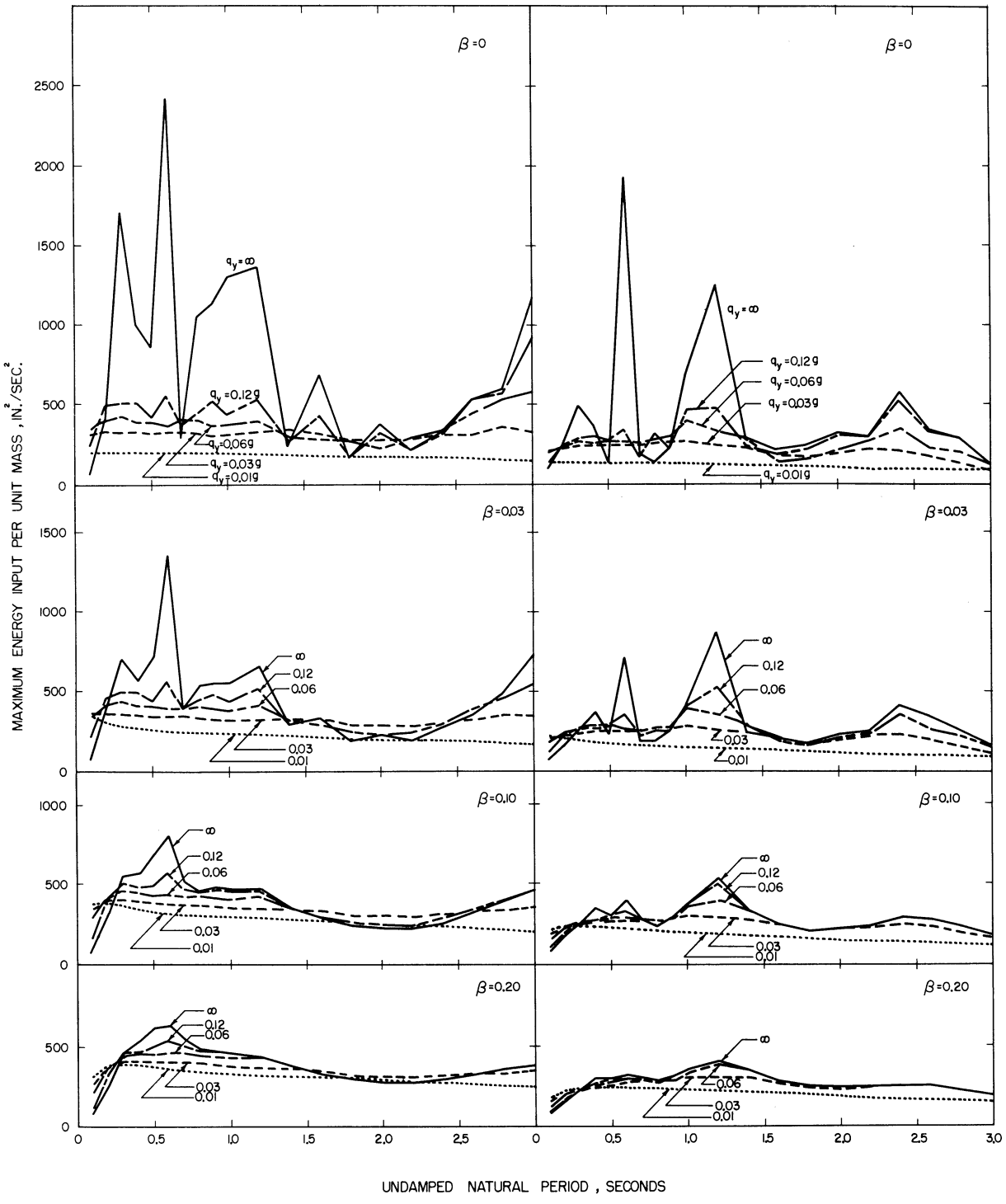

Figure 21. Energy Input Spectra, Olympia, Washington, Earthquake of April 13, 1949. Components: N80°E (left), N10°W (right).

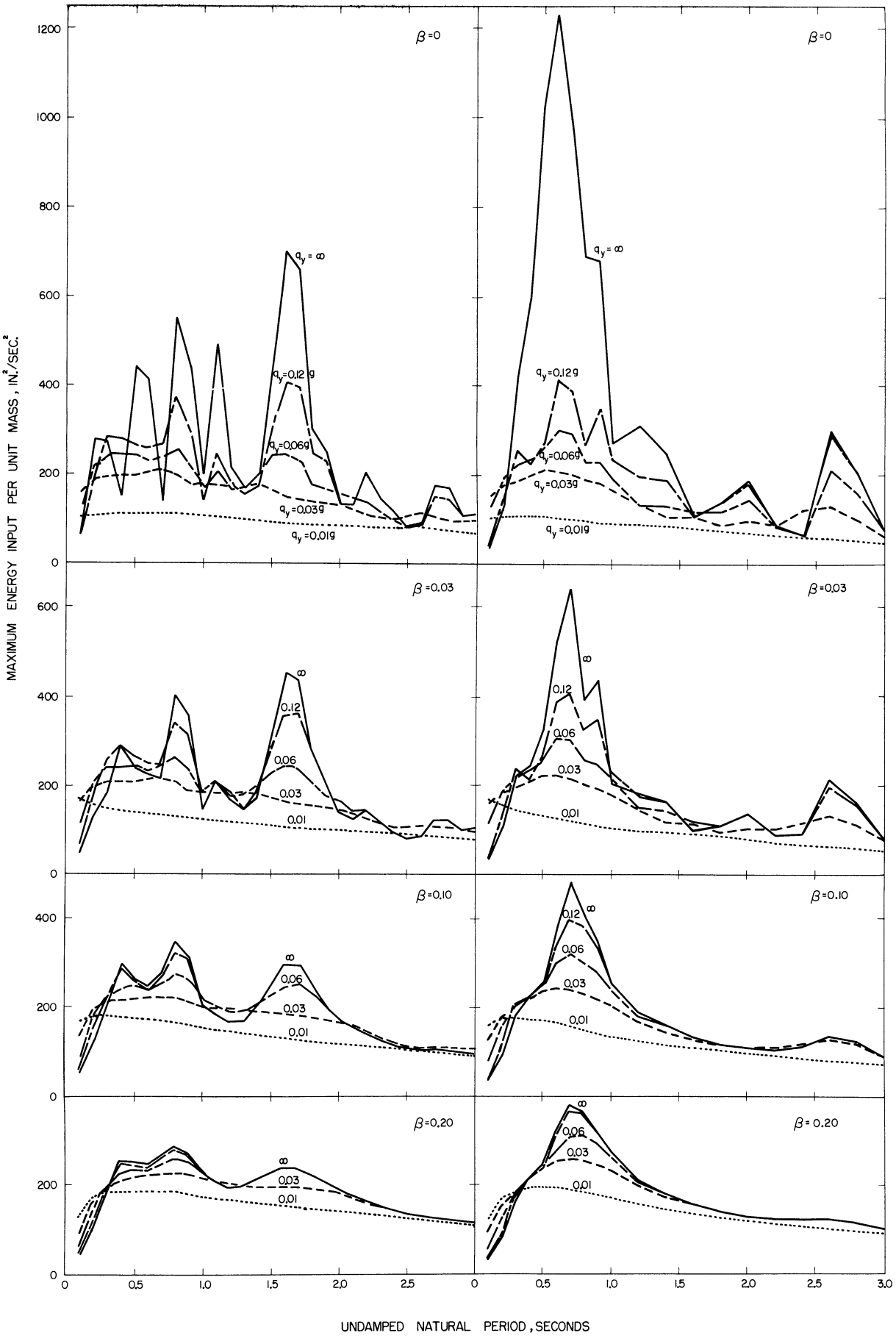

Figure 22. Energy Input Spectra, Taft, California, Earthquake of July 21, 1952. Components: N69°W (left), S21°W (right).

yield levels ranging from 0.01 g up to completely elastic. These figures permit a comparison of the values of maximum energy input or total dissipated energy calculated for the undamped case with the corresponding values calculated for different values of damping. This comparison shows the following.

1. For the undamped and completely elastic energy-input curve, small variations in the natural period induce large variations in this curve. At all levels of yielding, damping has a smoothing effect upon the input- and total dissipated-energy curves.
2. At yield levels as low as 0.03 g and 0.01 g, an increase in damping is accompanied by an increase in the energies. At higher yield levels, especially for the elastic case, variations in damping do not induce any decisive variations in the input- and total dissipated-energy curves.

Figures 23 and 24, studied with respect to the effect of variations in the natural period upon the input- and total dissipated-energy curves, also show that the above functions are almost independent of the natural period of the system at yield levels as low as 0.03 g and 0.01 g and at all levels of damping.

Finally, these figures show that the input- and total dissipated-energy curves are very similar qualitatively and quantitatively; hence, the observations made from the energy-input curves of Figures 19-22 could also be made from the total dissipated-energy curves, if the latter were presented in the same fashion as those shown in Figures 19-22.

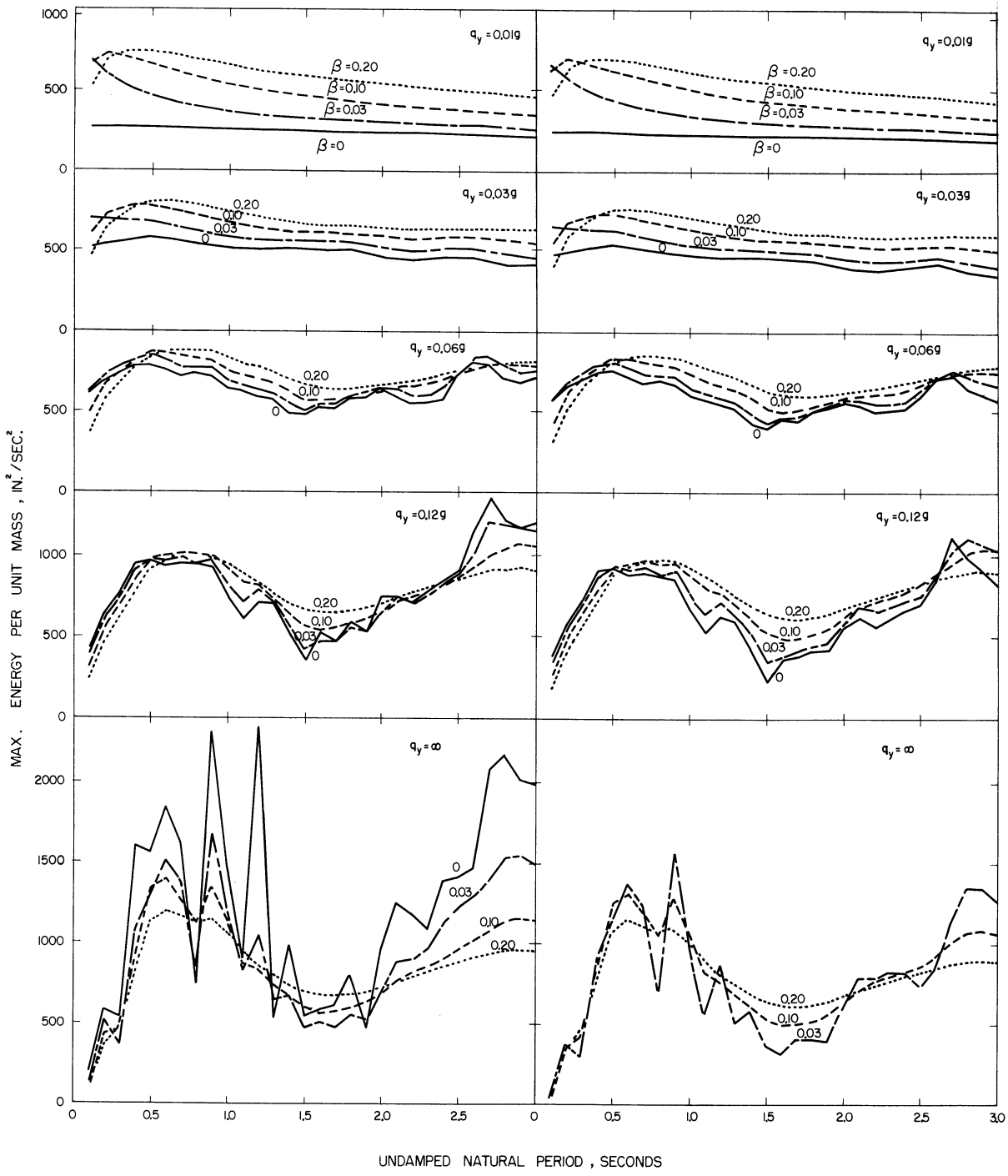

Figure 23. Energy Input Spectrum (left), Total Dissipated Energy Spectrum (right), El Centro, California, Earthquake of May 18, 1940. Component N-S.

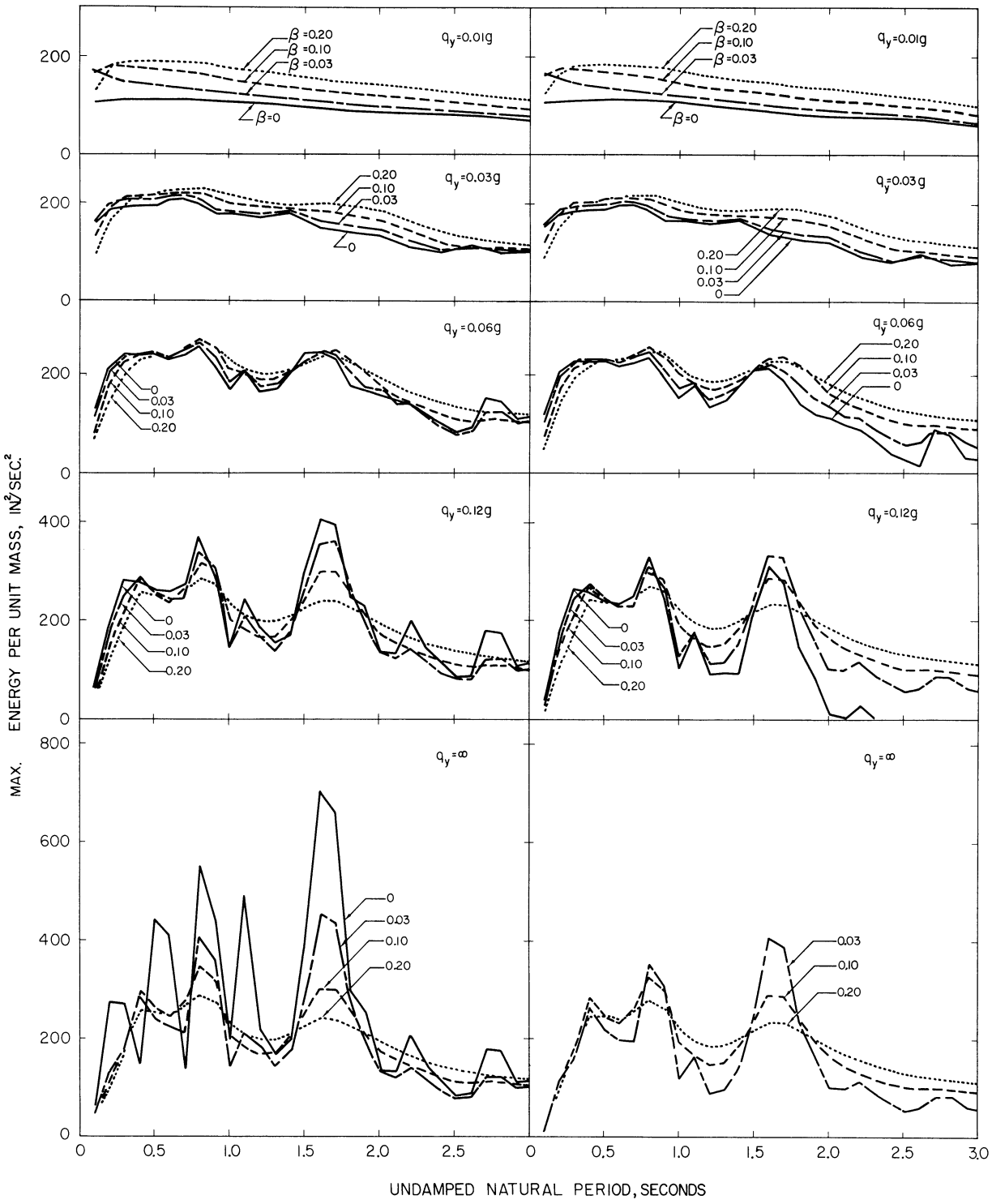

Figure 24. Energy Input Spectrum (left), Total Dissipated Energy Spectrum (right), Taft, California, Earthquake of July 21, 1952. Component N69° W.

CHAPTER VI

ELASTO-PLASTIC ACTION AS A REDUCING FACTOR OF THE SEISMIC LATERAL LOAD COEFFICIENTS CALCULATED FROM COMPLETELY ELASTIC DYNAMIC ANALYSIS

This chapter shows that elasto-plastic action can effectively reduce the seismic lateral load coefficients which have been calculated from completely elastic dynamic analysis.

Each time an earthquake analysis was run and the end of the accelerogram was reached, the computer evaluated the response and energy components. It was then instructed to calculate the sum of the absolute values of all displacements in the plastic region in both directions. This sum, to be referred to as the total plastic displacement, is obtained by dividing the energy dissipated through plastic deformation per unit mass by the considered yield level.

Figures 25-28 show the values of total plastic displacement plotted against natural period, for values of damping varying from 0 to 0.20 of critical damping and at fixed yield levels of 0.06 g and 0.12 g. In each of these plots the limiting elastic displacement, designated by x_y, is also plotted against natural period and is represented by a dotted curve.

These figures show that an increase in damping is accompanied by a decrease in the total plastic displacement at both yield levels of 0.06 g and 0.12 g; and also, that increasing the yield level from 0.06 g to 0.12 g reduces the total plastic displacement. This reduction becomes more appreciable at higher levels of damping.

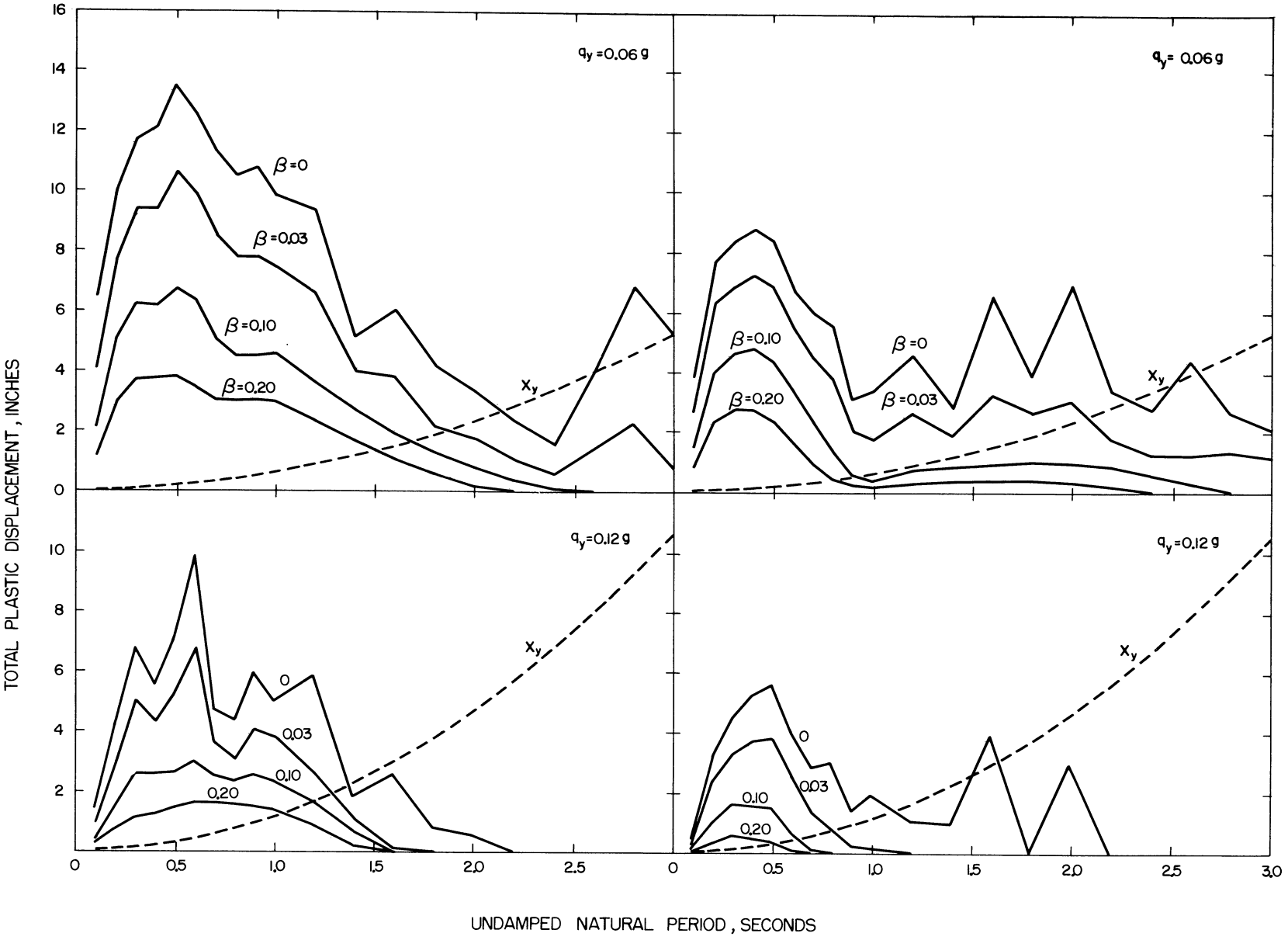

Figure 25. Total Plastic Displacements, El Centro, California, Earthquake of December 30, 1934. Components: N-S (left), E-W (right).

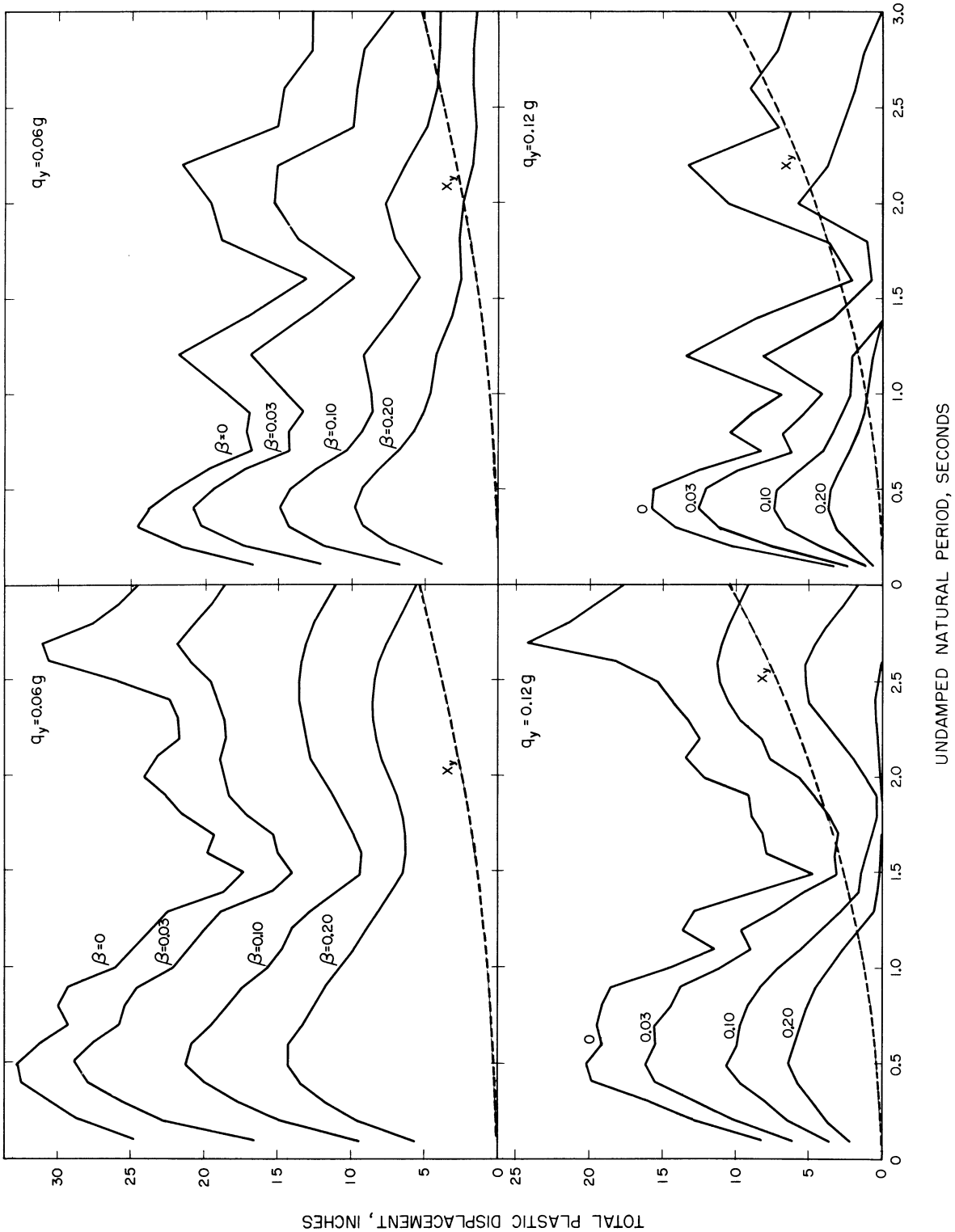

Figure 26. Total Plastic Displacements, El Centro, California, Earthquake of May 18, 1940. Components: N-S (left), E-W (right).

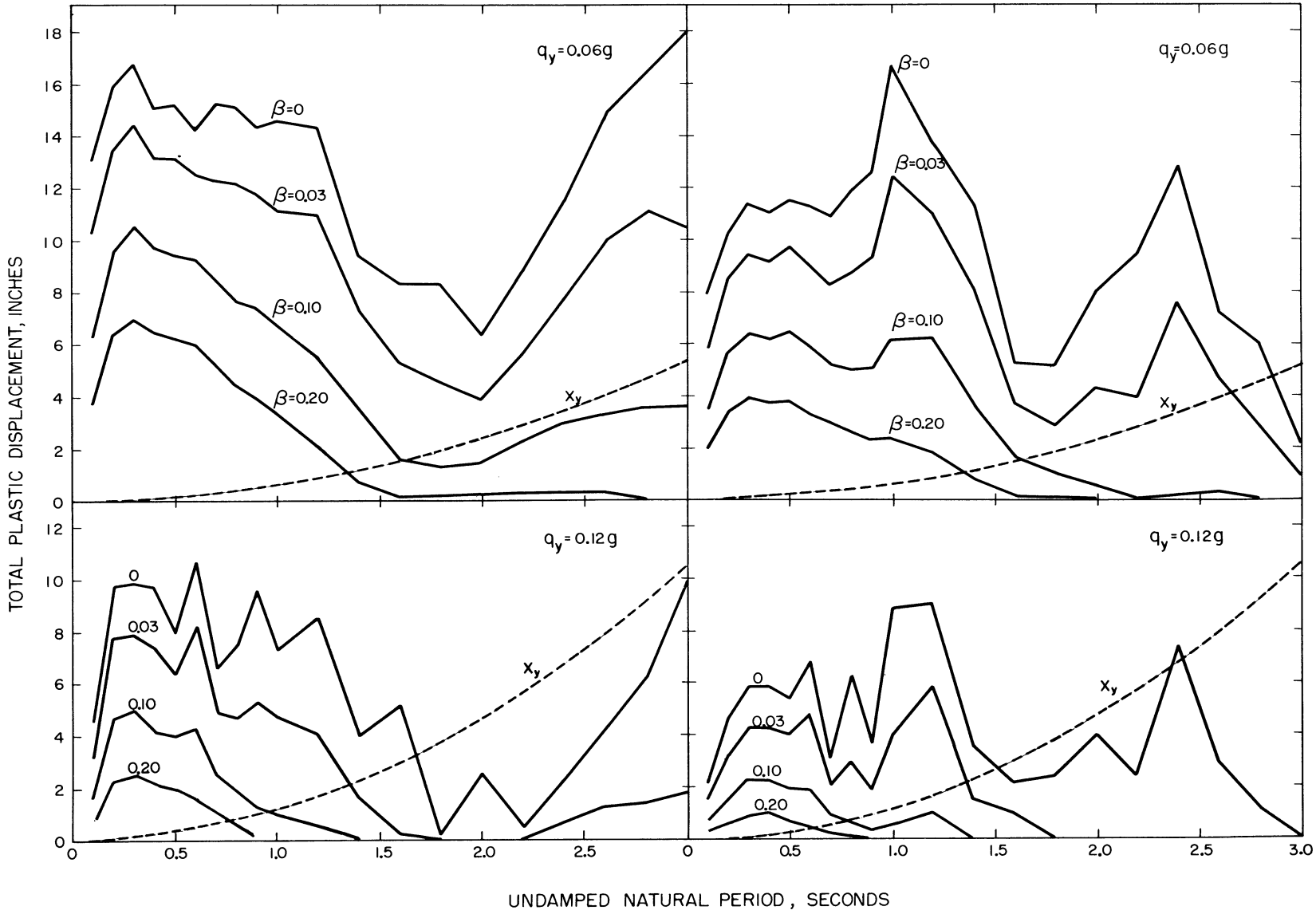

Figure 27. Total Plastic Displacements, Olympia, Washington, Earthquake of April 13, 1949. Components: N80°E (left), N10°W (right).

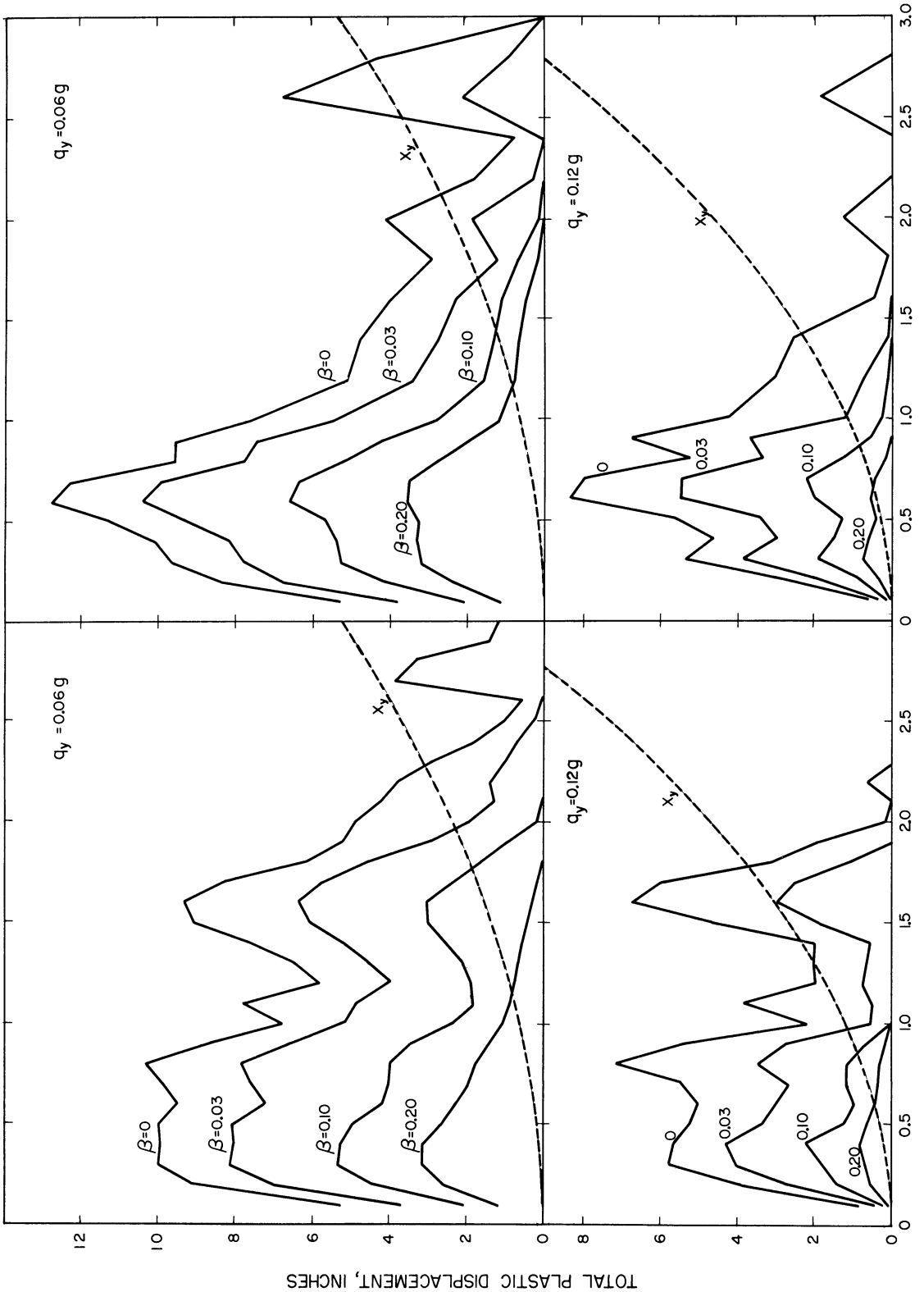

Figure 28. Total Plastic Displacements, Taft, California, Earthquake of July 21, 1952. Components: N69°W (left), S21°W (right).

The results obtained from each earthquake analysis indicated that in most cases yielding occurs in both directions, for the total plastic displacement is generally larger than the maximum magnitude of the displacement in the plastic region. As the permissible total plastic displacement may be reached long before the displacement in the plastic region reaches its permissible magnitude, it seems that the total plastic displacement could be the controlling response parameter if energy absorption through plastic deformation is incorporated into earthquake-resistant design.

The effect of elasto-plastic action as a reducing factor of the seismic lateral load coefficients has been analyzed by J. A. Blume,[12,13] R. M. Sheth,[7] and A. S. Veletsos and N. M. Newmark[20] with the maximum magnitude of displacement in the plastic region as the controlling response parameter.

To make the total plastic displacement the controlling response parameter in analyzing the reducing effect of elasto-plastic action on the seismic coefficients, the following definitions are made.

Let

$$\left.\begin{aligned} C_y &= \frac{q_y}{g} \\ C_r &= \frac{C_y}{C} = \text{the reduction coefficient} \end{aligned}\right\}, \qquad (6.1)$$

and

$$R_d = \frac{x_y + x_p}{x_y} = \text{the elasto-plastic ductility ratio}$$

where

C_y is the coefficient which, multiplied by the acceleration due to gravity, determines the yield level of the system,

C_r is the coefficient resulting from elasto-plastic action which reduces the seismic lateral load coefficient,

C is the seismic lateral load coefficient as shown by Equation (3.14) and is directly obtained from the plots of Figures 5-8,

x_y is the limiting elastic displacement and is obtained from the plots of Figures 25-28, (L)

x_p is the total plastic displacement consisting of the sum of the absolute values of all displacements in the plastic region in both directions and is obtained from the plots of Figures 25-28. (L)

C_r and R_d were calculated from Equation (6.1) using the results obtained from computer analyses involving yield levels of 0.06 g and 0.12 g for accelerograms of the four strongest U. S. earthquakes on record. Then the reduction coefficient was plotted against the elasto-plastic ductility ratio (Figures 29 and 30).

Figure 29 shows the points plotted for all values of damping varying from 0 to 0.20 of critical damping. The points are scattered over a band falling generally between two curves, also shown in the figure, which have been traced so as to enclose most of the plotted points, and which have no theoretical background. Only a few of the plotted points (about 12%) are found outside the two curves, which can thus be considered as limiting the quantitative reduction effect of elasto-plastic action for values of damping ranging from 0 to 0.20 of critical damping.

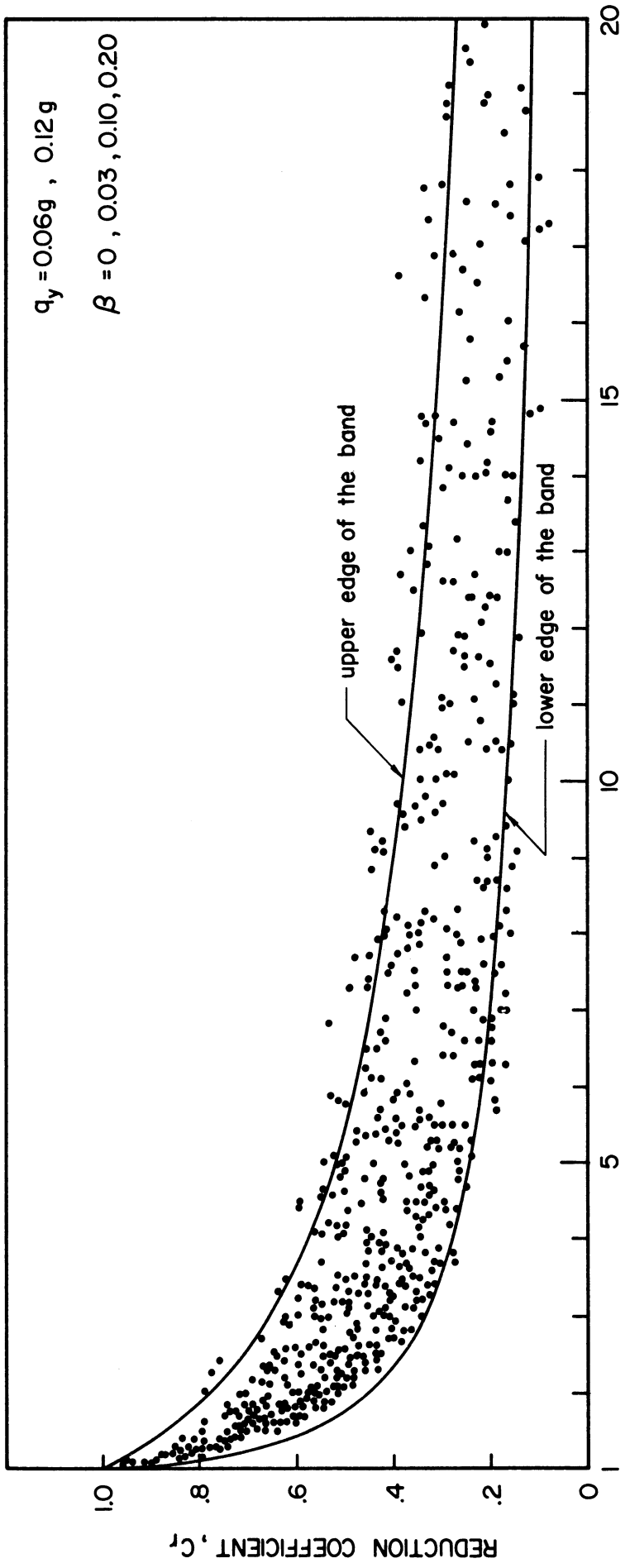

Figure 29. Reduction Coefficients (plotted for all the considered values of damping).

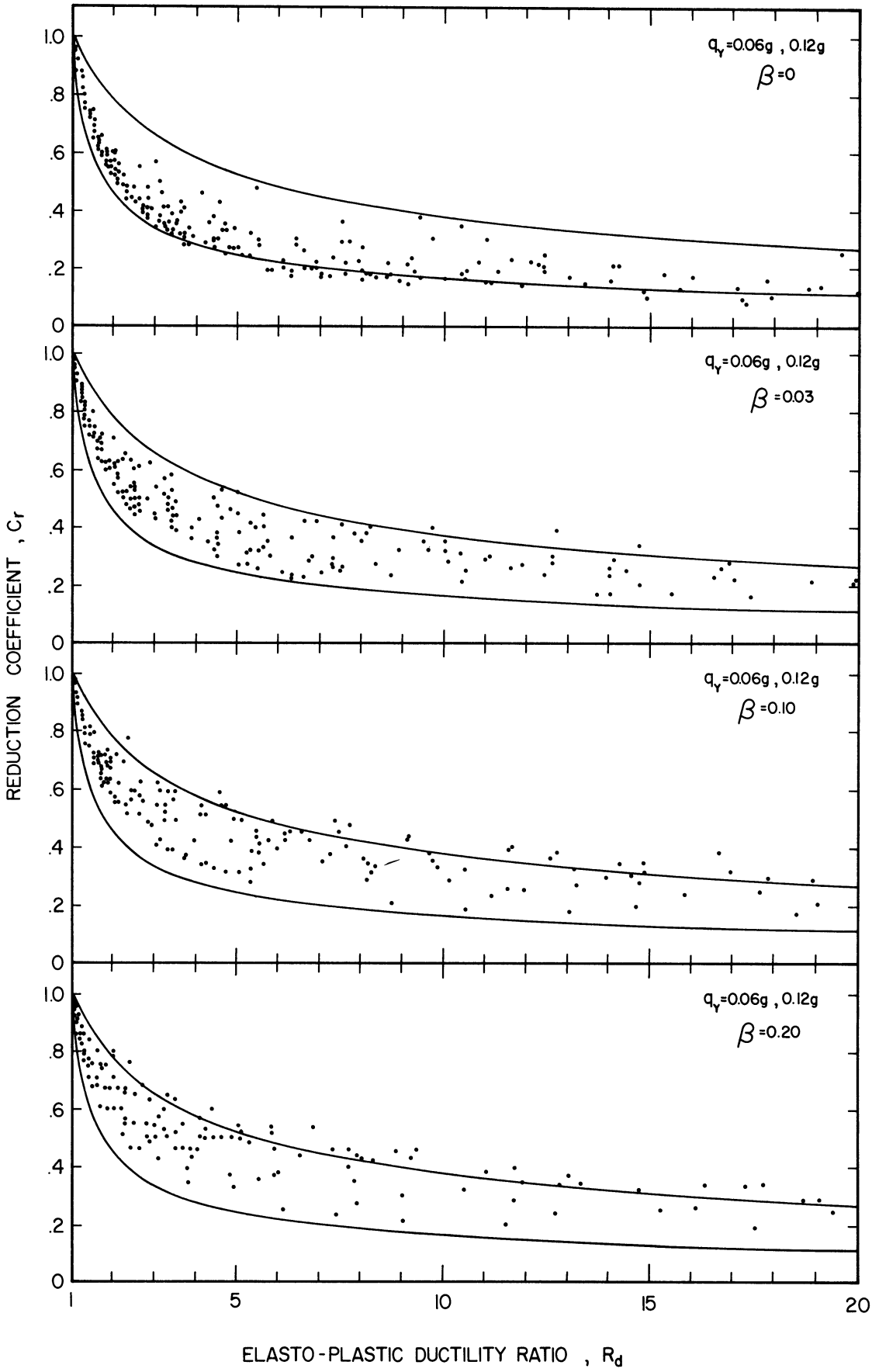

Figure 30. Reduction Coefficients (plotted for fixed values of damping).

Figure 30, where the points are plotted for fixed values of damping ranging from 0 to 0.20 of critical damping, shows that, on the average, the points calculated from the undamped case seem to approach the lower edge of the band, whereas those calculated for 0.20 of critical damping seem to approach the upper edge. This means that elasto-plastic action is more effective at lower levels of damping.

Turning back to Figures 19-22, the observation referring to the relation between yield level decrease and energy input decrease confirms that Professor Housner's hypothesis, made in his limit design approach, is on the average conservative. This hypothesis assumes that the maximum energy imparted to an overstressed building (in which the structural elements are stressed beyond the elastic limit) is not greater than it would have been had that building behaved completely elastically. On the basis of the above hypothesis, Housner's limit design criterion is that a building should be capable of absorbing energy through plastic deformation of the structural elements equal to the difference between the maximum strain energy that would have been stored in that building were it behaving completely elastically and the strain energy which the building can actually store when the yield point is reached.

Based on the above criterion and on a unit mass basis,

$$D = U_e - U_a \tag{6.2}$$

where

D is the energy to be absorbed through plastic deformation per unit mass, (L^2T^{-2})

U_e is the maximum strain energy that would have been stored per unit mass were the building behaving completely elastically, (L^2T^{-2})

U_a is the actual strain energy capacity per unit mass when the yield point is reached. (L^2T^{-2})

Equation (6.2) can be rewritten as follows:

$$U_e = U_a + D \ . \tag{6.3}$$

From Equation (3.10),

$$U_e = \frac{1}{2} \ S_v^2 \tag{6.4}$$

and from Equations (5.3) and (5.9), respectively,

$$U_a = \frac{1}{2} \ q_y x_y \tag{6.5}$$

and

$$D = q_y x_p \ . \tag{6.6}$$

Then, using Equations (6.4), (6.5), and (6.6), Equation (6.3) becomes:

$$\frac{1}{2} S_v^2 = \frac{1}{2} q_y x_y + q_y x_p \ . \tag{6.7}$$

Multiplying both sides of Equation (6.7) by $\frac{2}{q_y x_y}$ gives:

$$\frac{1}{q_y x_y} S_v^2 = 1 + 2 \frac{x_p}{x_y} \tag{6.8}$$

or

$$\frac{1}{q_y x_y} S_v^2 = 2 \frac{x_y + x_p}{x_y} - 1 \ . \tag{6.9}$$

From Figure 10,

$$x_y = \frac{Q_y}{k} \quad . \tag{6.10}$$

In view of Equations (6.10), (4.7), and (3.3),

$$x_y = \frac{q_y m}{k} = q_y \left(\frac{T}{2\pi}\right)^2 \quad . \tag{6.11}$$

Using Equations (6.9) and (6.11),

$$\left(\frac{1}{q_y}\right)^2 \left(\frac{2\pi}{T} S_v\right)^2 = 2 \frac{x_y + x_p}{x_y} - 1 \quad . \tag{6.12}$$

With Equations (3.14) and (6.1) which give, respectively,

$$\frac{2\pi}{T} S_v = Cg$$

and

$$q_y = C_y g \quad ,$$

Equation (6.12) becomes:

$$\left(\frac{C}{C_y}\right)^2 = 2 \frac{x_y + x_p}{x_y} - 1 \quad . \tag{6.13}$$

According to Equation (6.1),

$$\frac{C}{C_y} = \frac{1}{C_r} \quad \text{and} \quad \frac{x_y + x_p}{x_y} = R_d \quad .$$

Hence Equation (6.13) can be rewritten as follows:

$$\left(\frac{1}{C_r}\right)^2 = 2 R_d - 1 \tag{6.14}$$

or

$$C_r = \sqrt{\frac{1}{2 R_d - 1}} \quad . \tag{6.15}$$

From Equation (6.15) C_r was calculated for different values of R_d. Then C_r, the reduction coefficient, was plotted against R_d, the elasto-plastic ductility ratio as shown in Figure 31.

Figure 32 is obtained by superposing the band of Figure 29 over the curve of Figure 31 plotted from Equation (6.15). The new figure shows that the curve of Figure 31 lies within the lower portion of the band.

From Figures 30 and 32, it appears that the reduction coefficient as determined from Equation (6.15), is on the average conservative for the undamped case and for values of damping not exceeding 0.03 of critical damping. But, at levels of damping between 0.03 and 0.20 of critical damping, it appears that the reduction coefficient would be generally conservative if obtained from the upper edge of the band which is given by:

$$C_r = \sqrt{\frac{3}{2 R_d + 1}} \quad . \tag{6.16}$$

In view of the above, if we assume that the load-deflection characteristics of a single-story building can be described by an idealized curve of the elasto-plastic type, then energy absorption through inelastic deformation can be incorporated into strong-motion earthquake-resistant design simply by multiplying the seismic lateral load coefficient obtained from completely elastic dynamic analysis by the reduction coefficient.

Admittedly, the reduction coefficient as determined quantitatively from above has its limitations, since the complex load-deflection characteristics of a building have been described by an idealized curve of the elasto-plastic type. Nevertheless, the use of the reduction-coefficient concept in strong-motion earthquake-resistant design seems realistic and practicable.

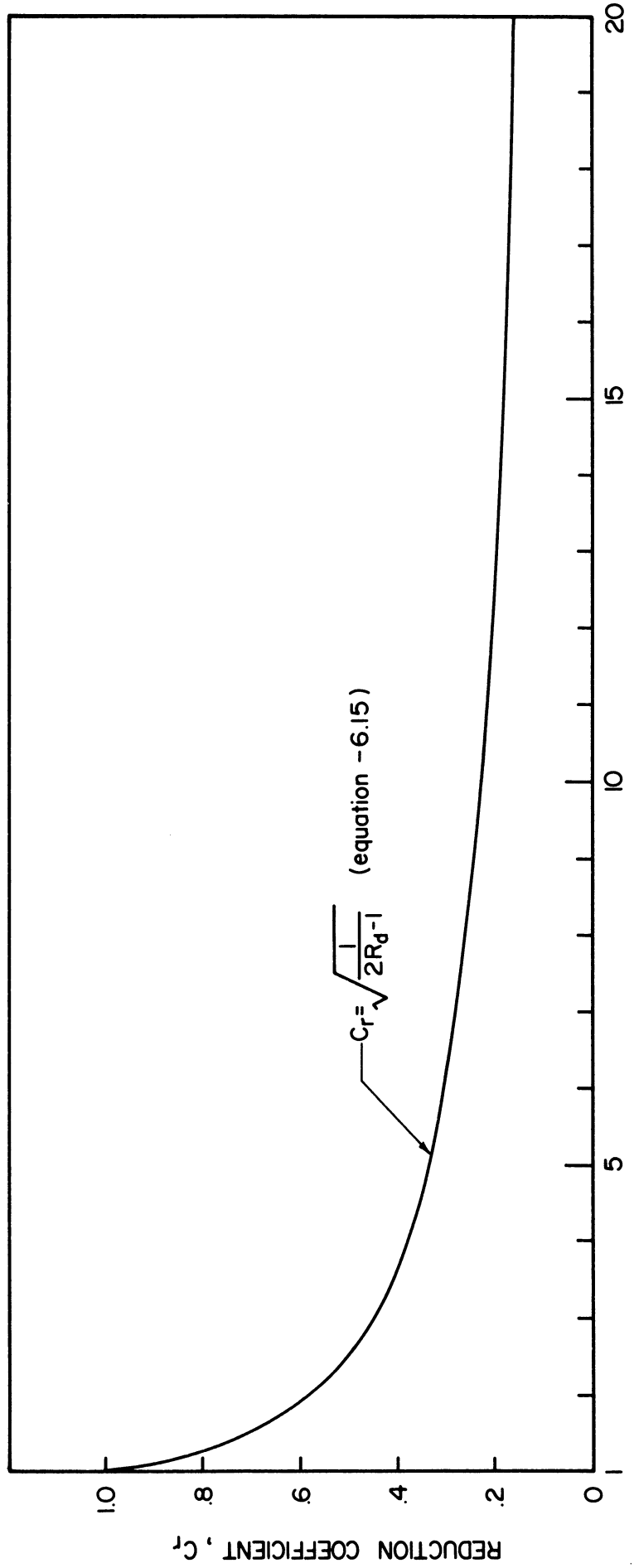

Figure 31. Reduction Coefficient Curve Plotted from Equation (6.15).

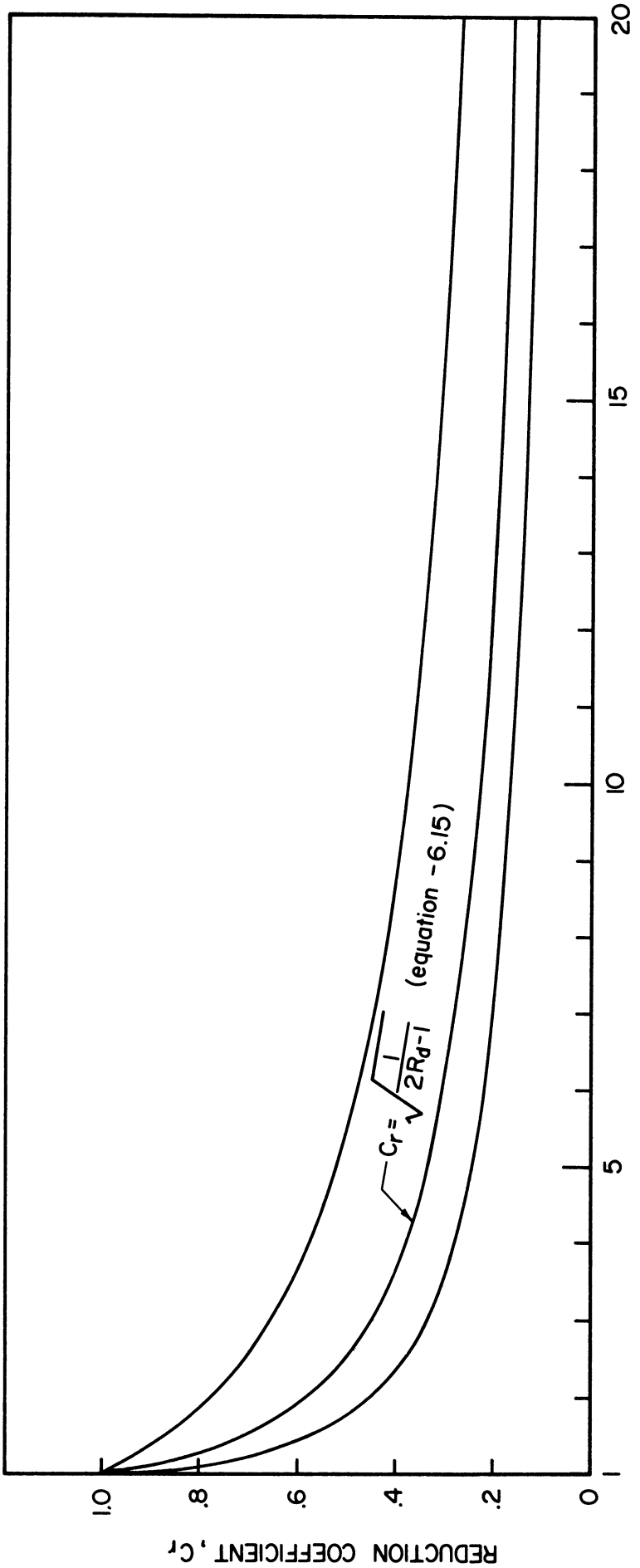

Figure 32. Superposition of the Band of Figure 29 over the Curve Plotted from Equation (6.15).

Experiments have been conducted in the U.S.A. and elsewhere in which structural materials were tested in order to study the relationship between load and deflection at the elastic and inelastic stages of loading.

In experiments conducted at Stanford University,[1,2] the ultimate strength of one-story shear wall panels (plain and reinforced concrete as well as brick) was investigated. Conditions affecting the behavior of the shear wall panels, such as plain or reinforced concrete panels, brick panels with or without boundary frame, and panel proportions, were also investigated. These tests have provided some useful and practical relationships, permitting one to predict approximately the load-deflection relation at the elastic and inelastic phases of loading when these walls are subjected to static unidirectional shear loadings.

In experiments conducted at MIT,[3] the static and dynamic load-deflection relations in the elastic and inelastic stages of loading were investigated for more than 200 reinforced concrete beams simply supported. The beams were loaded at midspan transversely with a static load or a step load representing an idealized dynamic load; after a first downward loading, the beams were turned over and a second downward loading (a reverse loading) was applied. These tests have shown that the reinforced concrete beams had greater resistance to a dynamic loading than to a static loading and that the reverse loading was more critical in the case of a static loading than in the case of a dynamic loading. The dynamic load-deflection curves for the two directions of loading were almost similar.

In experiments conducted at Tokyo University,[3] 25 small models of earthquake-resistant walls (consisting of reinforced concrete panels

monolithically poured with bounding reinforced concrete frames) were tested with the purpose of investigating how the load-deflection curve is affected by varying the amount of reinforcing steel in the panels. For this, the walls were loaded to within the inelastic region and then reverse-loaded to within the negative inelastic region by using static loads; the loading and reverse loading were carried for five half-cycles. Despite a visible cracking in the panels, the yield load was not appreciably lowered in the successive half-cycles, but there was a progressive decrease in the slope with which the yield load was reached. An increase in reinforcing steel was accompanied by an increase in yield strength.

The characteristics of some load-deflection curves obtained from the above and other experiments can be reasonably represented by a curve of the elasto-plastic type, while the characteristics of other load-deflection curves can be only crudely represented by the above type of curve.

In the experimental study of load-deflection relations, structural materials have exhibited pronounced hysteretic properties. However, almost none of the experiments reported to date investigated these hysteretic properties when structural materials are subjected to reverse-loading cycles after the limiting elastic displacement is far exceeded. Therefore, before introducing the reduction-coefficient concept in actual design, more experimental work is needed to determine permissible values of x_p.

CHAPTER VII

AN INVESTIGATION OF THE BEHAVIOR OF SIMPLE BUILDINGS WITH BILINEAR HYSTERESIS DURING EARTHQUAKES

After studying the behavior of simple buildings with elasto-plastic hysteresis, it seemed of interest to investigate the behavior of the same buildings with another type of hysteresis and to compare the results. Idealized bilinear (elastic-strain-hardening) hysteresis, described by the force-displacement curve shown in Figure 33, was chosen for study because it can be a reasonable representation of the load-deflection characteristics of some structural materials and because of its relative simplicity.

Idealized bilinear hysteresis could also describe the over-all response of a steel-framed building with masonry walls when subjected to an earthquake strong enough to cause relative sliding of the masonry blocks[21] (this presupposes that the load-deflection characteristics of the masonry walls can be approximately represented by a curve of the elasto-plastic type with hysteresis upon reversal of strain). In the early part of the response when the amplitude of vibration is small, the steel frame together with the masonry provide the restoring forces. Then, as the amplitude of vibration increases causing relative sliding of the masonry blocks, the burden of providing the restoring forces is thrown upon the steel frame; during this part of the response, although the masonry does not contribute any more to the stiffness of the building, the relative sliding of the blocks (acting perhaps somewhat in the nature of Coulomb frictional forces), will provide an additional source of energy absorption.

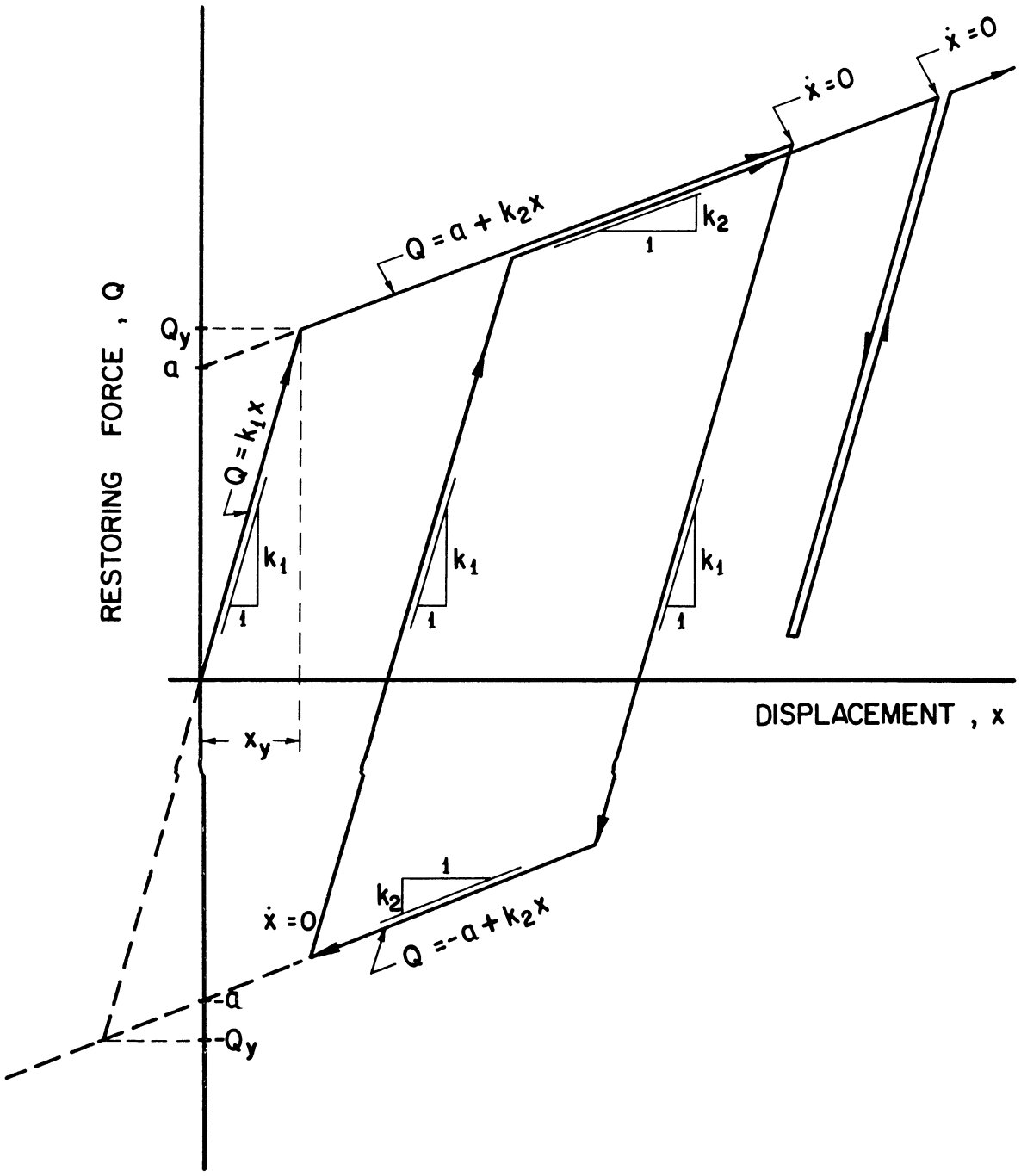

Figure 33. Idealized Force-Displacement Diagram.

For reasons of mathematical convenience and in the absence of information on the behavior of structural materials subjected to reverse-loading cycles after the limiting elastic displacement is far exceeded, it was assumed that a system cannot yield safely when the magnitude of the restoring force Q exceeds twice the value of the yield strength Q_y. Therefore all bilinear analyses were made with the limitation that $|Q|$ was not to exceed $2Q_y$; to this effect the computer was instructed to discontinue the solution whenever $|Q|$ exceeded $2Q_y$, and to proceed to the next solution.

The equations developed in the study of the behavior of simple buildings with elasto-plastic hysteresis were used after certain modifications were made. The equations leading to these modifications are developed below.

Assuming that the strength characteristics of the restoring force Q can be represented by the bilinear curve shown in Figure 33, the restoring force-displacement relations will read as follows.

Let

$$a = Q_y - k_2 x_y$$

then

$$\left.\begin{aligned}
\dot{Q} &= k_1 \dot{x} \quad \text{if} \quad -a + k_2 x < Q < a + k_2 x \\
&\quad \text{or if} \quad Q = a + k_2 x \quad \text{and} \quad \dot{x} < 0 \\
&\quad \text{or if} \quad Q = -a + k_2 x \quad \text{and} \quad \dot{x} > 0 \\
\dot{Q} &= k_2 \dot{x} \quad \text{if} \quad Q = a + k_2 x \quad \text{and} \quad \dot{x} \geq 0 \\
&\quad \text{or if} \quad Q = -a + k_2 x \quad \text{and} \quad \dot{x} \leq 0
\end{aligned}\right\}, \qquad (7.1)$$

where

k_1 is the stiffness in the elastic region (FL^{-1})

and

k_2 is the stiffness in the inelastic region. (FL^{-1})

If we define

$$\left.\begin{aligned} T &= 2\pi\sqrt{\frac{m}{k_1}} = \text{the undamped elastic period} \\ \text{and} \\ \zeta &= \frac{k_2}{k_1} \end{aligned}\right\}, \qquad (7.2)$$

then the foregoing differential relations, reduced to a unit mass basis, will read as follows:

$$\left.\begin{aligned} \dot{q} = \left(\frac{2\pi}{T}\right)^2 \dot{x} \qquad & \text{if} \quad -a + \zeta\left(\frac{2\pi}{T}\right)^2 x < q < a + \zeta\left(\frac{2\pi}{T}\right)^2 x \\ & \text{or if} \quad q = a + \zeta\left(\frac{2\pi}{T}\right)^2 x \quad \text{and} \quad \dot{x} < 0 \\ & \text{or if} \quad q = -a + \zeta\left(\frac{2\pi}{T}\right)^2 x \quad \text{and} \quad \dot{x} > 0 \\ \dot{q} = \zeta\left(\frac{2\pi}{T}\right)^2 \dot{x} \qquad & \text{if} \quad q = a + \zeta\left(\frac{2\pi}{T}\right)^2 x \quad \text{and} \quad \dot{x} \geq 0 \\ & \text{or if} \quad q = -a + \zeta\left(\frac{2\pi}{T}\right)^2 x \quad \text{and} \quad \dot{x} \leq 0 \end{aligned}\right\}. \qquad (7.3)$$

From Figure 33 and the above equation, $\dot{D}$, the rate of energy dissipated through inelastic deformation, has to obey the following relations:

$$\left.\begin{aligned} \dot{D} = 0 \qquad & \text{if} \quad -a + \zeta\left(\frac{2\pi}{T}\right)^2 x < q < a + \zeta\left(\frac{2\pi}{T}\right)^2 x \\ & \text{or if} \quad q = a + \zeta\left(\frac{2\pi}{T}\right)^2 x \quad \text{and} \quad \dot{x} \leq 0 \\ & \text{or if} \quad q = -a + \zeta\left(\frac{2\pi}{T}\right)^2 x \quad \text{and} \quad \dot{x} \geq 0 \\ \dot{D} = (1-\zeta)\left[a+\zeta\left(\frac{2\pi}{T}\right)^2 x\right]\dot{x} \quad & \text{if} \quad q = a + \zeta\left(\frac{2\pi}{T}\right)^2 x \quad \text{and} \quad \dot{x} > 0 \\ \dot{D} = (1-\zeta)\left[-a+\zeta\left(\frac{2\pi}{T}\right)^2 x\right]\dot{x} \quad & \text{if } q = -a + \zeta\left(\frac{2\pi}{T}\right)^2 x \quad \text{and} \quad \dot{x} < 0 \end{aligned}\right\}. \qquad (7.4)$$

Again, to overcome the difficulty caused by the discontinuity of $\dot{q}$ and $\dot{D}$ whenever the system was entering the inelastic region, the differential relations which appear in Equations (7.3) and (7.4) were replaced

by the following equivalent difference relations:

$$
\left.
\begin{aligned}
&\text{If} \quad -a \le q + \left(\frac{2\pi}{T}\right)^2 \Delta x - \zeta\left(\frac{2\pi}{T}\right)^2 (x + \Delta x) \le a \ , \\
&\text{then} \\
&\qquad \Delta q = \left(\frac{2\pi}{T}\right)^2 \Delta x \\
&\text{and} \\
&\qquad \Delta D = 0 \\
&\text{If} \quad q + \left(\frac{2\pi}{T}\right)^2 \Delta x - \zeta\left(\frac{2\pi}{T}\right)^2 (x + \Delta x) > a \ , \\
&\text{then} \\
&\qquad \Delta q = a + \zeta\left(\frac{2\pi}{T}\right)^2 (x + \Delta x) - q \\
&\text{and} \\
&\qquad \Delta D = \left\{q + \Delta q - \frac{\zeta}{2(1-\zeta)} \left(\frac{2\pi}{T}\right)^2 \left[\Delta x - \left(\frac{T}{2\pi}\right)^2 \Delta q\right]\right\} \left[\Delta x - \left(\frac{T}{2\pi}\right)^2 \Delta q\right] \\
&\text{If} \quad q + \left(\frac{2\pi}{T}\right)^2 \Delta x - \zeta\left(\frac{2\pi}{T}\right)^2 (x + \Delta x) < -a \ , \\
&\text{then} \\
&\qquad \Delta q = -a + \zeta\left(\frac{2\pi}{T}\right)^2 (x + \Delta x) - q \\
&\text{and} \\
&\qquad \Delta D = \left\{q + \Delta q - \frac{\zeta}{2(1-\zeta)} \left(\frac{2\pi}{T}\right)^2 \left[\Delta x - \left(\frac{T}{2\pi}\right)^2 \Delta q\right]\right\} \left[\Delta x - \left(\frac{T}{2\pi}\right)^2 \Delta q\right]
\end{aligned}
\right\} \quad . \qquad (7.5)
$$

Bilinear analyses have been made for the N-S component of the El Centro, California, earthquake of May 18, 1940, and the N69°W component of the Taft, California, earthquake of July 21, 1952. The results were plotted against natural period for fixed values of damping and yield level, and for values of ζ varying from 0 (elasto-plastic hysteresis) to 0.25. Only the plots for the El Centro component are shown here because the plots for the Taft component generally follow the same pattern.

Figures 34-40 permit a comparison of the results obtained from the bilinear solutions with those obtained from the elasto-plastic solutions.

The spectral plots of lateral deflection presented in Figure 34 show that, in general, bilinear hysteresis, as compared to elasto-plastic hysteresis, slightly reduces the maximum lateral deflections of systems.

The plots of permanent set presented in Figure 35 show that, in general, the first increment of ζ, from 0 to 0.05, reduces the permanent set effectively. As it was thought that the complete time history of the response of a system might explain this reduction, the complete time history of the response of a number of systems was generated. Among the systems under study, the undamped system of period 1.2 sec responding to the El Centro earthquake was selected as an illustration because a small increment in ζ was accompanied by a large drop in permanent set; its complete responses, elastic, bilinear (with $\zeta = 0.05, 0.25$), and elasto-plastic ($\zeta = 0$), are plotted in Figure 36. These plots show that, as inelastic deformation progresses, the elasto-plastic system oscillates about a position of equilibrium which keeps shifting away from the zero position and in the positive direction while the bilinear system oscillates about a position of equilibrium which meanders less and less as ζ increases. This means that for the elasto-plastic system most of the yielding occurs in the positive inelastic region, whereas for the bilinear system the total inelastic displacements in the positive and negative inelastic regions seem to become nearly equal, which explains the smaller permanent set. From these observations, one could say that, as inelastic deformation progresses, the bilinear system wanders less than the elasto-plastic system, thus causing a smaller permanent set.

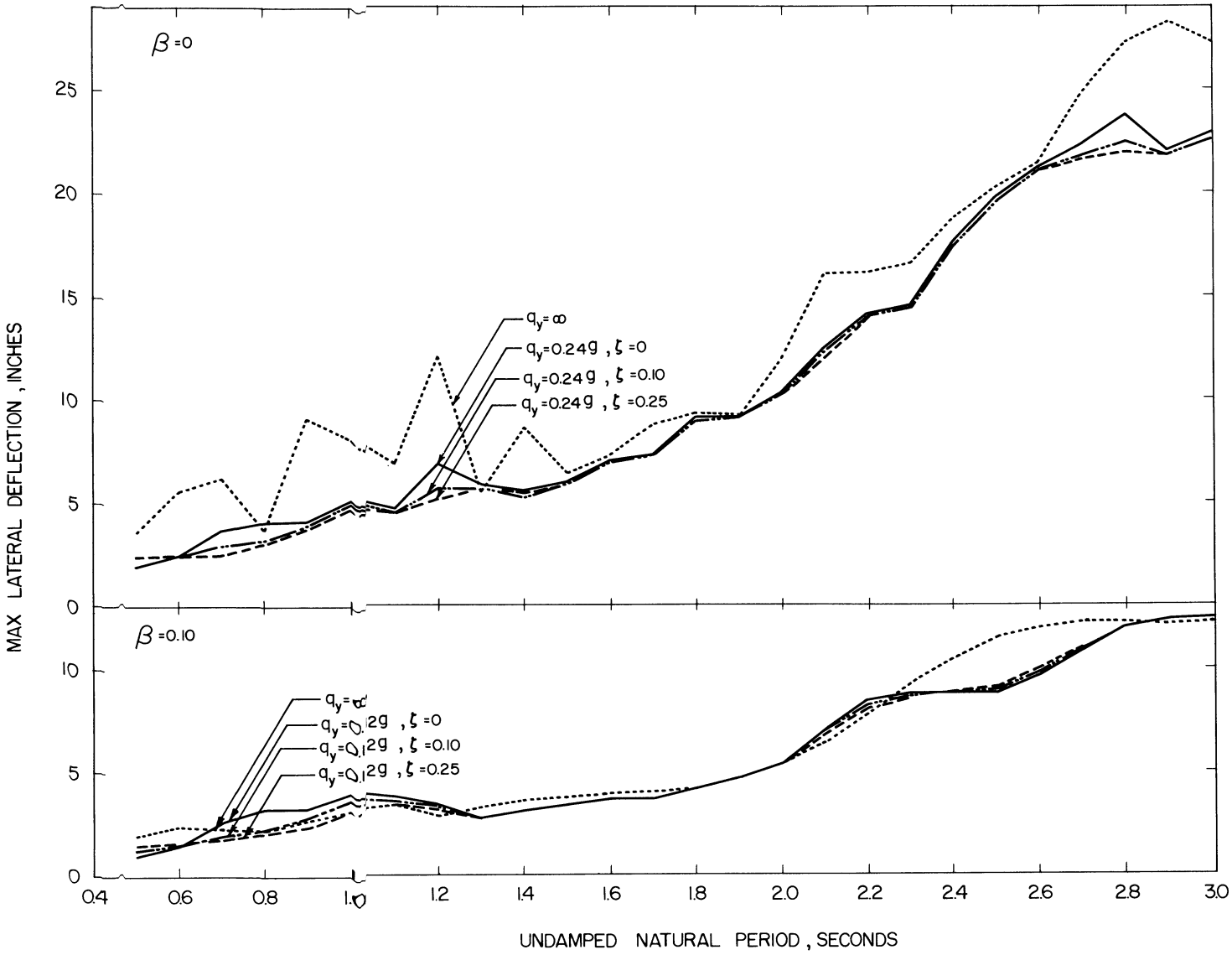

Figure 34. Lateral Deflection Spectrum, El Centro, California, Earthquake of May 18, 1940. Component N-S.

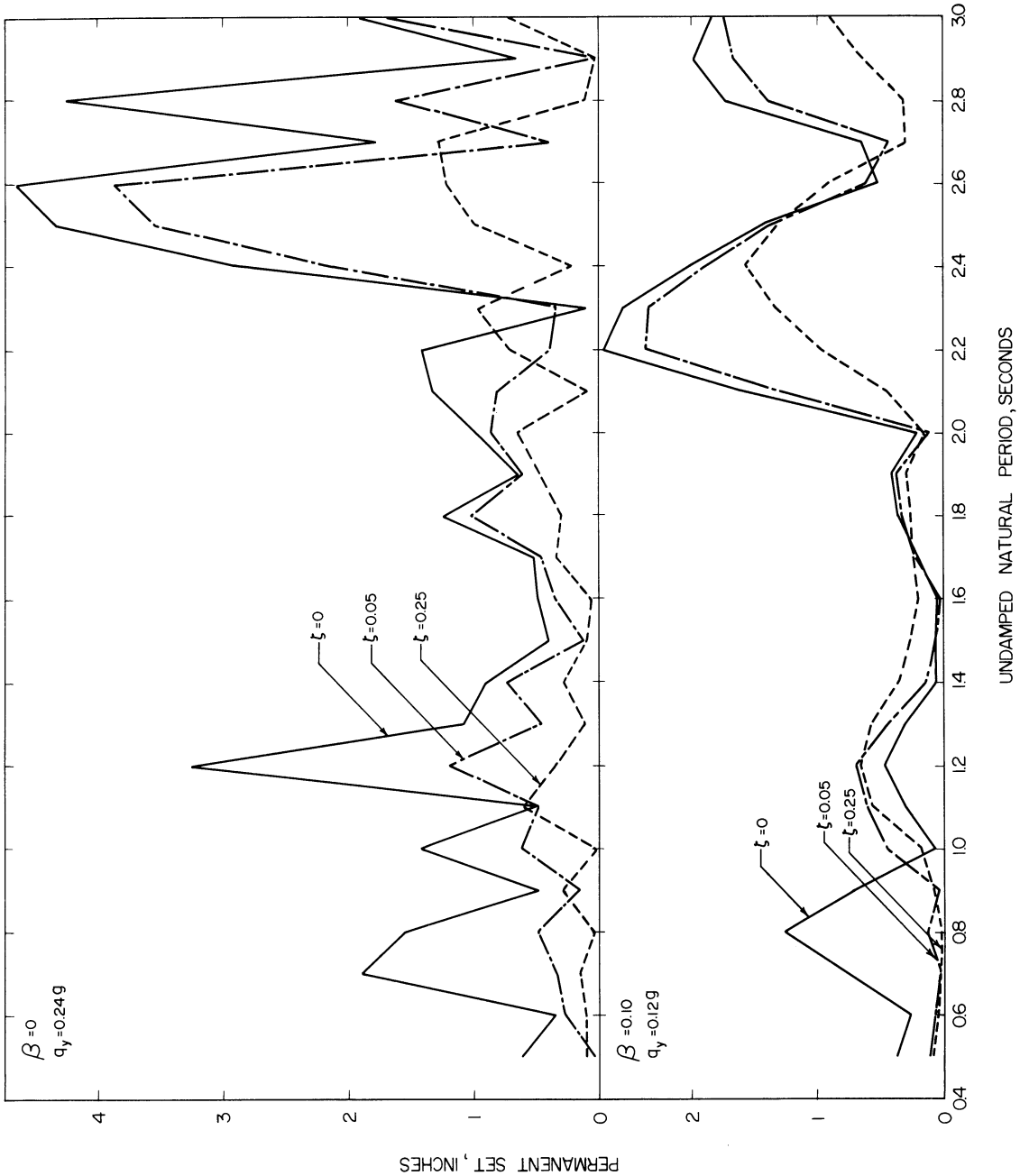

Figure 35. Permanent Sets, El Centro, California, Earthquake of May 18, 1940. Component N-S.

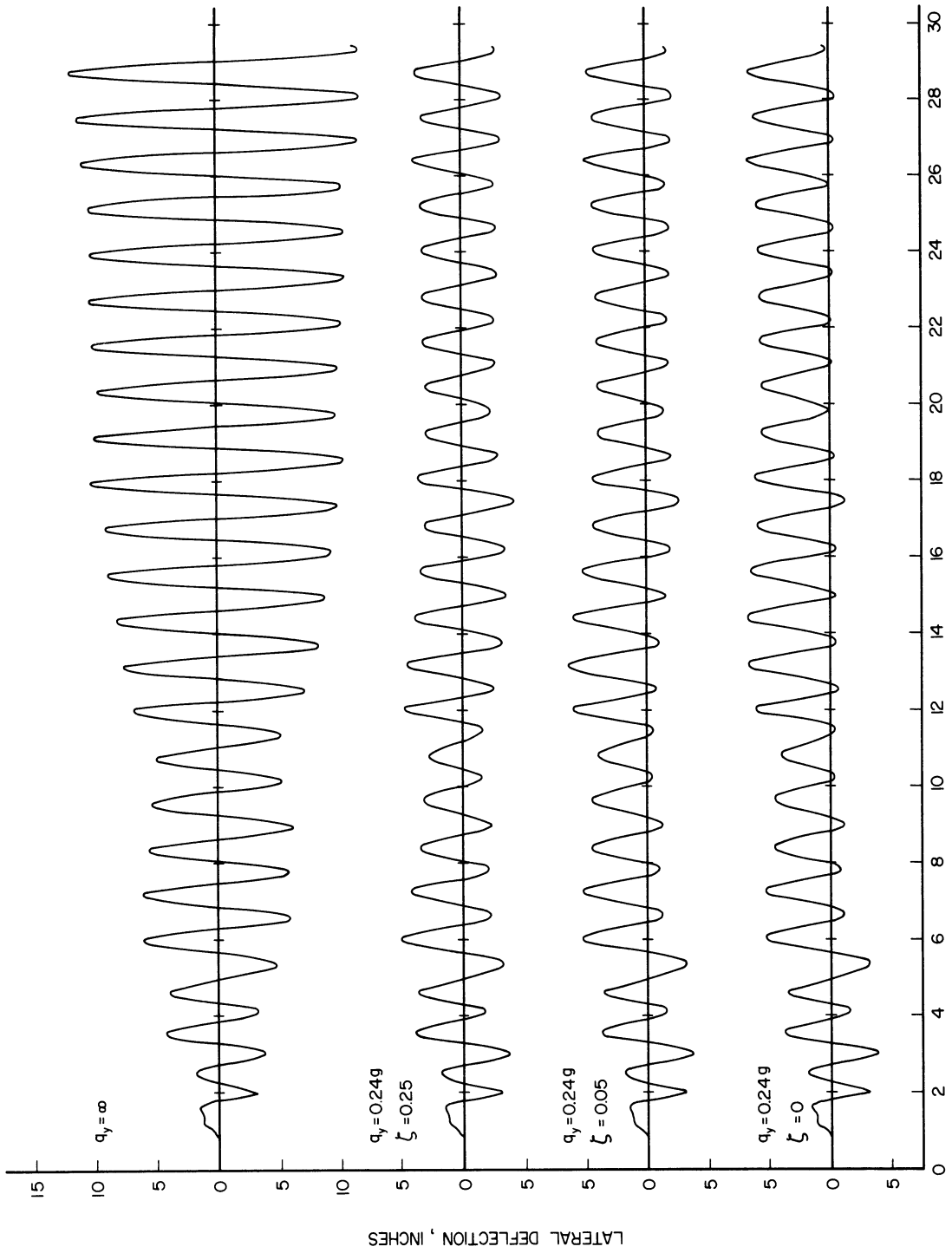

Figure 36. Response of Undamped System with Natural Period 1.2 sec., El Centro, California, Earthquake of May 18, 1940. Component N-S.

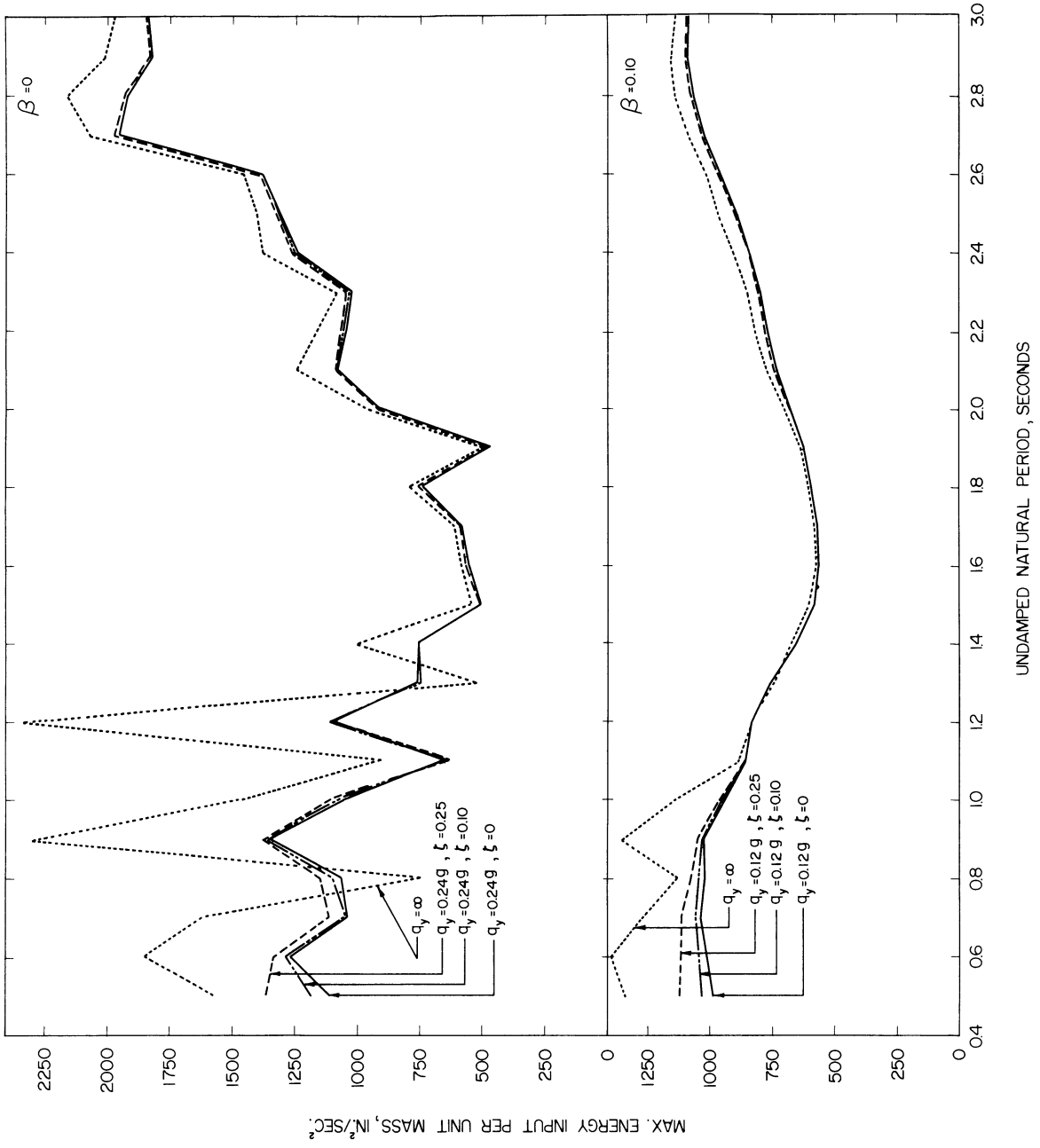

Figure 37. Energy Input Spectrum, El Centro, California, Earthquake of May 18, 1940. Component N-S.

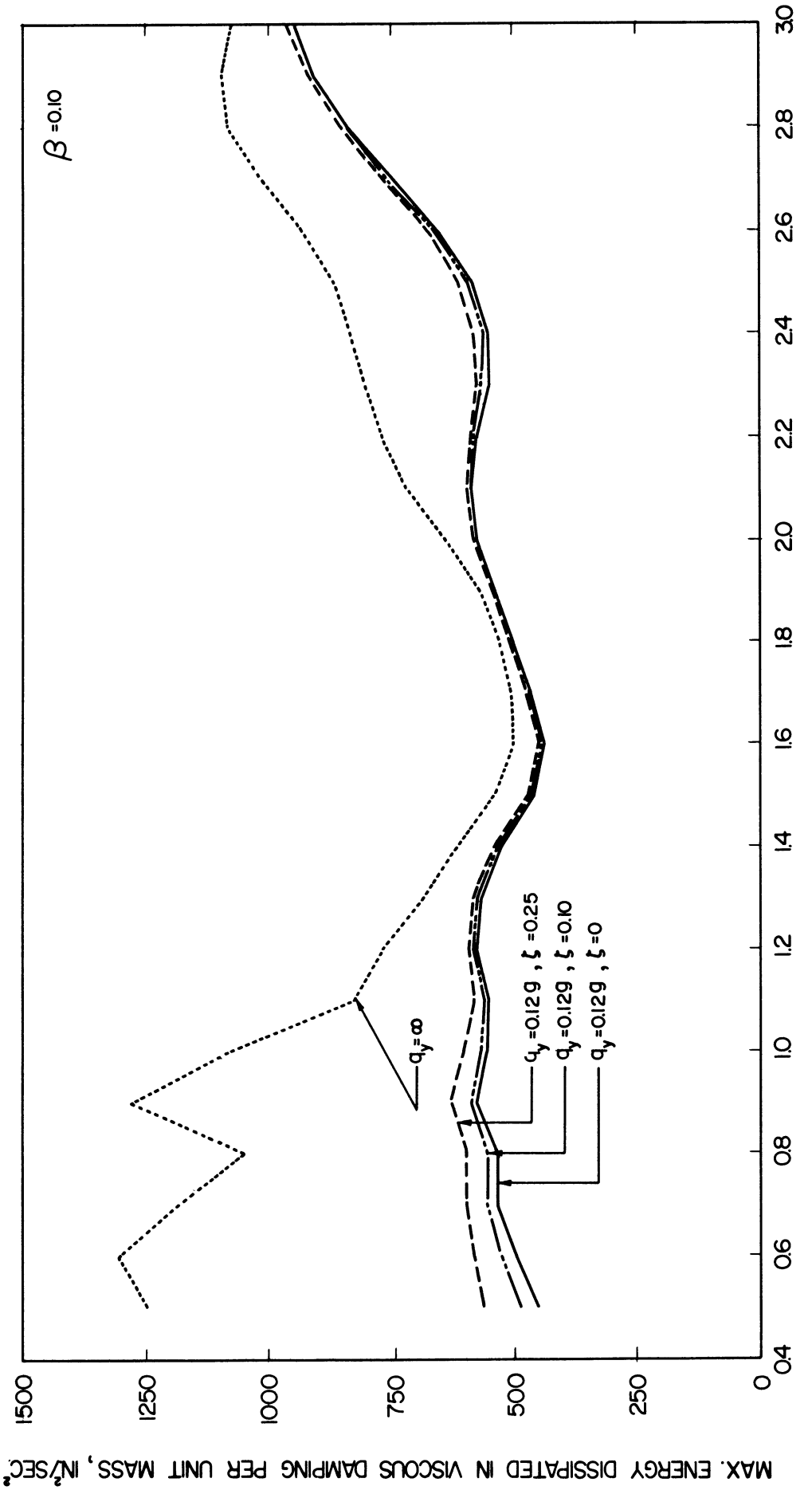

Figure 38. Maximum Energy Dissipated in Viscous Damping, El Centro, California, Earthquake of May 18, 1940. Component N-S.

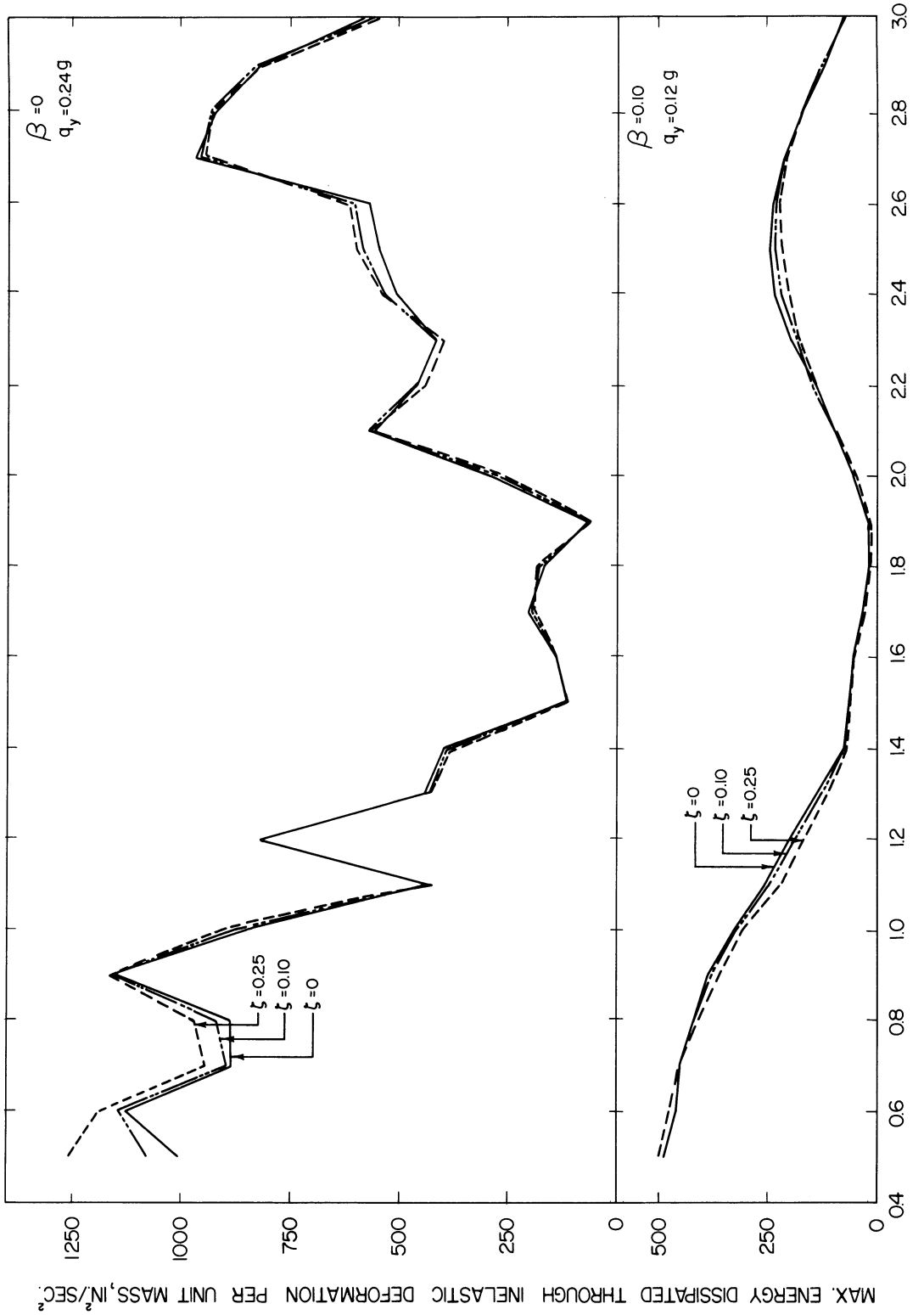

Figure 39. Maximum Energy Dissipated through Inelastic Deformation, El Centro, California, Earthquake of May 18, 1940. Component N-S.

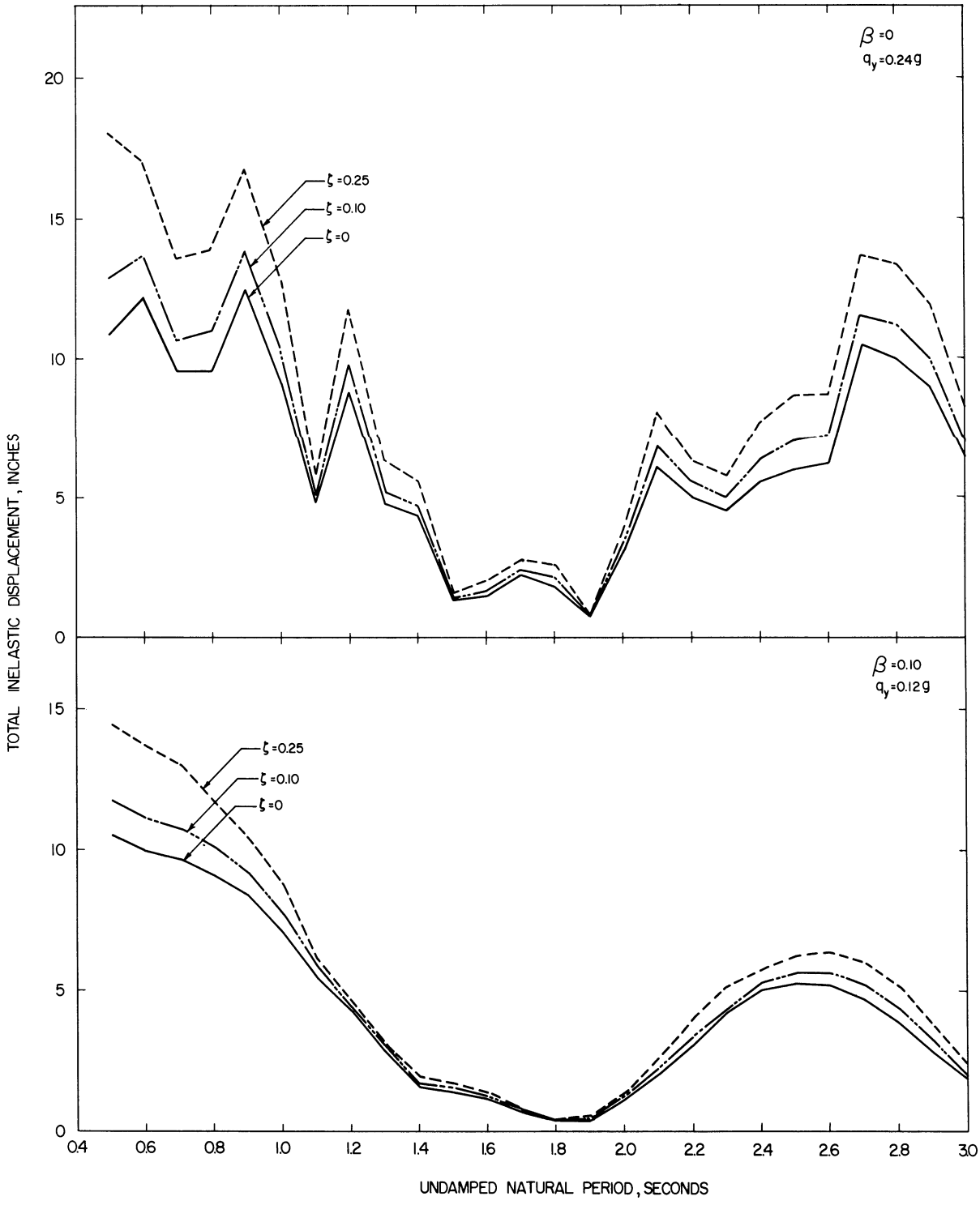

Figure 40. Total Inelastic Displacements, El Centro, California, Earthquake of May 18, 1940. Component N-S.

Incidentally, also in Figure 36, a comparison of elastic with either type of inelastic response shows that inelastic action reduces the magnitude of maximum lateral deflection effectively and the amplitude of oscillation considerably.

The spectral plots of energy input, energy dissipated in viscous damping, and energy dissipated through inelastic deformation presented in Figures 37, 38, and 39 show practically no difference between the energy curves of bilinear systems and the energy curves of elasto-plastic systems.

The plots of total inelastic displacement presented in Figure 40 show that, in general, bilinear hysteresis, as compared to elasto-plastic hysteresis, increases the total inelastic displacement.

The maximum magnitude attained by q in bilinear solutions of a number of systems was used as yield level to run elasto-plastic solutions for the same systems, as shown in Figure 41. The results, together with the results obtained from the corresponding bilinear solutions, are tabulated in Tables I and II. A comparison of the results obtained from the elasto-plastic solutions with those obtained from the bilinear solutions shows that in general the elasto-plastic solutions generated slightly larger values of energy input and lateral deflections, larger permanent sets, but smaller total inelastic displacements.

As bilinear analyses were made for only two earthquake components and limited combinations of structural parameters, no broad conclusions can be drawn from the above observations. Nevertheless, for the particular examples used in these analyses, there is practically no difference between bilinear hysteresis (in which the yield strength of a system keeps increasing within a certain limit) and elasto-plastic hysteresis (in which the yield strength of a system remains constant).

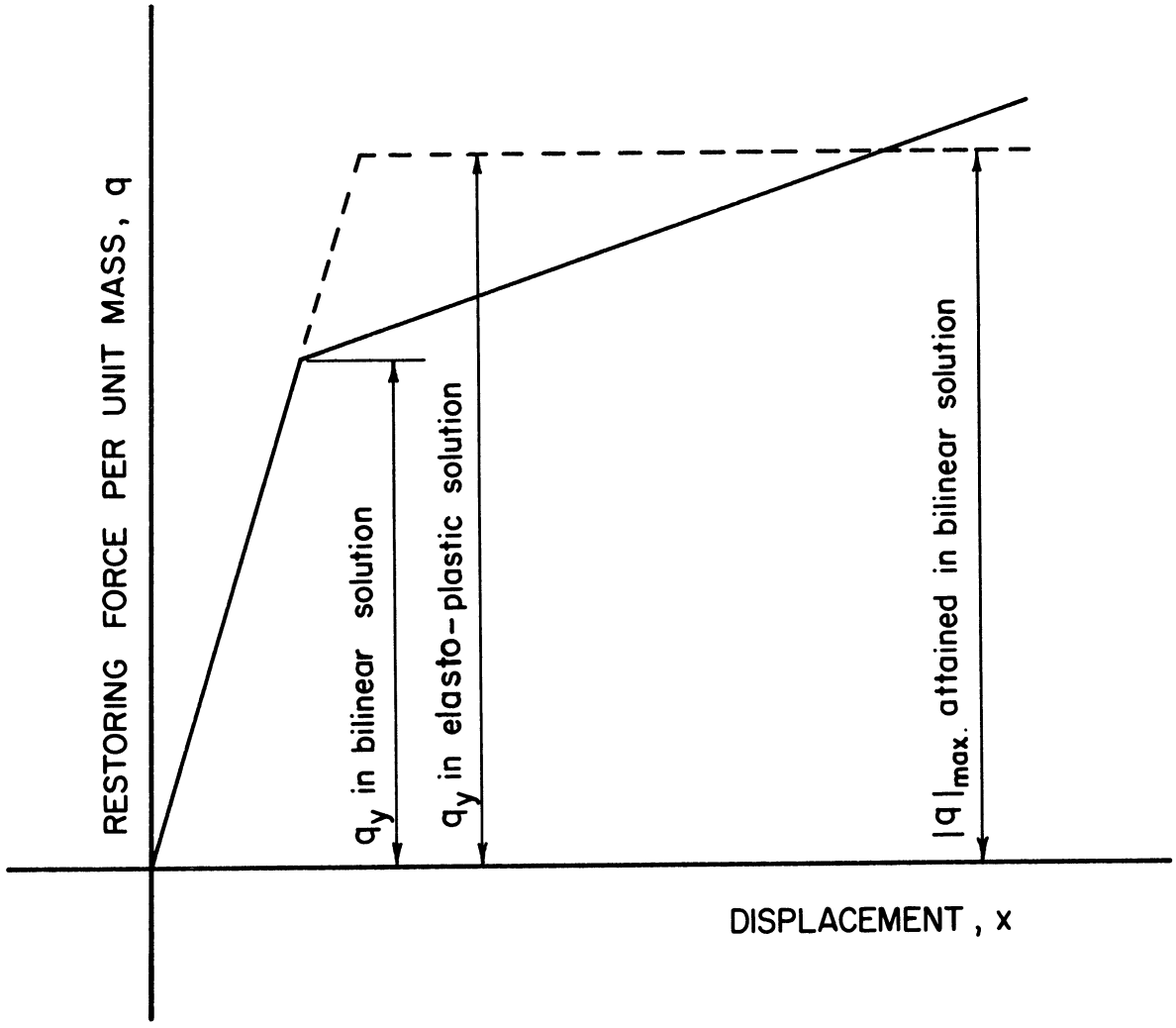

Figure 41. Elasto-Plastic Solution with q_y Equal to the Maximum Magnitude of q Attained in the Bilinear Solution.

TABLE I

RESPONSE OF ELASTO-PLASTIC AND BLLINEAR
UNDAMPED SYSTEMS TO EL CENTRO EARTHQUAKE

T sec	BILINEAR SOLUTION, $\zeta = .10$ $\beta = 0$, $q_y = .24$ g					ELASTO-PLASTIC SOLUTION $\beta = 0$				
	$\lvert q \rvert_{max}$ in/sec^2	E_{max} in^2/sec^2	$\lvert x \rvert_{max}$ in.	$\lvert x_r \rvert$ in.	x_p in.	q_y in/sec^2	E_{max} in^2/sec^2	$\lvert x \rvert_{max}$ in.	$\lvert x_r \rvert$ in.	x_p in.
.50	.295 g	1184	1.93	.04	12.89	.295 g	1159	1.97	.45	9.00
.60	.285 g	1283	2.44	.16	13.66	.285 g	1400	2.72	.39	11.13
.70	.276 g	1051	2.87	.07	10.67	.276 g	1102	3.30	1.29	8.49
.80	.266 g	1101	3.13	.13	10.99	.266 g	1074	3.36	.32	8.41
.90	.265 g	1354	3.90	.25	13.78	.265 g	1431	4.03	.46	11.83
1.00	.266 g	1077	4.91	.29	10.31	.266 g	1095	4.95	1.72	8.19
1.20	.256 g	1115	5.64	.47	9.77	.256 g	1169	7.21	3.52	8.54
1.40	.243 g	757	5.26	.59	4.63	.243 g	760	5.44	.79	4.16
1.60	.244 g	561	6.96	.23	1.65	.244 g	562	6.96	.38	1.33
1.80	.244 g	752	9.00	.80	2.06	.244 g	753	9.05	1.10	1.63
2.00	.242 g	916	10.26	.79	3.33	.242 g	916	10.47	1.01	2.98

TABLE II

RESPONSE OF ELASTO-PLASTIC AND BILINEAR
DAMPED SYSTEMS TO EL CENTRO EARTHQUAKE

T sec	BILINEAR SOLUTION, ζ = .10 β = .10, q_y = .12 g					ELASTO-PLASTIC SOLUTION β = .10				
	$\lvert q \rvert_{max}$ in /sec^2	E_{max} in^2/sec^2	$\lvert x \rvert_{max}$ in.	$\lvert x_r \rvert$ in.	x_p in.	q_y in /sec^2	E_{max} in^2/sec^2	$\lvert x \rvert_{max}$ in.	$\lvert x_r \rvert$ in.	x_p in.
.50	.160 g	1030	1.27	.0	11.78	.160 g	1042	1.31	.06	7.44
.60	.149 g	1045	1.44	.06	11.10	.149 g	1076	1.57	.05	7.66
.70	.148 g	1061	1.92	.08	10.76	.148 g	1092	2.24	.38	7.20
.80	.144 g	1043	2.27	.08	10.09	.144 g	1073	3.59	1.78	7.33
.90	.143 g	1027	2.78	.11	9.16	.143 g	1081	3.05	.83	6.86
1.00	.145 g	942	3.66	.51	7.70	.145 g	995	3.58	.31	5.36
1.20	.131 g	827	3.26	.82	4.41	.131 g	838	3.19	.77	3.46
1.40	.124 g	652	3.05	.21	1.72	.124 g	652	3.04	.14	1.46
1.60	.122 g	558	3.57	.07	1.21	.122 g	557	3.57	.01	1.04
1.80	.121 g	587	4.15	.31	.35	.121 g	587	4.15	.31	.31
2.00	.122 g	676	5.29	.03	1.16	.122 g	677	5.22	.01	.89

CHAPTER VIII

AN INVESTIGATION OF THE EFFECT OF INELASTIC ACTION ON THE BEHAVIOR OF MULTI-STORY BUILDINGS SUBJECTED TO EARTHQUAKES

The investigations described in the preceding chapters were restricted to one-story buildings. To see whether inelastic action has similar effects on the behavior of multi-story buildings, an attempt was made to extend the study to multi-story idealized shear buildings.

In this investigation the following simplifying assumptions were made:

1. The building is rigidly built upon a firm ground.
2. The masses of the building are concentrated at the respective floor levels.
3. The floors are infinitely rigid, whereas the columns are relatively flexible; therefore all lateral deformation of the building is due to the flexure of the columns.
4. The shear resistance-deflection characteristics within each story can be represented by an idealized curve. Two types of curves were considered: the elasto-plastic and the bilinear.
5. The damping forces in the building are viscous; the coefficient of viscous damping is a linear combination of the mass and stiffness. It is also assumed that the fractions of critical damping are equal in the first and second modes.

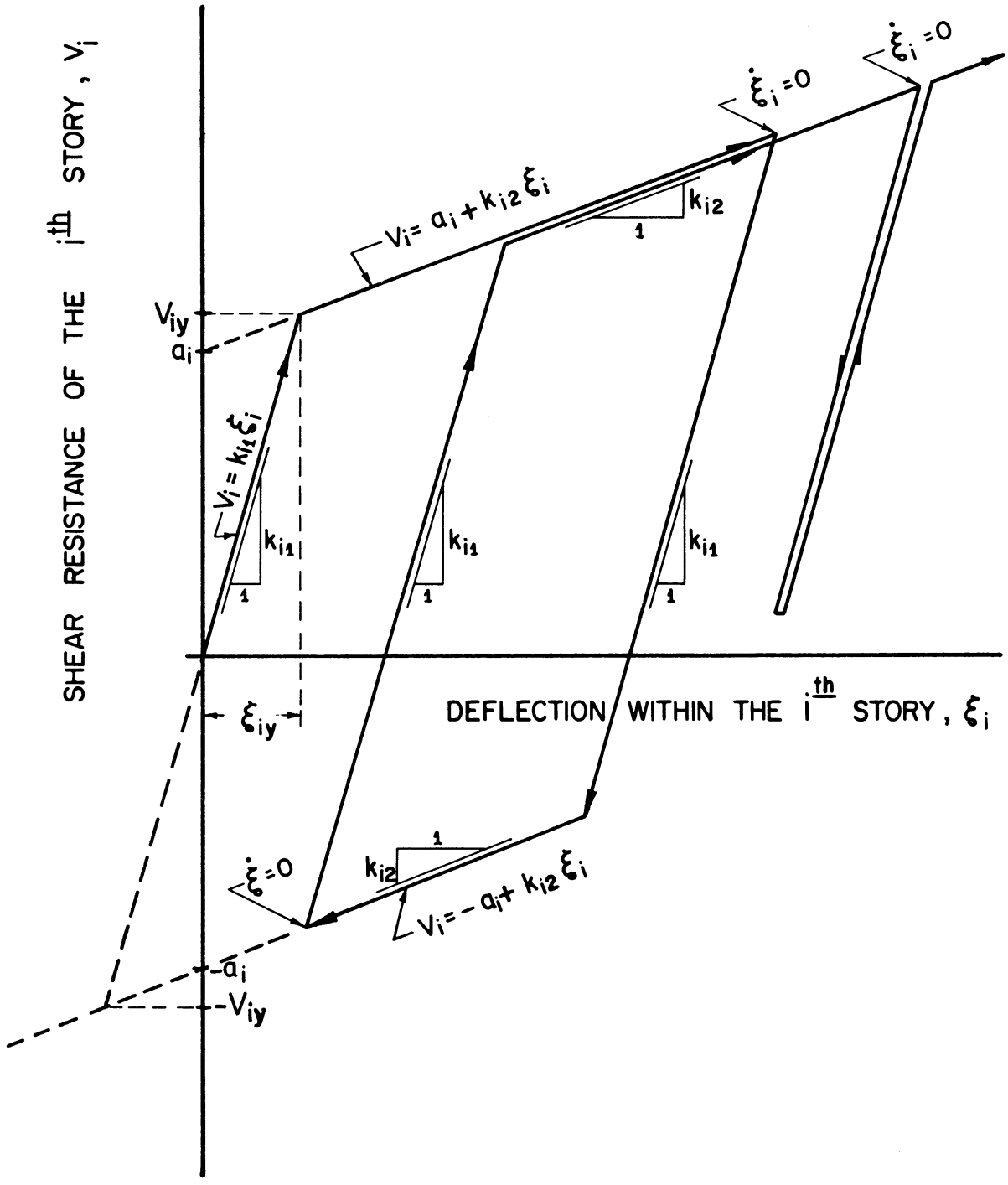

Figure 42. Idealized Shear-Deflection Diagram.

Assuming that the shear resistance-deflection characteristics within each story can be represented by a curve of the elasto-plastic type or the bilinear type (the elasto-plastic type being a special case of the bilinear type when $k_2 = 0$), as shown in Figure 42, then the shear resistance-deflection relations for the i-th story will read as follows.

Let

$$a_i = V_{iy} - k_{i2}\xi_{iy}$$

then

$$\left.\begin{aligned}
\dot{V}_i &= k_{i1}\dot{\xi}_i \quad \text{if} \quad -a_i + k_{i2}\xi_i < V_i < a_i + k_{i2}\xi_i \\
&\quad \text{or if} \quad V_i = a_i + k_{i2}\xi_i \quad \text{and} \quad \dot{\xi}_i < 0 \\
&\quad \text{or if} \quad V_i = -a_i + k_{i2}\xi_i \quad \text{and} \quad \dot{\xi}_i > 0 \\
\dot{V}_i &= k_{i2}\dot{\xi}_i \quad \text{if} \quad V_i = a_i + k_{i2}\xi_i \quad \text{and} \quad \dot{\xi}_i \geq 0 \\
&\quad \text{or if} \quad V_i = -a_i + k_{i2}\xi_i \quad \text{and} \quad \dot{\xi}_i \leq 0
\end{aligned}\right\} , \quad (8.1)$$

where

$$\xi_i = x_i - x_{i-1}$$

and where

V_{iy} is the yield shear strength of the i-th story, (F)

V_i is the shear resistance of the i-th story, a function of time, (F)

k_{i1} is the stiffness of the i-th story when in the elastic region, (FL^{-1})

k_{i2} is the stiffness of the i-th story when in the inelastic region, (FL^{-1})

x_i is the lateral displacement of the i-th floor level relative to the ground, a function of time, (L)

ξ_i is the lateral deflection within the i-th story, a function of time, (L)

ξ_{iy} is the limiting elastic lateral deflection within the i-th story, (L)

and dots denote differentiation with respect to time.

If Q_i is the resistance force exerted on m_i, the concentrated mass at the i-th floor level, then

$$Q_i = V_i - V_{i+1} \, . \tag{8.2}$$

If P_i is the damping force exerted on m_i, then, based on assumption 5,

$$P_i = \alpha m_i \dot{x}_i + \gamma [k_{i1}(\dot{x}_i - \dot{x}_{i-1}) - k_{(i+1)1}(\dot{x}_{i+1} - \dot{x}_i)] \, , \tag{8.3a}$$

where α is a constant of dimension T^{-1} and γ is a constant of dimension T. Under the assumption that the fractions of critical damping are equal in the first and second modes, the constants α and γ can be obtained from:(5)

$$\left.\begin{aligned} \alpha &= \frac{4\pi}{T_1 + T_2}\beta \\ \gamma &= \frac{T_1 T_2}{\pi(T_1 + T_2)}\beta \end{aligned}\right\} \, , \tag{8.3b}$$

where

T_1 is the fundamental (first-mode) elastic period (T)

and

T_2 is the second-mode elastic period. (T)

If R_i is the restoring force exerted on m_i, then, in view of Equations (8.2) and (8.3a),

$$R_i = \alpha m_i \dot{x}_i + \gamma [k_{i1}(\dot{x}_i - \dot{x}_{i-1}) - k_{(i+1)1}(\dot{x}_{i+1} - \dot{x}_i)] + V_i - V_{i+1} \tag{8.4}$$

and the equation of motion for the lateral displacement of the i-th floor level will read as follows:

$$m_i(\ddot{x}_i+\ddot{y}) + \alpha m_i\dot{x}_i + \gamma[k_{i1}(\dot{x}_i-\dot{x}_{i-1}) - k_{(i+1)1}(\dot{x}_{i+1}-\dot{x}_i)] + V_i - V_{i+1} = 0 \ . \quad (8.5)$$

If $f(t)$ is the force exerted on the structure by the foundation, then

$$f(t) = -[\alpha \sum_{i=1}^{N} m_i\dot{x}_i + \gamma k_{11}\dot{x}_1 + V_1] \quad (8.6)$$

and the energy input is

$$E(t) = -\int_0^t [\alpha \sum_{i=1}^{N} m_i\dot{x}_i + \gamma k_{11}\dot{x}_1 + V_1]\,\dot{y}\,d\tau \ . \quad (8.7)$$

The strain energy is

$$U(t) = \frac{1}{2}\sum_{i=1}^{N}\frac{V_i^2}{k_{i1}} \ . \quad (8.8)$$

The kinetic energy is

$$K(t) = \frac{1}{2}\sum_{i=1}^{N} m_i(\dot{x}_i + \dot{y})^2 \ . \quad (8.9)$$

The energy dissipated through viscous damping is

$$L(t) = \int_0^t \left\{ \sum_{i=1}^{N} \{\alpha m_i\dot{x}_i^2 + \gamma[k_{i1}(\dot{x}_i-\dot{x}_{i-1}) - k_{(i+1)1}(\dot{x}_{i+1}-\dot{x}_i)]\dot{x}_i\} \right\} d\tau \ . \quad (8.10)$$

$\dot{D}_i$, the rate of energy dissipated through inelastic deformation in the i-th story, has to obey the following relations:

$$
\begin{aligned}
\dot{D}_i &= 0 && \text{if } -a_i + k_{i2}\xi_i < V_i < a_i + k_{i2}\xi_i \\
& && \text{or if } V_i = a_i + k_{i2}\xi_i \text{ and } \dot{\xi}_i \leq 0 \\
& && \text{or if } V_i = -a_i + k_{i2}\xi_i \text{ and } \dot{\xi}_i \geq 0 \\
\dot{D}_i &= (1-\zeta_i)(a_i+k_{i2}\xi_i)\dot{\xi}_i && \text{if } V_i = a_i + k_{i2}\xi_i \text{ and } \dot{\xi}_i > 0 \\
\dot{D}_i &= (1-\zeta_i)(-a_i+k_{i2}\xi_i)\dot{\xi}_i && \text{if } V_i = -a_i + k_{i2}\xi_i \text{ and } \dot{\xi}_i < 0
\end{aligned}
\qquad \cdot \quad (8.11)
$$

where by definition

$$\zeta_i = \frac{k_{i2}}{k_{i1}}$$

Again, to adapt the equation of motion to the Runge-Kutta procedure of numerical integration, the second-order differential equation was replaced by two simultaneous first-order differential equations. In view of this adjustment, let

$$
\begin{aligned}
&\dot{x}_i = v_i \\
&\text{then} \\
&\dot{v}_i = \ddot{x}_i = -\left\{\ddot{y}+\alpha v_i + \frac{\gamma}{m_i}[k_{i1}(v_i-v_{i-1})-k_{(i+1)1}(v_{i+1}-v_i)] + \frac{1}{m_i}(V_i-V_{i+1})\right\}
\end{aligned}
\qquad \cdot \quad (8.12)
$$

The energy integrals (8.7) and (8.10) were adapted to the Runge-Kutta procedure by replacing each energy integral by its rate of change. From Equation (8.12)

$$\dot{x}_i = v_i$$

and if we define

$$\dot{y} = z \ ,$$

then

$$
\begin{aligned}
\dot{E} &= -\left[\alpha \sum_{i=1}^{N} m_i v_i + \gamma k_{11} v_1 + V_1\right] z \\
\dot{L} &= \sum_{i=1}^{N} \left\{\alpha m_i v_i^2 + \gamma[k_{i1}(v_i-v_{i-1}) - k_{(i+1)1}(v_{i+1}-v_i)]\, v_i\right\}
\end{aligned}
\qquad . \quad (8.13)
$$

To overcome the difficulty caused by the discontinuity of $\dot{V}_i$ and $\dot{D}_i$ whenever the i-th story was entering the inelastic region, the differential relations of Equations (8.1) and (8.11) were replaced by the following equivalent difference relations:

If

$$-a_i \leq V_i + k_{il}\Delta\xi_i - \zeta_i k_{il}(\xi_i+\Delta\xi_i) \leq a_i \quad ,$$

then

$$\Delta V_i = k_{il}\Delta\xi_i$$

and

$$\Delta D_i = 0$$

If

$$V_i + k_{il}\Delta\xi_i - \zeta_i k_{il}(\xi_i + \Delta\xi_i) > a_i \quad ,$$

then

$$\Delta V_i = a_i + \zeta_i k_{il}(\xi_i + \Delta\xi_i) - V_i$$

and

$$\Delta D_i = [V_i + \Delta V_i - \frac{\zeta_i k_{il}}{2(1-\zeta_i)} (\Delta\xi_i - \frac{\Delta V_i}{k_{il}})](\Delta\xi_i - \frac{\Delta V_i}{k_{il}})$$

If

$$V_i + k_{il}\Delta\xi_i - \zeta_i k_{il}(\xi_i + \Delta\xi_i) < - a_i \quad ,$$

then

$$\Delta V_i = -a_i + \zeta_i k_{il}(\xi_i + \Delta\xi_i) - V_i$$

and

$$\Delta D_i = [V_i + \Delta V_i - \frac{\zeta_i k_{il}}{2(1-\zeta_i)} (\Delta\xi_i - \frac{\Delta V_i}{k_{il}})](\Delta\xi_i - \frac{\Delta V_i}{k_{il}})$$

. (8.14)

Without affecting the above developed equations, the following additional assumptions were made: all stories of the building have equal

height; all masses of the building concentrated at the respective floor levels are equal; k_1, the stiffness in the elastic region and V_y, the yield shear strength, vary along the height of the building at the same rate.

As prescribed by some current building codes, the base yield shear strength V_{iy} was distributed over the floor levels of the building in proportion to the product of the mass at each level times its height above the ground, and then from this distribution the yield shear strength was established along the height of the building. This and the above assumptions yielded a triangular first-mode shape.

Based on the above, if m is the mass concentrated at each floor level, for a given fundamental period T_1 and for a given number of stories N, the ratio $\frac{k_{11}}{m}$ was obtained from:

$$\frac{k_{11}}{m} = \frac{N(N+1)}{2} \left(\frac{2\pi}{T_1}\right)^2 \quad , \tag{8.15}$$

and the values of k_{i1} $(i=2,3,\ldots,N)$ and V_{iy} $(i=2,3,\ldots,N)$ were obtained in terms of k_{11} and V_{1y}, respectively, from:

$$\left.\begin{aligned} k_{i1} &= \left(1 - \frac{i(i-1)}{N(N+1)}\right) k_{11} \quad (i=2,3,\ldots,N) \\ V_{iy} &= \left(1 - \frac{i(i-1)}{N(N+1)}\right) V_{1y} \quad (i=2,3,\ldots,N) \end{aligned}\right\} \quad . \tag{8.16}$$

In this investigation, four-story idealized shear buildings with elasto-plastic or bilinear hysteresis were considered. Analyses were made for the N-S component of the El Centro, California, earthquake of May 18, 1940, for different values of T_1, β, r (r denoting the ratio of the base yield shear strength to the total weight of the building),

and ζ. The results plotted against T_1 are shown in the figures which follow.

Figure 43 presents spectral plots of lateral deflection within each story and permits a comparison of the deflections calculated from elasto-plastic behavior with the corresponding ones calculated from completely elastic behavior ($r = \infty$). This comparison shows that, on the average, a decrease in r is not accompanied by an increase in lateral deflection until r gets below 0.06. The same figure shows that damping reduces lateral deflections effectively for all values of r.

Figure 44 presents plots of the permanent set within each story, resulting from elasto-plastic action. The permanent sets corresponding to $r = 0.06$ with $\beta = 0.05$ (a possible value encountered in actual multi-story buildings) seem to be within acceptable limits.

Figure 45 presents spectral plots of energy input per unit mass and permits a comparison of the values of maximum energy input calculated from elasto-plastic behavior with the corresponding values calculated from completely elastic behavior. This comparison shows that, in general, a decrease in r is accompanied by a decrease in energy input.

Figure 46 presents spectral plots of energy input per unit mass and of total energy dissipated per unit mass. In this figure the curves obtained from four-story elasto-plastic buildings are drawn in solid line and the curves obtained from one-story elasto-plastic buildings are drawn in dotted line. A comparison of the two sets of curves shows that the curves of four-story buildings are in general above those of one-story buildings, but qualitatively they are closely similar; when r gets as low as 0.03, the curves tend to agree also quantitatively.

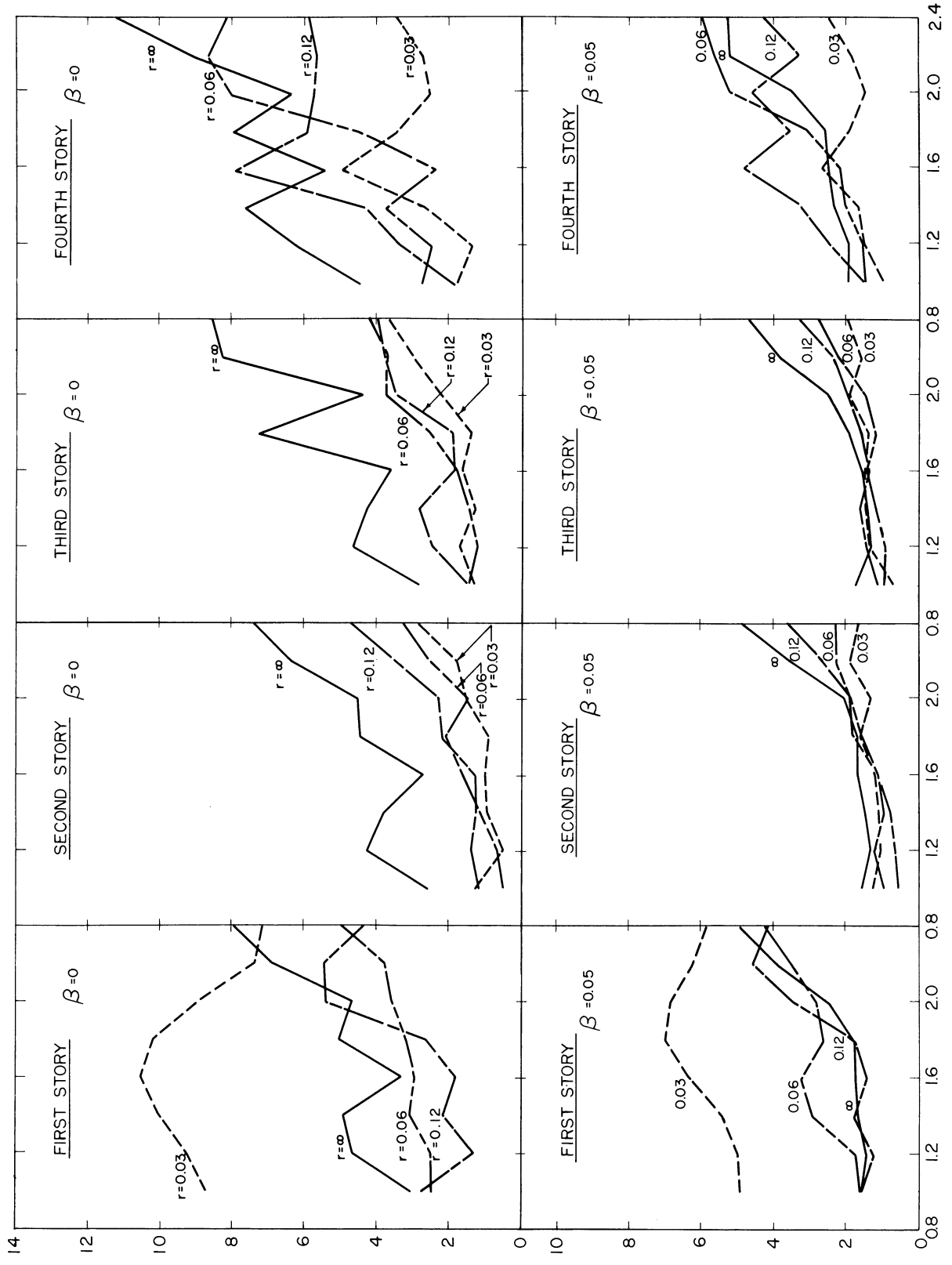

Figure 43. Lateral Deflection Spectra, El Centro, California, Earthquake of May 18, 1940. Component N-S.

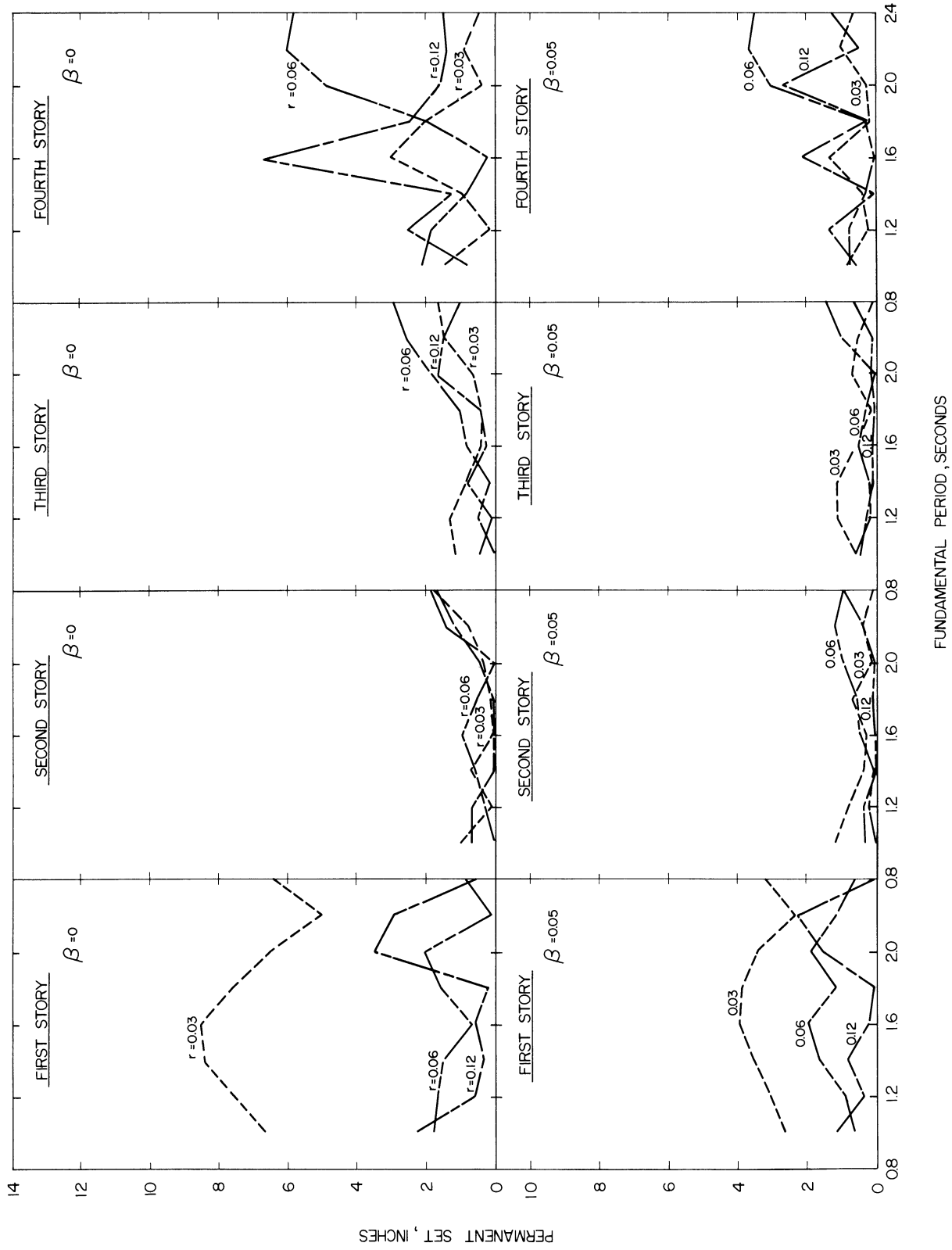

Figure 44. Permanent Sets, El Centro, California, Earthquake of May 18, 1940. Component N-S.

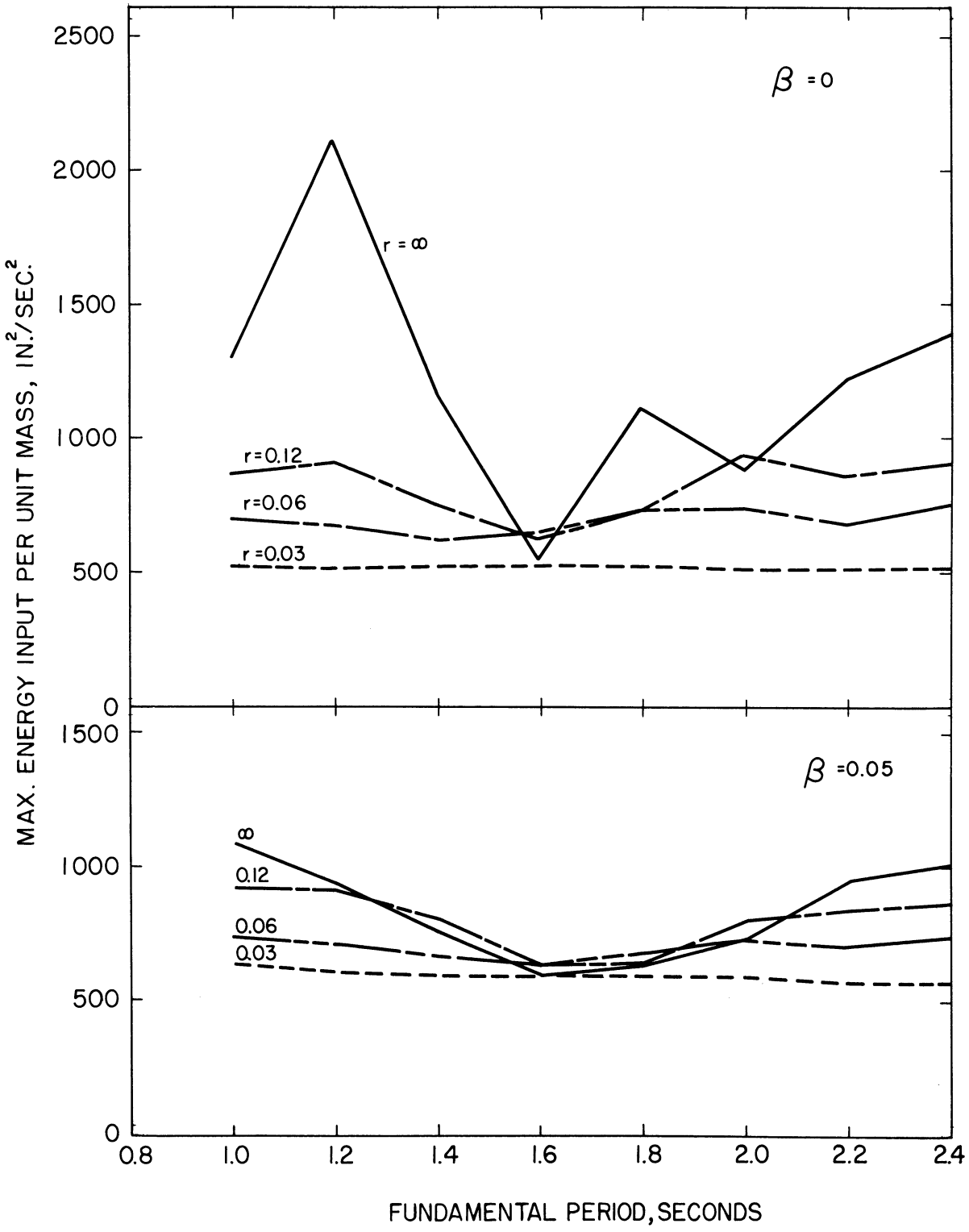

Figure 45. Energy Input Spectrum, El Centro, California, Earthquake of May 18, 1940. Component N-S.

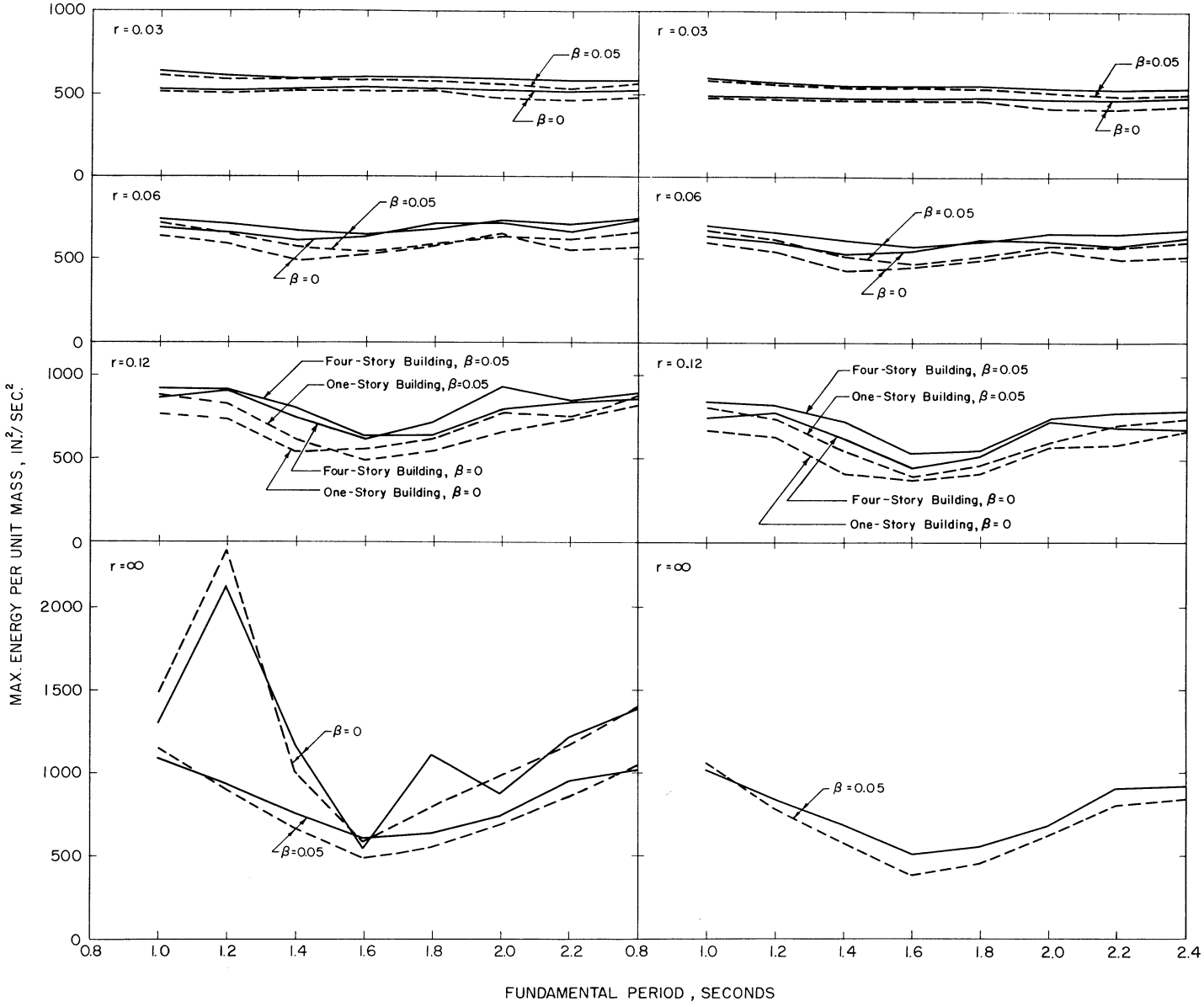

Figure 46. Energy Input Spectrum (left), Total Dissipated Energy Spectrum (right), El Centro, California, Earthquake of May 18, 1940. Component N-S.

Figures 47-52 present plots of results obtained from bilinear solutions and corresponding elasto-plastic solutions. A comparison of results shows that, in general, bilinear action reduces the lateral deflection somewhat and the permanent set effectively, but it increases the total inelastic displacement; practically no difference in noted between the energy curves obtained from either type of solution.

Figure 52 also shows that the inelastic deformation in the fourth story is considerably larger than in any other story although the distribution of the base yield shear strength was established from a triangular loading.

Analyses were made only for one earthquake component, four-story buildings, and limited combinations of structural parameters; yet, on the basis of the above observations, it might be expected that under inelastic action one-story and multi-story buildings will exhibit similar behavior. But before extending the limit design concepts, discussed in Chapter VI, to multi-story buildings, further investigations, beyond the scope of this study, are needed to determine the relation between the structural parameters and the distribution of inelastic deformation among the stories of a building, because this distribution cannot be readily predicted.

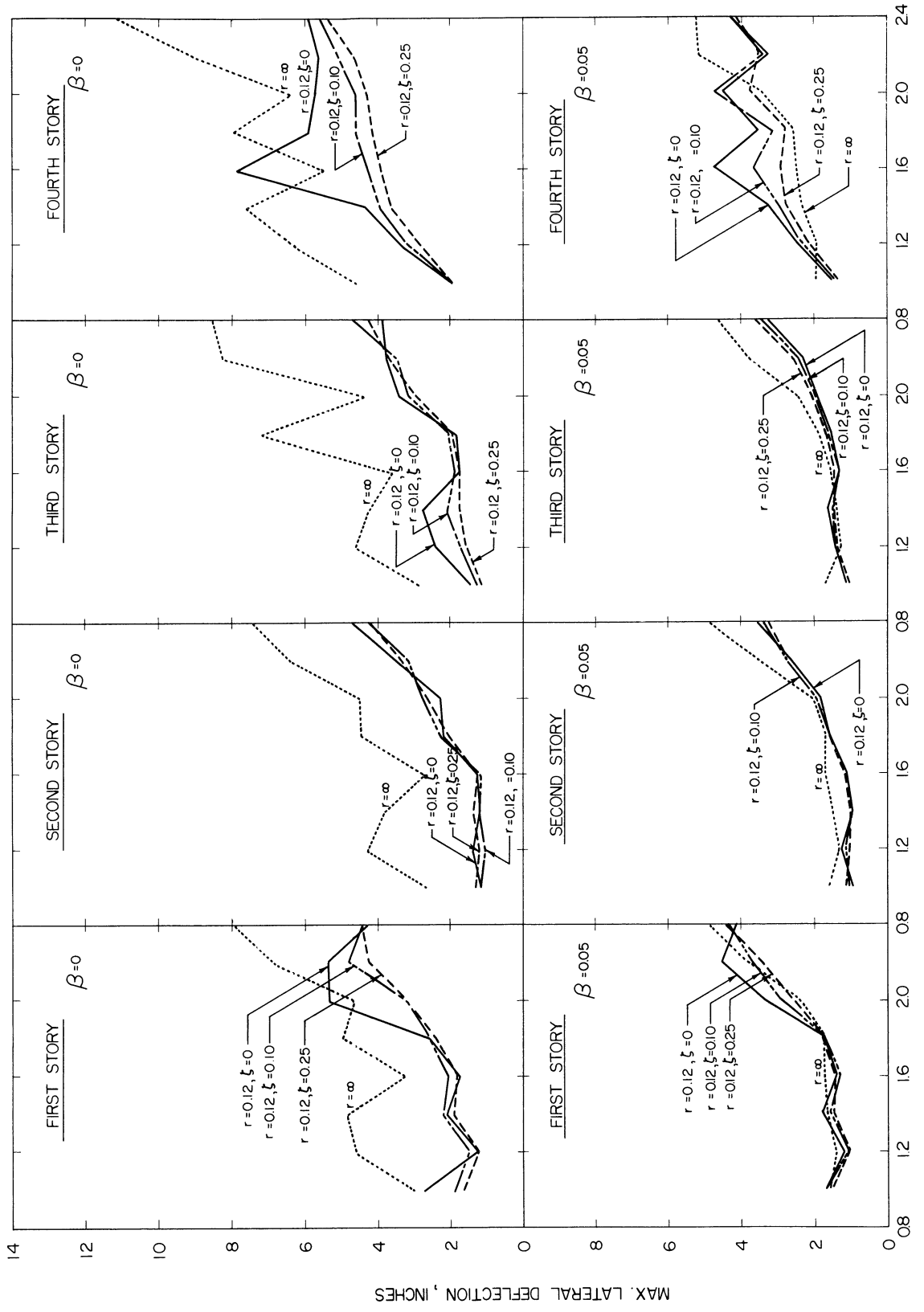

Figure 47. Lateral Deflection Spectra, El Centro, California, Earthquake of May 18, 1940. Component N-S.

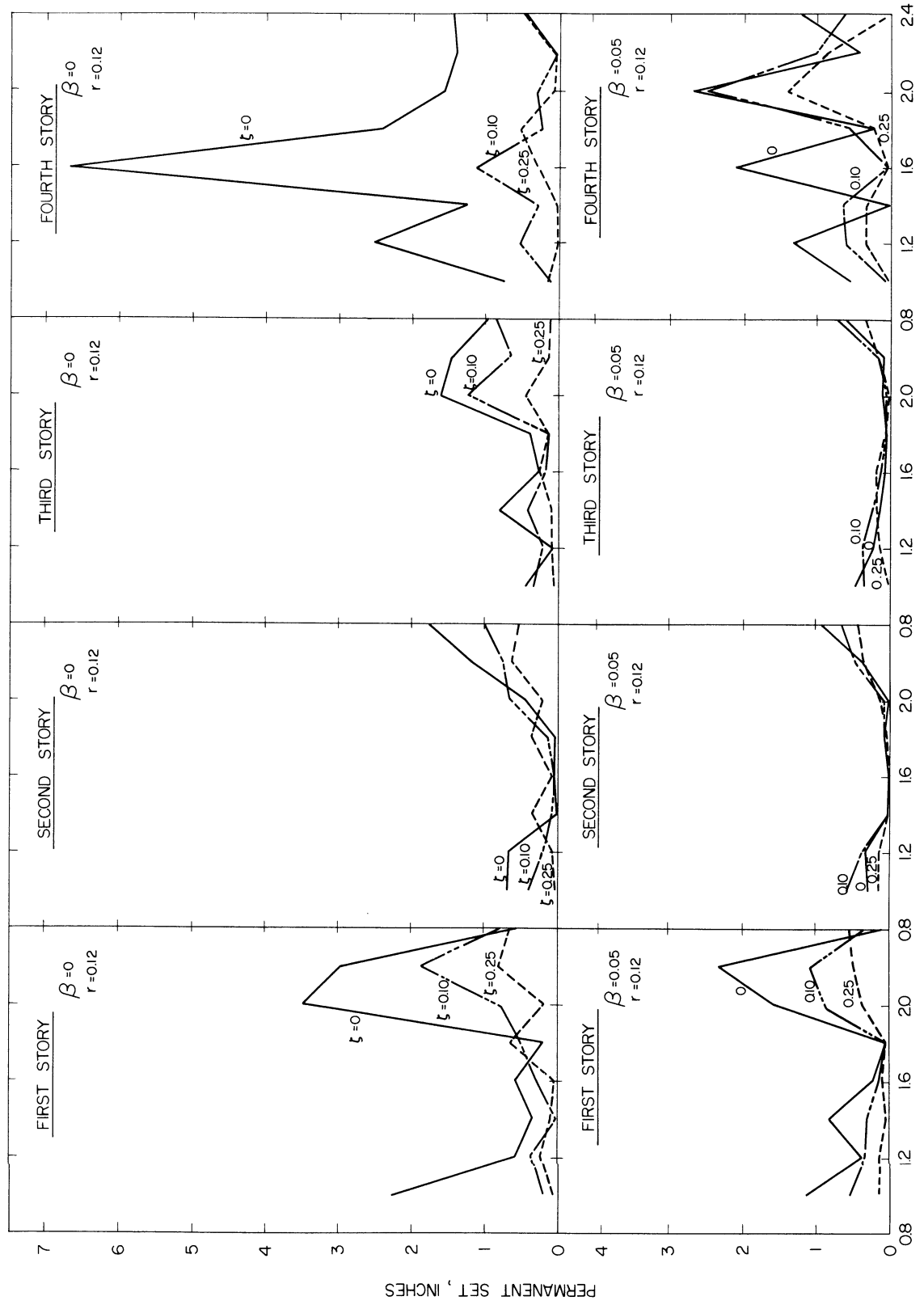

Figure 48. Permanent Sets, El Centro, California, Earthquake of May 18, 1940. Component N-S.

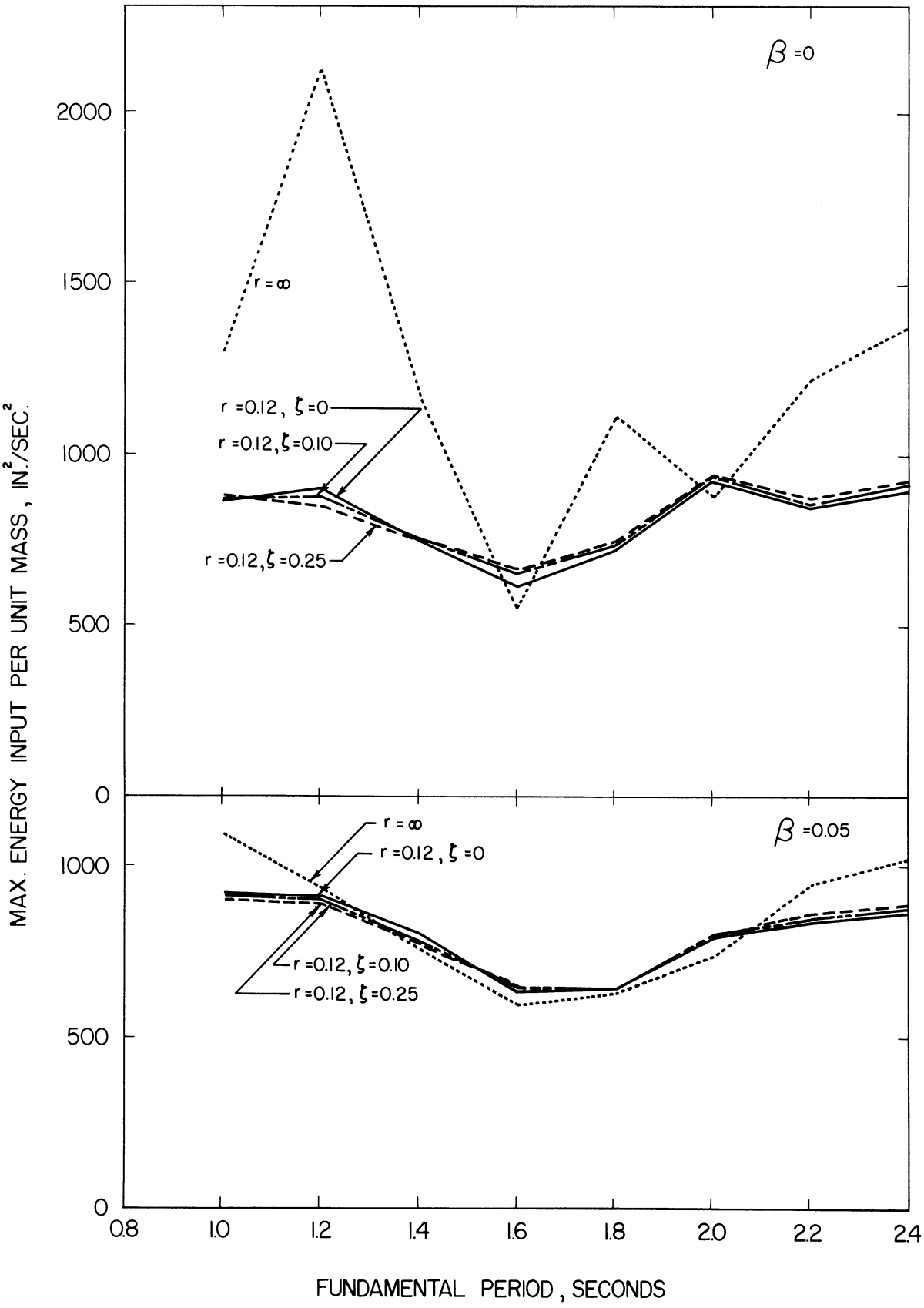

Figure 49. Energy Input Spectrum, El Centro, California, Earthquake of May 18, 1940. Component N-S.

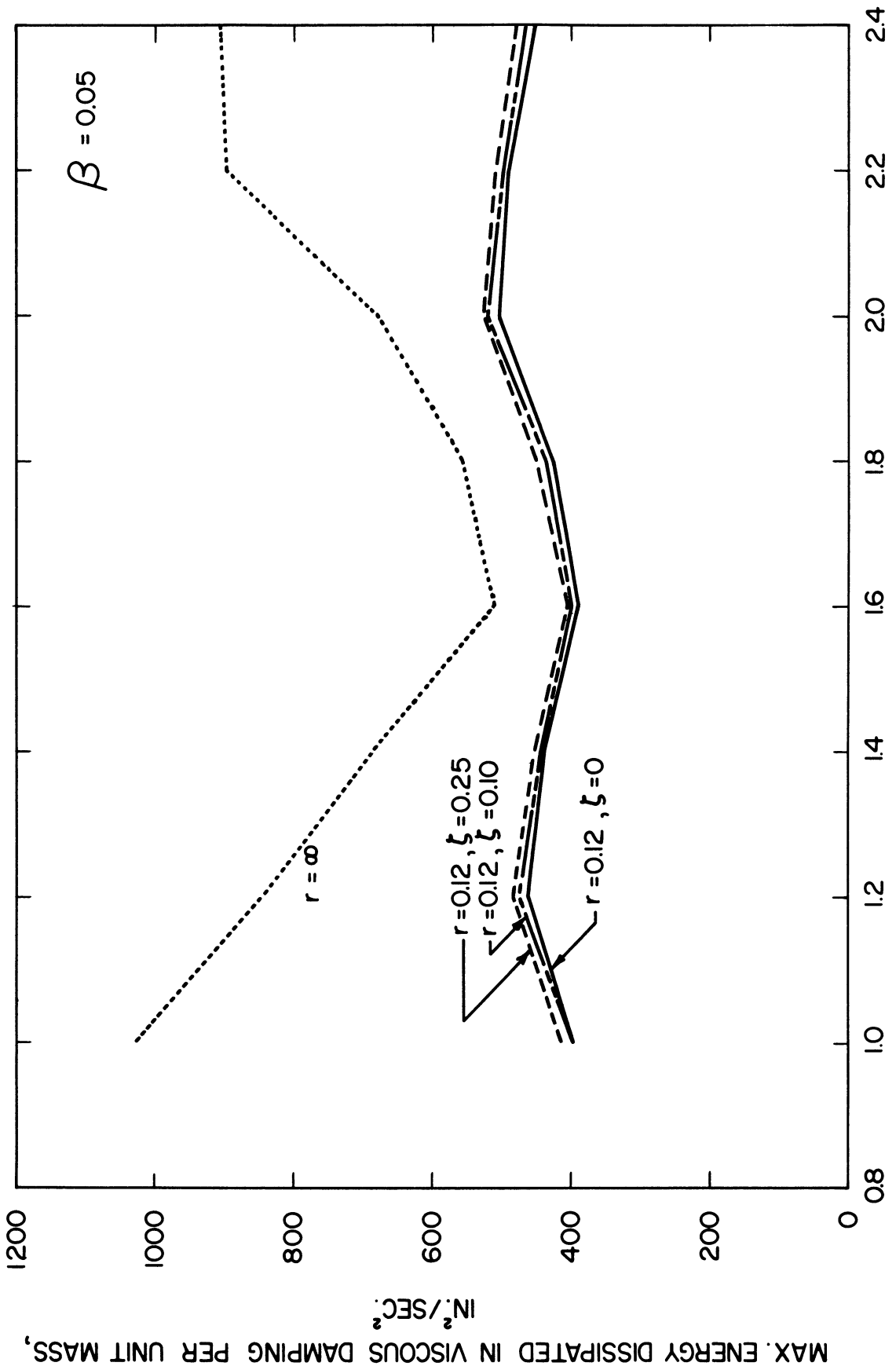

Figure 50. Maximum Energy Dissipated in Viscous Damping, El Centro, California, Earthquake of May 18, 1940. Component N-S.

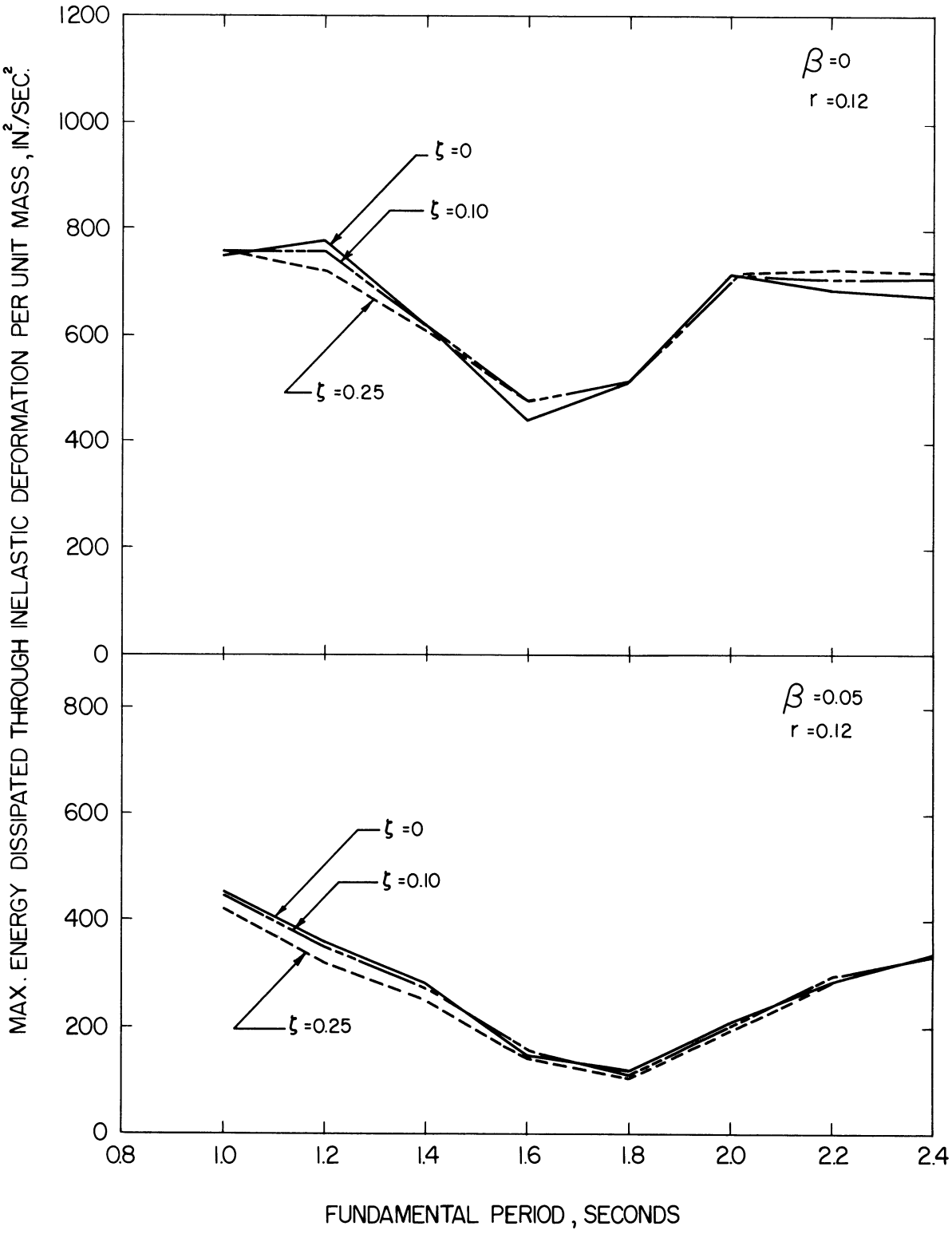

Figure 51. Maximum Energy Dissipated through Inelastic Deformation, El Centro, California, Earthquake of May 18, 1940. Component N-S.

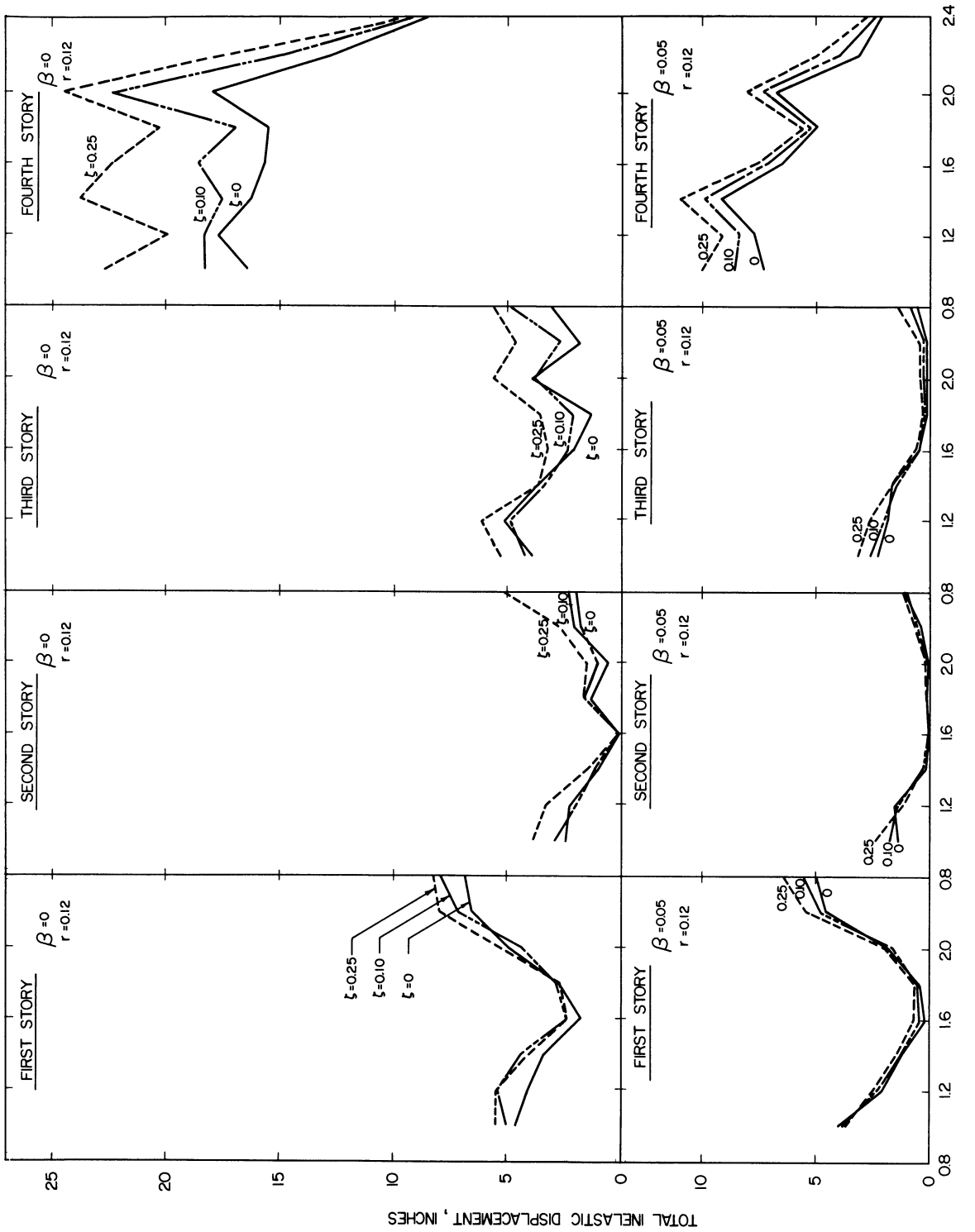

Figure 52. Total Inelastic Displacement, El Centro, California, Earthquake of May 18, 1940. Component N-S.

CHAPTER IX

SUMMARY AND CONCLUSIONS

A study of the behavior of buildings subjected to earthquakes has been presented, in which buildings with elasto-plastic or bilinear hysteresis have been considered. All the investigations were carried out with the aid of an IBM-704 digital computer. The results were presented in graphic and tabular form.

In Chapter I, the object of the study was introduced and some of the recent investigations on the inelastic response of buildings to earthquake forces were described briefly.

Chapter II described the method adopted in this study for the translation of the earthquake accelerogram records into punched-card accelerograms to be used as input data by the computer. The accelerogram records considered were those of the four strongest U.S. earthquakes on record.

In Chapter III, linear dynamic analysis was reviewed. The seismic lateral load coefficient (ratio of maximum base shear to weight of building) was evaluated for different buildings, for each horizontal component of the earthquakes under study. The results indicated seismic coefficients as high as 0.55 for buildings represented by linear dynamic systems, even if the buildings were damped as heavily as 0.20 of critical damping. The apparent discrepancy between the seismic coefficients obtained from linear dynamic analysis and those stipulated by building codes was attributed mainly to the fact that linear dynamic analysis ignores

energy dissipated through inelastic deformation. This dissipation of energy is recognized by engineers as an important factor in explaining the observed behavior of buildings during strong-motion earthquakes.

Chapter IV analyzed the response to earthquakes of simple buildings with elasto-plastic hysteresis. The effect of elasto-plastic action on lateral deflections and permanent sets was investigated, because buildings with hysteresis might become unusable as a result of large permanent sets, even though the structural elements might still have adequate strength for structural safety. The maximum lateral deflections of different buildings were evaluated for different levels of yield strength, for all horizontal earthquake components. Levels of yield strength as low as 0.03 and 0.01 of gravity were considered to determine the extent to which the yield strength of buildings can be lowered without causing lateral deflections significantly larger than those calculated for the same buildings, had they behaved linearly. The results were plotted, in the form of families of curves, against natural period, for levels of yield strength ranging from completely elastic down to 0.01 of gravity and for values of damping ranging from 0 to 0.20 of critical damping.

In Chapter V, the energy relations for the energy input and its components were developed for simple buildings with elasto-plastic hysteresis subjected to earthquakes. The maximum values of the energy functions for different buildings were evaluated for all horizontal earthquake components. The computed values of energy input and total dissipated energy were presented in the form of families of curves as in the preceding chapter. The curves permitted the study of the relation between the plotted energies and the three structural parameters, namely, natural period (stiffness),

damping, and yield strength. Significantly, these curves permitted a comparison of the values of the total energy imparted to buildings with elasto-plastic hysteresis with those values calculated for the same buildings had they behaved linearly.

Chapter VI analyzed the effect of elasto-plastic action in reducing the seismic lateral load coefficients calculated from linear dynamic analysis. Based on the results of the investigations described in the preceding chapters, the reduction effect was evaluated, using the total plastic displacement as the controlling response parameter. This parameter consists of the sum of the absolute values of all displacements in the plastic region in both directions. The results were expressed in terms of a reduction coefficient defined as the ratio of the actual yield strength of a building to the strength that would have been required for that building if it were to respond linearly to the considered earthquake.

Chapter VII investigates the behavior of simple buildings with bilinear hysteresis subjected to earthquakes. Only two horizontal earthquake components and limited combinations of structural parameters were analyzed. Results from this investigation and those which preceded permitted a comparison of bilinear with elasto-plastic hysteresis.

In Chapter VIII, an attempt was made to extend the above described investigations to multi-story idealized shear buildings, to see whether, under inelastic action, one-story and multi-story buildings would exhibit similar behavior. Only one horizontal earthquake component, four-story buildings, and limited combinations of structural parameters were analyzed.

From the results of the investigations presented herein, the following conclusions can be drawn.

The spectral plots of lateral deflection show that simple buildings with elasto-plastic hysteresis and values of yield level not lower than 0.06 of gravity will undergo lateral deflections seldom exceeding those calculated for the same buildings had they behaved linearly, and often lower. For the same buildings the plots of permanent set show that the lateral deflections remaining at the end of the earthquake seem to be within acceptable limits for the values of damping and natural period generally encountered in buildings. Therefore it appears that strong-motion earthquake-resistant design incorporating energy absorption through plastic deformation can be attempted, provided that the yield level is not lower than 0.06 of gravity. Lower values may severely affect the lateral deflection and permanent set, and thus might make the building unusable, even though the structural elements may still have adequate strength for structural safety.

For all the considered values of damping, the spectral plots of energy input show that, on the average, a decrease in yield level is accompanied by a decrease in the total energy imparted to simple buildings with elasto-plastic hysteresis. This could explain the fact that buildings designed for relatively low seismic lateral loads have withstood major earthquakes.

The above relation between yield level decrease and energy input decrease confirms that Professor Housner's hypothesis, made in his limit design approach, is on the average conservative. This hypothesis assumes that the maximum energy input imparted to a building with hysteresis is not greater than it would have been if that building had behaved linearly.

The spectral plots of energy input also show that at high values of yield level, especially in the case of linear behavior, variations in the fractions of critical damping do not induce any decisive variations in the energy-input curves. But at low values of yield level an increase in damping is accompanied by an increase in energy input.

Finally, the same plots show that either type of energy dissipation, through plastic deformation or through damping, removes effectively the irregular peaks of the elastic undamped energy-input curves.

From the plots of the reduction coefficient it appears that, for the considered values of damping, the quantitative reduction effect of elasto-plastic action is generally limited by two curves bounding the band over which the plotted points are scattered. Only a few of these points are found outside the band. From the same plots it also appears that elasto-plastic action is more effective at lower levels of damping.

From linear dynamic analyses of past earthquakes, one can estimate the maximum strain energy U_e that is likely to be stored in a building if the latter were to respond completely elastically to a future earthquake. Knowing the properties of the structural elements, one can estimate D, the amount of energy which that building can dissipate through plastic deformation. Housner's limit design criterion is that a building should be capable of actually storing as strain energy the difference between U_e and D. On the basis of this criterion, Equation (6.15) was developed. This equation gives the reduction coefficient as a function of the permissible total plastic displacement.

By superposing the band of Figure 29 over the curve plotted from Equation (6.15), it appears that, for the earthquakes considered,

the reduction coefficient as determined from Equation (6.15) is generally conservative for values of damping not exceeding 0.03 of critical damping, while at levels of damping between 0.03 and 0.20 of critical damping, the reduction coefficient would be generally conservative if obtained from the upper edge of the band, given by Equation (6.16).

Based on the foregoing, energy absorption through inelastic deformation can be incorporated into strong-motion earthquake-resistant design simply by multiplying the seismic lateral load coefficient obtained from linear considerations by the reduction coefficient.

Admittedly, the reduction coefficient as determined quantitatively from the above has its limitations since the complex load-deflection characteristics of a building have been described by an idealized relation of the elasto-plastic type. Nevertheless, the use of the reduction-coefficient concept in strong-motion earthquake-resistant design seems realistic and practicable.

In the experimental study of load-deflection relations,[1-3] structural materials have exhibited pronounced hysteretic properties. However, almost none of the experiments reported to date investigated these hysteretic properties when structural materials are subjected to reverse-loading cycles after the limiting elastic displacement is far exceeded. Therefore, before introducing the reduction-coefficient concept to actual design, more experimental work is needed to determine permissible values of total plastic displacement.

When the results obtained from buildings with bilinear hysteresis are compared with those obtained from the same buildings with elasto-plastic

hysteresis, it appears that, as inelastic deformation progresses, the elasto-plastic system oscillates about a position of equilibrium which generally keeps shifting away from the zero position while the bilinear system generally wanders less, thus causing a smaller permanent set. Otherwise, for the particular examples used in the analyses, there is practically no difference between bilinear and elasto-plastic hysteresis.

On the basis of the results obtained after the study was extended to four-story idealized shear buildings, it appears that, under inelastic action, one-story and multi-story buildings exhibit similar behavior. But before extending the limit design concepts discussed above to multi-story buildings, further investigations are needed to determine the relation between the structural parameters and the distribution of inelastic deformation among the stories of a building, because this distribution cannot be readily predicted. However, the results obtained in this study should contribute to a better understanding of the behavior of buildings during earthquakes, which, it is hoped, will eventually lead to the improvement of earthquake-resistant design procedures.

APPENDIX A

EQUIVALENT ONE-MASS SYSTEM GIVING THE SAME BASE SHEAR AS THE r-th MODE OF THE MULTI-MASS SYSTEM

The uncoupled equation of motion in the r-th mode of an undamped multi-mass system subjected to an earthquake ground motion is given by:

$$\ddot{u}_r + \left(\frac{2\pi}{T_r}\right)^2 u_r = - \ddot{y} \frac{\sum_{i=1}^{N} m_i \phi_{ir}}{\sum_{i=1}^{N} m_i \phi_{ir}^2} \qquad (A.1)$$

where

u_r is the modal displacement. (L)

The displacement of the i-th mass relative to the ground if the system vibrated in the r-th mode is

$$x_{ir} = \phi_{ir} u_r \ . \qquad (A.2)$$

Denoting by s_{ij} the stiffness coefficient which is defined as the force that would be exerted on the i-th mass when the configuration of the system is $x_j = 1$ unit length and all other $x = 0$, the restoring force exerted on the i-th mass in the r-th mode is

$$Q_{ir} = \sum_{j=1}^{N} s_{ij} x_{jr} \ . \qquad (A.3)$$

From Equations (A.2) and (A.3),

$$Q_{ir} = \sum_{j=1}^{N} s_{ij} \phi_{jr} u_r \ . \qquad (A.4)$$

But as

$$\sum_{j=1}^{N} s_{ij} \phi_{jr} = \left(\frac{2\pi}{T_r}\right)^2 m_i \phi_{ir} \ ,$$

Equation (A.4) becomes:

$$Q_{ir} = \left(\frac{2\pi}{T_r}\right)^2 m_i \phi_{ir} u_r \quad . \tag{A.5}$$

The base shear in the r-th mode is

$$V_{Br} = \sum_{i=1}^{N} Q_{ir} = \left(\frac{2\pi}{T_r}\right)^2 \sum_{i=1}^{N} m_i \phi_{ir} u_r \quad . \tag{A.6}$$

The equation of motion for the equivalent one-mass system corresponding to the r-th mode of the multi-mass system is

$$\ddot{x}_{er} + \left(\frac{2\pi}{T_r}\right)^2 x_{er} = - \ddot{y} \quad . \tag{A.7}$$

The base shear for the equivalent one-mass system is

$$V_{Br} = k_{er} x_{er} \quad . \tag{A.8}$$

From the first definition made in Equation (3.3),

$$k_{er} = \left(\frac{2\pi}{T_r}\right)^2 m_{er} \quad . \tag{A.9}$$

With this, Equation (A.8) can be rewritten as follows:

$$V_{Br} = \left(\frac{2\pi}{T_r}\right)^2 m_{er} x_{er} \quad . \tag{A.10}$$

From the differential Equations of motion (A.1) and (A.7),

$$u_r = \frac{\sum_{i=1}^{N} m_{ir} \phi_{ir}}{\sum_{i=1}^{N} m_i \phi_{ir}^2} \; x_{er} \quad . \tag{A.11}$$

For equal base shears the right side of Equation (A.10) will be equated to the right side of Equation (A.6), after expressing u_r in terms of x_{er} as given by Equation (A.11).

Hence

$$\left(\frac{2\pi}{T_r}\right)^2 m_{er}x_{er} = \left(\frac{2\pi}{T_r}\right)^2 \frac{\left[\sum_{i=1}^{N} m_i\phi_{ir}\right]^2}{\sum_{i=1}^{N} m_i\phi_{ir}^2} x_{er}$$

or

$$m_{er} = \frac{\left[\sum_{i=1}^{N} m_i\phi_{ir}\right]^2}{\sum_{i=1}^{N} m_i\phi_{ir}^2} \quad . \tag{A.12}$$

According to Equations (A.5) and (A.6), the vertical distribution of the base shear V_{Br} is determined from:

$$F_{ir} = V_{Br} \frac{m_i\phi_{ir}}{\sum_{i=1}^{N} m_i\phi_{ir}} \quad . \tag{A.13}$$

APPENDIX B

FORMULAS USED IN THE RUNGE-KUTTA THIRD-ORDER PROCEDURE

In brief, the Runge-Kutta method for the evaluation of a variable at time $t + h$ (h being a specified time interval) from that at time t is based on the use of suitably chosen slopes within the specified time interval h. The third-order procedure uses three such slopes and by multiplying each slope by h, three candidate increments in the variable are obtained. The final choice for the increment is a weighted average of the above three increments.

Let us assume the differential equations to have the form

$$\left.\begin{aligned} \dot{x}_1 &= f_1 (x_1, x_2, \ldots, x_n, t) \\ \dot{x}_2 &= f_2 (x_1, x_2, \ldots, x_n, t) \\ &\vdots \\ \dot{x}_n &= f_n (x_1, x_2, \ldots, x_n, t) \end{aligned}\right\} , \qquad \text{(B.1)}$$

where

x_i $(i = 1, 2, \ldots, n)$ are the dependent variables,

t is the independent variable,

and dots define differentiation with respect to t.

The three candidate increments in the variable are defined as follows:

$$\left.\begin{aligned} \delta_{io} &= h\, f_i(x_1,\ldots,x_n,t) \\ \delta_{i1} &= h\, f_i(x_1+p\delta_{1o},\ldots,x_n+ p\delta_{no},t + p\, h) \\ \delta_{i2} &= h\, f_i(x_1+ (q-r)\delta_{1o} + r\delta_{11},\ldots,x_n+ (q-r)\delta_{no} + r\delta_{n1} ,t + q\, h) \end{aligned}\right\} \qquad \text{(B.2)}$$

and the final increment in the variable obtained as a weighted average of the above three increments is defined as follows:

$$x_i(t+h) - x_i(t) = \ell\delta_{io} + m\delta_{i1} + n\delta_{i2} \quad . \tag{B.3}$$

The symbols p, q, r, ℓ, m, and n which appear in Equations (B.2) and (B.3) are determined by expanding both sides of Equation (B.3) in powers of h by means of Taylor's series expansion and equating coefficients of the powers up through h^3. In so doing, the following four equations with six unknowns are obtained:

$$\left.\begin{aligned} \ell + m + n &= 1 \\ mp + nq &= 1/2 \\ mp^2 + nq^2 &= 1/3 \\ npr &= 1/6 \end{aligned}\right\} \tag{B.4}$$

There are many solutions to Equation (B.4). The solution shown below,

$$\left.\begin{aligned} \ell &= 1/4 \\ m &= 0 \\ n &= 3/4 \\ p &= 1/3 \\ q &= 2/3 \\ r &= 2/3 \end{aligned}\right\} \quad , \tag{B.5}$$

is advantageous because the number of arithmetic operations is reduced as a result of $m = q - r = 0$ and for this reason it has been selected for use in this study.

REFERENCES

1. Benjamin, J. R. and Williams, H. A. "Behavior of Reinforced Concrete Shear Walls." Trans. A.S.C.E., 124, 1959.

2. Benjamin, J. R. and Williams, H. A. "The Behavior of One-Story Brick Shear Walls." Journal of the Structural Division, A.S.C.E., July, 1958.

3. Jacobsen, L. S. Frictional Effects in Composite Structures Subjected to Earthquake Vibrations. Stanford University, March, 1959.

4. Tanabashi, R. "Studies on the Non-Linear Vibrations of Structures Subjected to Destructive Earthquakes." Proceedings of the First World Conference on Earthquake Engineering, Berkeley, California, June, 1956.

5. Berg, G. V. Analysis of Structural Response to Earthquake Forces. University of Michigan, Report No. IP-291, Ann Arbor, May, 1958.

6. Bycroft, G. N., Murphy, M. J., and Brown, K. J. "Electrical Analog for Earthquake Yield Spectra." Journal of the Engineering Mechanics Division, A.S.C.E., October, 1959.

7. Sheth, R. M. Effect of Inelastic Action on the Response of Simple Structures to Earthquake Motions. M.S. Thesis, University of Illinois, Dept. of Civil Engineering, 1959.

8. Penzien, J. "Dynamic Response of Elasto-Plastic Frames." Journal of the Structural Division, A.S.C.E., July, 1960.

9. Penzien, J. "Elasto-Plastic Response of Idealized Multi-Story Structures Subjected to a Strong Motion Earthquake." Proceedings of the Second World Conference on Earthquake Engineering, Tokyo, Japan, July, 1960.

10. Housner, G. W. "Limit Design of Structures to Resist Earthquakes." Proceedings of the First World Conference on Earthquake Engineering, Berkeley, Calif., June, 1956.

11. Housner, G. W. "Behavior of Structures During Earthquakes." Journal of the Engineering Mechanics Division, A.S.C.E., October, 1959.

12. Blume, J. A. Closing discussion on "Structural Dynamics in Earthquake-Resistant Design." Trans. A.S.C.E., 125, 1960.

13. Blume, J. A. Discussion on "Electrical Analog for Earthquake Yield Spectra." Journal of the Engineering Mechanics Division, A.S.C.E., June, 1960.

14. Alford, J. L., Housner, G. W., and Martel, R. R. Spectrum Analyses of Strong-Motion Earthquakes. Earthquake Research Lab., Calif. Inst. Tech., August, 1951.

15. Anderson, A. W., et al., "Lateral Forces of Earthquake and Wind." Trans. A.S.C.E., 117, 1952.

16. Hudson, D. E. "Response Spectrum Techniques in Engineering Seismology." Proceedings of the First World Conference on Earthquake Engineering, Berkeley, Calif., June, 1956.

17. Clough, R. W. "Dynamic Effects of Earthquakes." Journal of the Structural Division, A.S.C.E., April, 1960.

18. Jacobsen, L. S. Discussion on "Structural Dynamics in Earthquake-Resistant Design." Trans. A.S.C.E., 125, 1960.

19. Berg, G. V. and DaDeppo, D. A. "Dynamic Analysis of Elasto-Plastic Structures." Journal of the Engineering Mechanics Division, A.S.C.E., April, 1960.

20. Veletsos, A. S. and Newmark, N. M. "Effect of Inelastic Behavior on the Response of Simple Systems to Earthquake Motions." Proceedings of the Second World Conference on Earthquake Engineering, Tokyo, Japan, July, 1960.

21. Caughey, T. K. "Random Excitation of a System with Bilinear Hysteresis." J. Appl. Mech., 27, December, 1960.